NOTICE

The quality of this microform is heavily dependent upon the quality of the original thesis submitted for microfilming. Every effort has been made to ensure the highest quality of reproduction possible.

If pages are missing, contact the university which granted the degree.

Some pages may have indistinct print especially if the original pages were typed with a poor typewriter ribbon or if the university sent us an inferior photocopy.

Reproduction in full or in part of this microform is governed by the Canadian Copyright Act, R.S.C. 1970, c. C-30, and subsequent amendments.

AVIS

La qualité de cette microforme dépend grandement de la qualité de la thèse soumise au microfilmage. Nous avons tout fait pour assurer une qualité supérieure de reproduction.

S'il manque des pages, veuillez communiquer avec l'université qui a conféré le grade.

La qualité d'impression de certaines pages peut laisser à désirer, surtout si les pages originales ont été dactylographiées à l'aide d'un ruban usé ou si l'université nous a fait parvenir une photocopie de qualité inférieure.

La reproduction, même partielle, de cette microforme est soumise à la Loi canadienne sur le droit d'auteur, SRC 1970, c. C-30, et ses amendements subséquents.

HYDROCRACKING BOSCAN HEAVY OIL WITH CATALYSTS CONTAINING A ZEOLITE COMPONENT

By

Rwaichi J.A. Minja

Ottawa, Ontario. June 1990

A Thesis

submitted to the School of Graduate Studies and Research

University of Ottawa

in partial fulfilment of the requirements

for the degree of Master of Applied Science

in Chemical Engineering.

ISBN 0-315-62301-2

UNIVERSITÉ D'OTTAWA
UNIVERSITY OF OTTAWA

ABSTRACT

In this study, hydrodesulphurization (HDS), hydrodenitrogenation (HDN), hydrodemetallization (HDM), and micro carbon residue (MCR) removal were investigated using residuum hydrocracking catalysts containing a zeolite component. It is well known that the strong Brønsted acid sites on the external surfaces of zeolite crystals increase the distillate yield and decrease the coke yield obtained when using fluid catalytic cracking (FCC) catalysts. However, comparatively few studies have been performed to investigate the possibility of improving resid hydrocracking catalysts by using zeolitic materials. Two families of catalysts were prepared each containing various amounts of zeolite (H-mordenite or HY). The first family of catalysts containing H-mordenite was tested at a pressure of 13.9 MPa and at temperatures of 400 and 450°C in an upward flow packed bed reactor. The results showed increased overall HDM, but decreased overall HDS, HDN, and MCR removal with increasing catalyst H-mordenite content. Analysis based on constant residence time and constant catalyst surface area, i.e., calculation of pseudo turnover frequency (PTOF) and PTOF per unit residence time, showed increased catalyst activity for all reactions with increasing

catalyst H-mordenite content. The second family of catalysts containing HY was tested at the same conditions, but at temperatures of 400 and 370°C. For these catalysts there was increased overall HDS, HDN, HDM, and MCR removal with increased HY content in the catalysts. Calculation of PTOF and PTOF per residence time also showed an increase in catalyst activity with the increasing catalyst HY content.

Benzofuran temperature programmed desorption (TPD) measurements showed that, the number of acid sites increased with increasing zeolite (H-mordenite or HY) content in the catalysts. Therefore it was suggested that, the enhanced activity of the catalysts was related to the increased number of acid sites caused by the addition of zeolite (H-mordenite or HY) in the catalysts.

CONTRIBUTIONS TO KNOWLEDGE

The following is an account of what was done in this study which contributes to a new knowledge:

1. Page 84 describes a new preparation method for catalysts containing a zeolite component, using a zeolite-oil paste.

3. In section 5.2 page 101, the HDS, HDN, and MCR experimental results for catalysts containing various concentrations of H-mordenite zeolite are discussed. The effect of increasing the amount of H-mordenite in the catalyst is discussed. These results were submitted for publication to the journal **Fuel**.

4. On page 117 experimental measurements showing increased HDM with increasing H-mordenite content in the catalysts are discussed. The results were submitted for publication to the journal **Energy and Fuels**.

5. On page 129 experimental results showing the effect of HY zeolite catalyst content on HDM are discussed. Although HY zeolite has been tested before in resid hydroprocessing catalysts, this work was different in that it provides the first HDM measurements that have been reported for zeolite containing catalysts.

ACKNOWLEDGEMENT

The completion of this study was possible not only because of my efforts, but also because many others offered financial support, helpful collaboration, guidance and encouragement. I am thankful to Swiss Development Corporation (SDC) for their financial support which enabled me to undertake this study. I wish to express my gratitude to the management of the Energy Research Laboratories (ERL) for allowing me to do research at ERL. My thanks to the technicians of the ERL analysis laboratory for analyzing my samples, and to all ERL staff whose help was vital to my work.

I am thankful to Dr. M. Ternan for his challenges, guidance and encouragement during the whole period. I am also thankful to my colleague H.T.H. Kimweri for his moral support and useful company throughout the duration of these studies. My sincere appreciation is extended to the professors, fellow students and the staff of the Chemical Engineering Department for their friendliness.

To my mother, father, sisters and brothers whose love, caring, encouragement, and prayers always continue to be the tools for my achievements.

NOMENCLATURE

A	Total membrane pore cross-sectional area, m^2
A_B	Empty reactor cross-sectional area, m^2
C	A constant in equation 11, atoms removed nm^{-2}
C_1	A constant in equation 6, atoms removed nm^{-2}
C_2	A constant which equals C/C_1
C_o	Initial concentration of species X, mol/L
C_x	Concentration of species X at time t, mol/L
ΔC	Concentration difference, kg/m^3
D	Measured diffusion Coefficient, m^2/s
D_B	Diffusivity of a solute molecule in a bulk phase solution, m^2/s
D_{eff}	Effective diffusivity of a solute molecule in a pore, m^2/s
d_p	pore diameter, m
E	Void fraction between catalyst particles in the reactor, m^3/m^3
J	Diffusivity flux, kg/s
k	Boltzmann's constant, J/K or reaction rate constant, s^{-1} or $mol^{-1}s^{-1}$
L	Pore length, m
P	Constant parameter in equation 3, [-]
r_m	Radius of a solute molecule, m
r_p	Pore radius, m
SA	Total catalyst surface area in a reactor, m^2

S_{BET}	Catalyst specific surface area determined by BET, m^2/kg
S_{Hg}	Catalyst specific surface area determined by mercury porosimetry, m^2/kg
T	Temperature, K
t	Time, s
$\tilde{U}_G$	Superficial gas velocity, m/s
V	Empty reactor volume, m^3
V_p	Specific pore volume, m^3/g
V^*	Volumetric gas flow rate, m^3/s
V^{**}	Feedstock feed rate at reactor condition, m^3/s
X	Represents heteroatoms (sulphur, nitrogen, nickel, or vanadium)
Y	Atomic mass of sulphur, nitrogen, nickel, or vanadium

Greek Symbols

α	Sulphur conversion, wt %
β	Nitrogen conversion, wt %
γ	MCR conversion, wt %
ϵ_G	Gas hold-up, m^3/m^3
η	Solvent viscosity, Pa.s
θ	Residence time or mean residence time, s
κ	Constant as defined in section 2.6, $s^{-1}L^{-1}$
λ	Ratio of r_m/r_p, m/m
ρ_L	Liquid density, kg/m^3

ρ_G	Gas density, kg/m^3
σ_L	Liquid surface tension, N/m
χ	Conversion or fractional conversion, [-]

Abbreviations

ART	Asphalt Residua Treating
BET	Brunauer, Emmett, and Teller
BF	Bottom Fraction
CMA	Cobalt-Molybdenum-Alumina
CM	Carboneous Molecule
DRES	Diffusion Reflection Electron Spectroscopy
EXAFS	Extended X-ray Absorption Fine Structure
FCC	Fluid Catalytic Cracking
H/C	Hydrogen to Carbon Atomic Ratio
HDM	Hydrodemetallization
HDN	Hydrodenitrogenation
HDO	Hydrodeoxygenation
HDS	Hydrodesulphurization
HOC	Heavy Oil Cracking
HPLC	High Pressure Liquid Chromatography
ICAP	Inductively Coupled Argon Plasma
LHSV	Liquid hourly space velocity
MES	Mossbauer Emission Spectroscopy
MCR	Micro carbon residue
PSA	Pressure Swing Absorption
PTOF	Pseudo turnover frequency

REY	Rare Exchanged Y
SEC	Size Exclusion Chromatography
SEM	Scanning Electron Microscopy
TOF	Turnover frequency
TPD	Temperature Programmed Desorption
TPO	Temperature Programmed Oven
VPO	Vapour Pressure Osmometry
XPS	X-ray Photoelectron Spectroscopy
XRD	X-ray Diffraction

CONTENTS

ABSTRACT (ii)

CONTRIBUTIONS TO KNOWLEDGE (iv)

ACKNOWLEDGEMENT (v)

NOMENCLATURE (vi)

LIST OF TABLES (xiv)

LIST OF FIGURES (xiv)

1 INTRODUCTION 1

1.1 General Description of Heavy Oils and Residua 1

1.2 Physical Structure and Characteristics of Heavy Oils and Residua 4

1.2.1 Structure and Size of Resid Molecules 6

1.2.2 Effect of Separation Technique on Molecular Weight and Size 9

1.3 Chemical Composition of Heavy Oils 12

1.3.1 Sulphur Compounds in Petroleum 12

1.3.2 Nitrogen Compounds in Petroleum 14

1.3.3 Oxygen Compounds in Petroleum 15

1.3.4 Metallic Constituents of Petroleum 15

1.3.5 Porphyrin Metal Compounds 17

1.3.6 Non-porphyrin Metal Compounds 17

1.4 Hydrocracking Reactions of Heavy oil and Residua 18

1.4.1 Thermal Cracking Reactions 18

1.4.2 Hydrogenation Reactions in the Absence of a Catalyst 19
1.4.3 Catalytic Cracking Reactions 20
1.4.4 Hydrogenation Reactions in the Presence of a Catalyst 21
1.5 Hydrocracking Catalysts for Heavy Oils and Residua 22
1.5.1 Historical Background 22
1.5.2 Composition of Resid Hydrocracking Catalysts. 23
1.5.3 Alumina Support 23
1.5.4 Molybdenum and its Role in Catalysts 24
1.5.5 Cobalt and Nickel Promoters 24
1.5.6 Other Catalyst Additives (Components) 25
1.5.7 Use of Zeolite in Catalysts 27
1.5.8 Effect of Zeolite in Hydrocracking Catalysts 29
1.5.9 Zeolites Used in This Study 31
1.5.10 Catalyst Particle Size 33
1.5.11 Pore Diffusion 34
1.5.12 Catalyst Pore Size and Surface Area 38
1.6 Catalyst Characterization Techniques 40
1.6.1 Correlation Between Catalyst Solid Structure and Catalytic Activity 40
1.6.2 Correlation of Sites and Activity of Catalysts 43

1.7 Catalyst Deactivation in Resid Hydrocracking 44

1.8 Processing Parameters 48

1.8.1 Hydrogen Pressure 49

1.8.2 Reactor Temperature 49

1.8.3 Liquid Hourly Space Velocity (LHSV) 50

1.9 Commercial Processes for Conversion of Heavy Oils and Residua Without the Use of Hydrogen 50

1.9.1 Thermal (Non-Catalytic) Conversion Processes 51

1.9.2 Catalytic Conversion 54

1.10 Commercial Resid Hydrocracking Processes 56

1.10.1 H-Oil Process 56

1.10.2 LC-Fining 57

1.10.3 VEBA-Combi-Cracking. 59

1.10.4 CANMET Hydrocracking Process 60

2 METHODOLOGY 61

2.1 Characterization of the Catalysts Made 61

2.1.1 Elemental Composition 61

2.1.2 Mercury Porosimetry 62

2.1.3 BET Surface Area 62

2.1.4 X-ray Diffraction 63

2.1.5 Benzofuran Temperature Programmed Desorption 65

2.2 Analysis of the Liquid Product Samples 67

2.2.1 Carbon and Hydrogen Determination 67

2.2.2 Sulphur Determination 67

2.2.3 Nitrogen Determination 68
2.2.4 Micro Carbon Residue (MCR) Determination 69
2.2.5 Measurement of Specific Gravity 69
2.3 Characterization of the Used Catalysts. 70
2.4 Calculation of PTOF 71
2.5 The Effect of Residence Time on PTOF 72

3 PROPERTIES OF MATERIALS 75

3.1 Properties of Boscan (Venezuela) Heavy Oil Used in This Study 75
3.2 Properties of Hydrocarbon Distillate Oil 77
3.3 Properties of the Catalysts Made 77

4 EXPERIMENTAL 82

4.1 Catalyst Preparation 82
4.1.1 CMA Paste Preparation 82
4.1.2 Preparation of Catalysts with H-mordenite Zeolite Component 84
4.1.3 Preparation of Catalysts with HY Zeolite Component 85
4.1.4 Catalyst Drying and Calcination 85
4.2 Hydrocracking Reaction Experiments 86
4.2.1 Catalyst Presulphiding 89
4.2.2 Evaluation of Catalysts with Mordenite Component 90
4.2.3 Evaluation of Catalysts with HY Component 90

4.2.3 Evaluation of Catalysts with HY Component 90

5 RESULTS AND DISCUSSION 91

5.1 Non-Catalytic Hydrocracking 91

5.2 Catalytic Hydrocracking with Catalysts Containing an H-mordenite Component 101

5.3 Catalytic Hydrocracking with Catalysts Containing an HY Component 121

5.4 Comparison Between Non-Catalytic Hydrocracking and Catalytic Hydrocracking 132

6 CONCLUSIONS AND RECOMMENDATIONS 139

6.1 Conclusions 139

6.2 Recommendations 141

7 REFERENCES 142

8 APPENDICES 154

Appendix-A Experimental Data 155

Appendix-B Calculations 158

Appendix-C Benzofuran TPD plots 163

LIST OF TABLES

1. Properties of Various Residua 3
2. Properties of Boscan Heavy Oil 76
3. Properties of Hydrocarbon Distillate Oil 76
4. Characteristics of Catalysts having an H-mordenite Component 80
5. Characteristics of Catalysts having an HY Component 81
6. Experimental Data: conversions, densities and Yield 155
7. Experimental Data: Gas Volumes and PTOF 156
8. Experimental Data: Analysis of Spent Catalysts 157

LIST OF FIGURES

1. ASTM Procedure for Separation of Petroleum. 5
2. Schematic Representation of an Asphaltene Cluster 8
3. Sulphur and Nitrogen Compounds in Petroleum 13
4. Porphine and Vanadium Metal Complex Structures 16
5. Effect of Pore Size in Pore Diffusion 37
6. X-ray Diffraction Patterns for Catalysts 64
7. Benzofuran Temperature Programmed Desorption 66
8. The Effect of Residence Time on PTOF 74
9. Experimental Set-up 87
10. Conversion versus Temperature for Non-catalytic Hydrocracking 92

11. Liquid Product Density versus Temperature for Non-catalytic Hydrocracking 94
12. Liquid Product Yield versus Temperature for Non-catalytic Hydrocracking 95
13. Change in H/C Atomic Ratio versus Temperature for Non-catalytic Hydrocracking 97
14. Metal Conversion versus Temperature for Non-catalytic Hydrocracking 99
15. Conversion versus Catalyst H-mordenite Zeolite Content 102
16. Specific Surface Area versus Catalyst H-mordenite Zeolite Content 103
17. Cumulative Mercury Intrusion Volume versus Catalyst Pore Diameter 105
18. Catalyst Pore Volume versus Catalyst H-mordenite Zeolite Content 106
19. Catalyst Bulk Density versus Catalyst H-mordenite Zeolite Content 108
20. PTOF versus Catalyst H-mordenite Zeolite Content 111
21. PTOF versus Apparent Residence Time 112
22. PTOF/θ versus Catalyst H-mordenite Zeolite Content 114
23. Effect of Diffusion on PTOF 115
24. Carbon Deposited versus Catalyst H-mordenite Content 117
25. Metal Conversion versus Catalyst H-mordenite Content 118
26. Conversion versus Catalyst HY Zeolite Content 122
27. Total Surface Area in the Reactor versus Catalyst HY Zeolite Content 123

28. PTOF versus Catalyst HY Zeolite Content 125
29. PTOF/θ versus Catalyst HY Content 126
30. Catalyst Pore Volume versus Catalyst HY Content 127
31. Carbon Deposited versus Catalyst HY Content 129
32. Metal Conversion versus Catalyst HY Content 130
33. Conversion versus Temperature for Catalytic Reactions 134
34. Temperature versus Liquid Product H/C Atomic Ratio 136
35. Effect of Temperature on Liquid Product Yield and Density 138
36. Temperature Programmed Desorption Plot for the Catalyst without a Zeolite Component 162
37. Temperature Programmed Desorption for the Catalyst with 10 wt % H-mordenite Zeolite Content 163
38. Temperature Programmed Desorption for the Catalyst with 20 wt % H-mordenite Zeolite Content 164
39. Temperature Programmed Desorption for the Catalyst with 20 wt % HY Zeolite Content 165

CHAPTER ONE

1.0 INTRODUCTION

The economies of all countries depend on energy, much of which is produced from petroleum crude oil. The depletion of the world's reserves of light crude oils is leading to an increase in utilization of heavy crude oils and residua. In Canada, the quantities of heavy oil reserves are comparable in magnitude to the light crude oil reserves in Saudi Arabia. In general, the properties of heavy crude oils are less desirable than those of light crude oils. The greater portion of large molecules in heavy oils is reflected in their boiling point distributions. As a result, heavy crude oils have to be converted to form lower boiling products. A variety of conversion processes have been developed. This thesis describes an experimental investigation of catalysts for one specific conversion process, heavy oil hydrocracking.

1.1 General Description of Heavy Oils and Residua

A recent definition of heavy oils (Heavy Oiler, 1989) has three categories of crude oils classified according to the density or American Petroleum Institute (API) gravity. If the gravity is less than 10°API (density greater than 1000 kg/m^3),

then the oil is extra heavy. If it's between 20-10°API (934-1000 kg/m^3), then it is classified as a heavy oil, and if the gravity is greater than 20°API (density less than 934 kg/m^3), it is classified as medium or light oil. Table 1 shows properties of various atmospheric residua and heavy crude oils (Quann **et al**, 1988 and Speight, 1981). Heavy crude oils have greater concentrations of polyaromatic asphaltenic structures in the 345°C+ atmospheric residuum fraction or 565°C+ vacuum residuum fraction (Quann **et al**, 1988). A crude oil residuum is broadly defined as the residue obtained from the crude oil after a nondestructive distillation has removed all of the volatile materials. Heavy oils are darker in colour and may even be black.

The asphaltene fraction of petroleum, heavy oils, and bitumens is the portion which precipitates when a large excess (40 volumes) of low-boiling liquid hydrocarbon (e.g. pentane) is added to (1 volume) of the petroleum or heavy oil. The asphaltenes are dark brown or black amorphous solids which do not melt prior to decomposition.

Another common property of heavy oils is micro carbon residue (MCR), i.e., the coke-forming tendency of the oil (alternatively, Ramsbottom carbon residue or Conradson carbon residue). MCR can sometimes be correlated with other properties, such as API gravity, sulphur, nitrogen, viscosity, and asphaltenes in the oil (Roberts, 1989 and Speight, 1981).

Table 1: Properties of Various Residua

Crude Oil Origin	Resid type	Gravity (°API)	Sulphur (wt %)	Nitrogen (wt %)	MCR (wt %)	Asphaltenes (wt %)	metals Nickel (ppm)	metals Vanadium (ppm)
Iranian Heavy	Ar	14.7	2.52	0.47	9.5	6.7	57	166
Kuwait	Ar	14.6	4.10	0.22	11.1	3.5	22	77
Arabian Heavy	Ar	12.7	4.24	0.28	12.3	10.3	28	78
Maya Mexico	Ar	8.8	4.50	0.54	18.3	15.0	70	433
Beta (California)	Ar	8.3	4.31	1.06	13.2	10.5	156	180
Hondo (California)	Ar	8.5	6.49	0.87	13.5	14.2	130	249
Jobo (Venezuela)	Ar	6.8	4.24	0.54	16.2	14.4	93	450
Bachaquero (Venezuela)	Ar	10.1	2.77	0.57	14.3	8.4	61	507
Boscan (Venezuela)	Ar	6.4	5.9	0.69	18.2	13.5	130	1553
Boscan (Venezuela)	Crude	10.3	5.6	-	14.0	12.6	117	1220
Athabasca (Canada)	Crude	5.9	4.9	0.41	14.9	11.4	86	167
Lloydminster (Canada)	Crude	14.5	4.3	-	8.1	-	40	100
Cold Lake (Canada)	Crude	10.0	4.4	0.39	12.8	10.8	62	164

Note: Ar = Atmospheric resid.

1.2 Physical Structure and Characteristics of Heavy Oils and Residua

Heavy oils are complex, wide boiling range mixtures of hydrocarbon and non-hydrocarbon organic compounds that extend from the simplest alkane to highly complex structures with molecular weights which may be as high as thousands of g/mol. Petroleum (light and heavy oils) can be fractionated into four generic types of materials with similar chemical properties, saturates, aromatics, resins, and asphaltenes. One of the separation methods is the 1985 standard ASTM (D2007) separation procedure which is based on solubility and chromatography (Quann **et al**, 1988 and Annual Book of ASTM Standards, 1986). The four generic components are shown in Figure 1.

As described previously asphaltenes are the precipitates obtained when a petroleum or bitumen is mixed with 40 volumes of a relatively light paraffin, usually pentane. Asphaltenes are considered to contain the most complex, high molecular weight, high boiling components and to constitute a solubility class of materials which consists primarily of highly polar and aromatic species. Asphaltenes are generally soluble in benzene, pyridine, and other polar solvents.

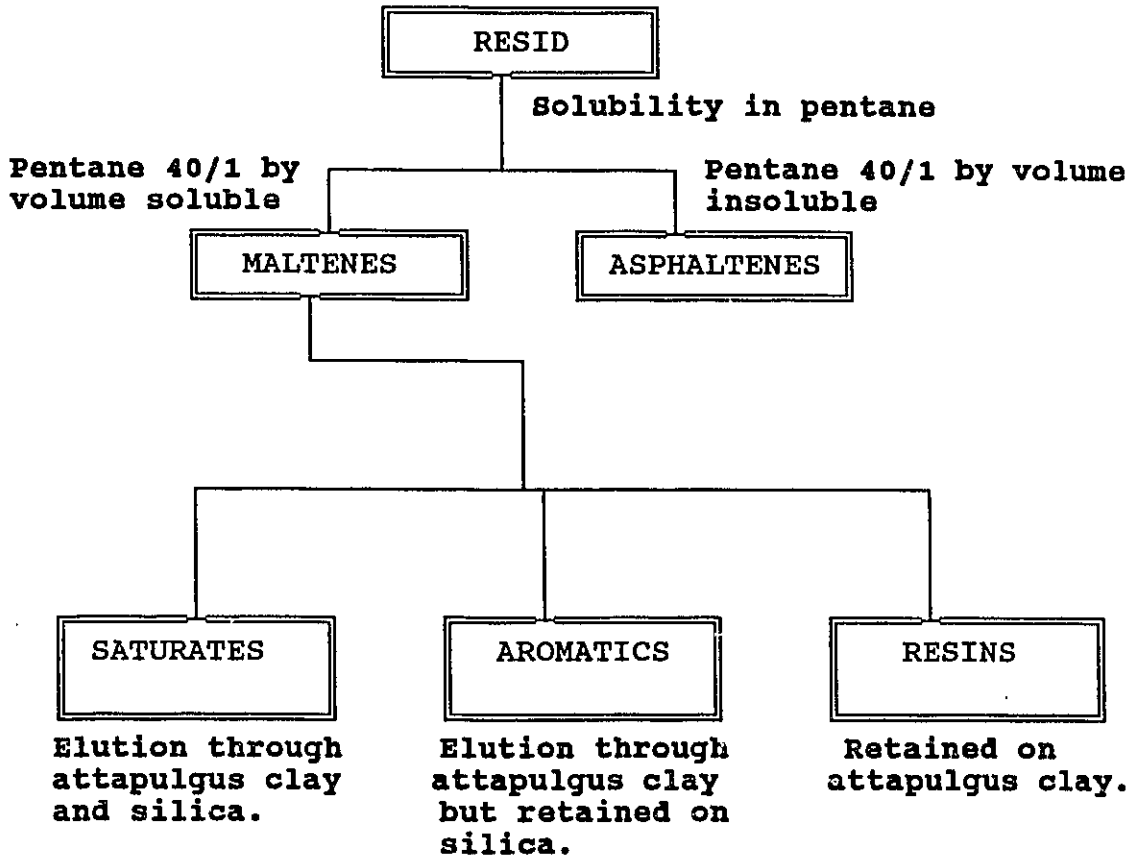

Figure 1.. The Standard ASTM (D2007) procedure for separation of asphaltenes and other generic components in petroleum.

The compounds in petroleum or bitumen which dissolve in light paraffins, such as pentane, are known as maltenes. Maltenes are separated into three subclasses using adsorption techniques. In the separation of maltenes, a column packed with layers of attapulgus clay and silica is employed. Resins are adsorbed on the attapulgus clay while the remaining solution (saturates and aromatics) are not. Further in the column the aromatics are adsorbed on the silica leaving only the saturates to flow out of the column. To obtain the resins, the upper portion of the bed in which the resins adsorbed is leached with 50/50 volume mixture of benzene and acetone. The amount of aromatics is the difference between the weight of the petroleum sample used and the sum of the weights of the asphaltenes, resins, and saturates (Quann **et al**, 1988 and Annual Book of ASTM standards, 1986). Although not an official ASTM method, Banerjee **et al** (1986) have described a technique to obtain the aromatics as a discrete fraction.

Resins are less polar, less aromatic, and of lower molecular weight than asphaltenes. Saturates and aromatics constitute the fractions of petroleum with the lowest molecular weight. Saturates have the highest H/C ratio (about 1.9) while asphaltenes have the lowest H/C ratio (about 1.2).

1.2.1 Structure and Size of Resid Molecules

The asphaltene fraction obtained by the heavy oil solubility

separation technique is the most complicated petroleum fraction in terms of molecular structure and size. This fraction contains a significant amount of the heteroatoms (S, N, and O) and metals (Ni and V).

The hypothetical structures of asphaltene molecules determined from their molecular weight, wt % elemental carbon, wt % aromatic carbon, wt % elemental hydrogen, and the types of hydrogen showed that asphaltenes are polycondensed aromatic nuclei bearing naphthenic and alkyl groups on their periphery (Speight, 1980 and Quann **et al**, 1988). The asphaltene molecular weights were determined by vapour pressure osmometry (VPO). Proton nuclear magnetic resonance (H-NMR) was used to give information about the types of hydrogen present and ^{13}C-NMR was used to determine the wt % of aromatic carbon. By using this information the probable molecular structures were formulated.

X-ray diffraction analysis of asphaltene macromolecular structure gives dimensions of the unit cell. Figure 2 shows a unit cell interlamellar distance (C/2), layer diameter (L_a), height of the unit cell (L_c), and number of lamellae (N_c) contributing to the micelle (Speight, 1980). The values of molecular weight and size of asphaltene molecules given in the literature vary with the method of determination used. Fractionation of asphaltenes by stepwise precipitation with hydrocarbon solvents (heptane to decane) separates the asphaltene by molecular weight. An X-ray diffraction method, indicated that the layer diameter was found to increase with molecular weight to a limiting value of about 1.6 nm (16 Å).

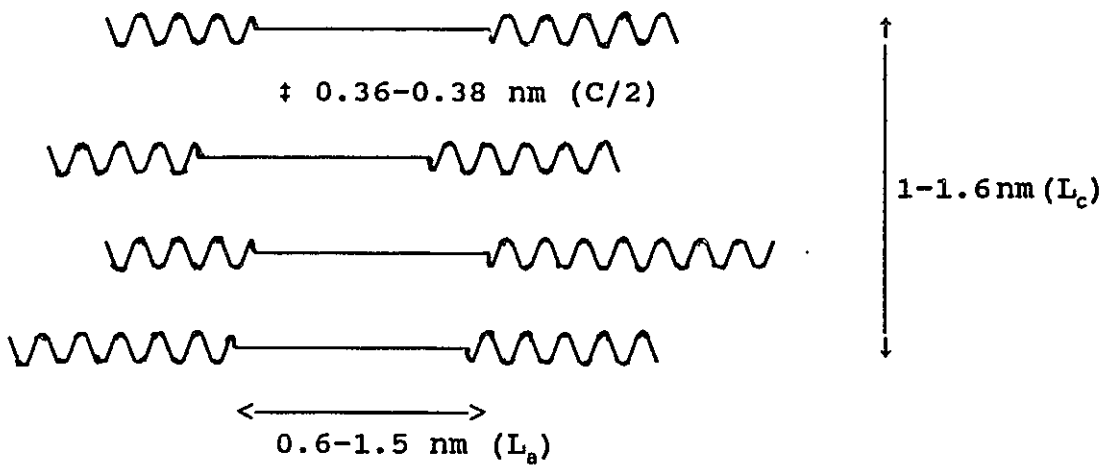

Figure 2: Schematic representation of an asphaltene cluster as deduced from X-ray diffraction patterns. The flat lines represent aromatic sheets and the attached zig-zag lines represent aliphatic chains.

1.2.2 Effect of Separation Technique on Molecular Weight and Size.

Boduszyski (1979) found that results obtained using the solubility method of separating heavy petroleum are dependent not only upon the alkane solvent used, but also upon the initial composition of the heavy oil. Separation of heavy petroleum into atmospheric equivalent boiling point (AEBP) and sequential elution fractionation (SEF) of the non-distillable fraction (Boduszyski, 1986) showed that compounds having similar molecular weights had a broad boiling point range. It was also shown that the heavy crude oils have high densities because they are rich in high-density naphthenes, aromatics, and compounds containing heteroatoms but poor in alkanes.

There are considerable variations in molecular weight values obtained by different methods; depending on the type of solvent used and the concentration of the asphaltenes in the solution. For example, ultracentrifuge studies (Quann **et al**, 1988) give molecular weights up to 300,000 whereas viscosity determinations give molecular weights of less than 2000. Determination of molecular weight by vapour pressure osmometry (VPO) has shown that the molecular weights depend on the nature of solvent and solution temperature during measurements (Kyriacou **et al**, 1988a). The higher molecular weights recorded by solubility class separation are caused by intermolecular association between asphaltene nuclei. Boduszyski (1979) suggested formation of aggregates of limited solubility because of association through hydrogen bonding.

A more suitable technique that separates resid molecules on the basis of compound class rather than solubility class has been developed. The method (Quann **et al,** 1988) can be used to separate a petroleum according to its chemical composition. Using an ion and resin chromatographic fractionation technique, the acidic and basic fractions of a residuum are isolated. The remaining fraction is separated into a neutral Lewis base fraction and a hydrocarbon (non-polar) fraction using coordination chromatography on ferric Attapulgas clay. Silica gel is then used to separate the non-polar fraction into saturate and aromatic hydrocarbons.

The polar (acid, base, and neutral Lewis base) fractions had high concentrations of heteroelements. By using IR spectroscopy, the acid fraction was found to contain mostly pyrroles with phenols and a small amount of carboxylic acids and quinolines. The base fraction had mostly pyridinic nitrogen, plus small amounts of amides and pyrroles. The neutral Lewis base fraction had mostly amide and pyrrole functional groups.

The molecular weights of the different fractions were determined by field ionization mass spectrometry (FIMS). These FIMS molecular weights of about 1000 were considerably lower than those obtained by other methods. This is evidence of intermolecular association which causes the high molecular weights obtained by other methods. The current view on asphaltenes is that they are primarily polar molecules of molecular weight 300-1000 (Quann **et al**, 1988).

Although there are other methods for separating heavy oils, the solubility method has been adopted as a standard because of its simplicity. It has the disadvantage of being dependent upon the chemical species present in each individual heavy oil and resid. Some VPO calculation methods (and other methods which require solvents to determine molecular weights) which extrapolate to infinitely dilute solutions are used to correct for molecular association. Champagne **et al**, 1985 used VPO and freezing point depression (FPD) without extrapolation to determine molecular weights of Athabasca bitumen fractions. They found that the non-distillable fraction had molecular weights ranging from 500 to 7000. They pointed out that the processes used to convert resid molecules do not use dilute solutions; therefore molecules will probably exist as aggregates.

The measured size of the asphaltene molecules, like molecular weight, is affected by intermolecular association. Molecular diameters for metal porphyrins of 1.2 to 1.5 nm have been reported (Quann **et al**, 1988), while asphaltenes isolated by precipitation from the crude oil have been reported (Quann **et al**, 1988) to have apparent average diameters of 7 to 9 nm. Other values of heavy oil molecular sizes reported were about 1.7 to 6 nm by viscosity measurements (Kyriacou **et al**, 1988a), about 4 to 14 nm by diffusion measurements (Kyriacou **et al**, 1988b), about 1.2 to 1.6 nm by X-ray diffraction (Takeuchi **et al**, 1983), a mean diameter of 6 to 20 nm by small angle neutron scattering (Ravey **et al**, 1988), and about 2 to 3 nm by high resolution electron microscopy (Quann **et al**, 1988). The large variation in the molecular size values obtained by different methods is caused by the asphaltene molecules forming micelles in solution.

1.3 Chemical Composition of Heavy Oils

Despite the fact that many studies have been performed, the chemical composition of petroleum remains largely undefined. On a molecular basis, petroleum contains hydrocarbons, organic compounds of sulphur, nitrogen, and oxygen, and sometimes a very small amount of metallic constituents.

The elemental composition (ultimate analysis) of petroleum, without considering their origin, varies only slightly over very narrow limits (Speight, 1980):

carbon	83.0 - 87.0 wt %;
hydrogen	10.0 - 14.0 wt %;
sulphur	0.05 - 6.0 wt %;
nitrogen	0.1 - 2.0 wt %;
oxygen	0.05 - 1.5 wt %.

Elemental composition is not used to classify petroleum because the ranges of the principle components carbon, and hydrogen are so narrow. On a scale of 0 to 100, the minor components sulphur, nitrogen and oxygen also have a small range. However, relative to one another they show larger variations. For example, sulphur contents of 0.05 to 6 wt % are different by two orders of magnitude. Nevertheles, the composition of the minor components is not used as a basis for classification.

1.3.1 Sulphur Compounds in Petroleum

The concentration of sulphur compounds in crude oils increases with the boiling point of the crude oil fraction.

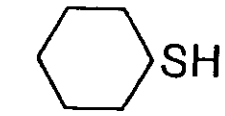

Cyclohexylthiol

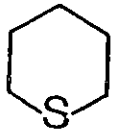

Thiacyclohexane

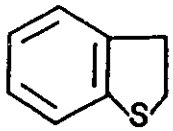

1-Thiaindan

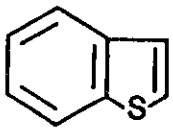

Benzothiophene

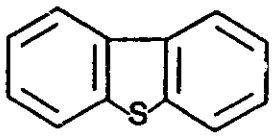

Dibenzothiophene

(a)

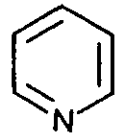

Pyridine

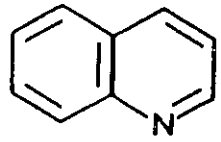

Quinoline

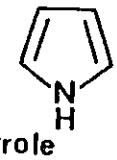

Pyrrole

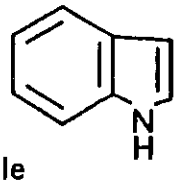

Indole

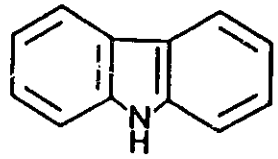

Carbazole

(b)

Figure 3: Sulphur and nitrogen compounds in petroleum. (a) Sulphur compounds and (b) nitrogen compounds

Studies (Speight, 1981) on the identification of sulphur containing constituents of crude oils have identified many of the sulphur compound types that occur in crude oils. These include different simple compounds like ethanethiol (CH_3CH_2SH) and diethyl sulphide/3-thiapentane ($CH_2CH_2SCH_2CH_3$) and polycyclic sulphides such as shown in Figure 3a (Speight, 1981). Benzothiophene and dibenzothiophene derivatives are the main sulphur compounds present in resid. The concentration of the various types of sulphur compounds varies remarkably among crude oils of different origins.

1.3.2 Nitrogen Compounds in Petroleum

There are two main nitrogen compounds in petroleum: basic and nonbasic. Figure 3b (Speight, 1981) shows types of common organic nitrogen compounds. The basic nitrogen compounds are composed mainly of pyridine homologue, while the nonbasic nitrogen compounds are usually of the pyrrole, indole and carbazole type. The basic group occurs throughout the boiling ranges of petroleum. The nonbasic group occurs in the higher boiling fractions of petroleum. The classifications of basic or nonbasic are defined by titration with perchloric acid in a 50-50 solution of glacial acetic acid and benzene. This method has indicated a ratio of 0.3 basic nitrogen to total nitrogen irrespective of the source of the crude (Speight, 1981).

Nitrogen metal complexes (porphyrins) are also constituents of petroleum and usually occur in the nonbasic portion of the nitrogen containing concentrate. The simplest porphyrin is porphine ($C_{20}H_{14}N_4$) (Figure 4a (Quann **et al**, 1988)). Porphine consists of four pyrrole molecules joined by methine (-C=) bridges. Porphyrins will be discussed later in describing metal containing compounds.

1.3.3 Oxygen Compounds in Petroleum

Most of the oxygen in petroleum compounds is contained in the high molecular weight compounds. The structure of higher molecular weight oxygen containing compounds is not well known. In lower molecular weight petroleum compounds oxygen occurs in the form of carboxylic acids and phenols.

1.3.4 Metallic Constituents of Petroleum

The two major metal constituents of petroleum are nickel and vanadium. Nickel and vanadium exist in petroleum as metal porphyrins and nonporphyrin metal complexes. These complexes may be distributed over a wide boiling range (350-650°C+) (Quann **et al**, 1988).

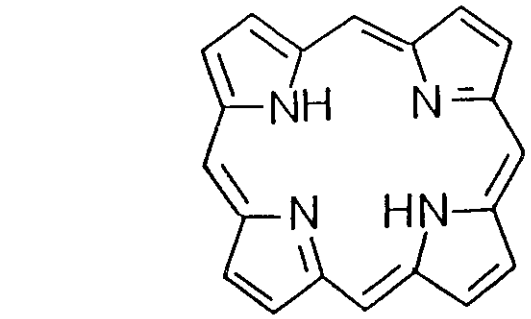

(a)

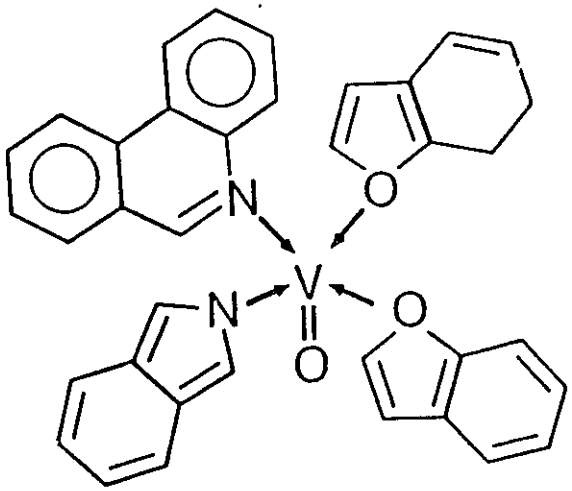

(b)

Figure 4: Porphine structure (a) and (b) Vanadium complex of tetradentate mixed ligands (example of non-porphyritic compounds)

1.3.5 Porphyrin Metal Compounds

The basic skeleton of porphyrin is porphine (Figure 4a (Quann et al, 1988)). Metalloporphyrins are formed by the chelation of metal ions into the porphyrin structures. This involves incorporation of the metal ion into the centre of the tetrapyrrole ring with the simultaneous displacement of two protons from the pyrrolic nitrogen atoms. Nickel is present in petroleum as Ni(II), and it sits in the plane of the four pyrrole rings comprising the porphyrin. Vanadium is present as V(IV), but exists in petroleum as the vanadyl VO^{2+}. The oxygen in the vanadyl group is perpendicular to the porphyrin plane and the vanadium atom lies 0.048 nm above the porphyrin plane. The amount of metal in petroleum which occurs as metal porphyrins varies according to concentration and origin of petroleum. Various crude oils have shown that the porphyrin metal content is less than 40 % of the total metal content (Quann et al, 1988).

1.3.6 Nonporphyrin Metal Compounds

Nonporphyrin metal compounds are not well characterized with respect to molecular structure. Non-porphyrinic metal complexes have been considered to be metal compounds composed of a wide variety of coordinated complexes involving inorganic forms of the metals and polar organic molecules. Nickel and vanadium non-porphyrinic compounds have been postulated (Quann et al,

1988). Figure 4b shows a vanadium complex of tetradentate mixed ligands as an example of non-porphyrinic compounds. There is no doubt about the existence of nonporphyrin metals. The presence of vanadyl compounds with molecular weights (determined by size exclusion chromatography (SEC) and high pressure liquid chromatography (HPLC)) less than that possible for vanadyl porphyrins has been established.

1.4 Hydrocracking Reactions of Heavy oil and Residua

Hydrocracking reactions involve cracking and hydrogenation reactions. The hydrocracking reactions in a catalytic system are both thermal and catalytic. Thermal reactions occur because the temperatures are high enough to permit some hydrogenation or cracking reactions, such as hydrogenolysis of larger molecules.

1.4.1 Thermal Cracking Reactions

Thermal cracking is a free radical chain reaction. The mechanism involved in thermal cracking decomposition is based on three reaction steps: (1) initiation by cleavage of a C-C bond, (2) propagation by β-scission of the primary radical giving an olefin and another radical, followed by the reaction of the other free radical with a normal molecule, and (3) termination of the chain reaction by action of two free radicals. The products of

hydrocarbon cracking are chiefly α-olefins (Blourl **et al**, 1985 and Speight, 1980).

Examples of free radical thermal cracking reactions are given below:

$CH_3(CH_2)_5CH_2CH_2(CH_2)_5CH_3$ ----> $2CH_3(CH_2)_5\dot{C}H_2$ Initiation step;

$CH_3(CH_2)_5\dot{C}H_2$ -----> $CH_3(CH_2)_3\dot{C}H_2 + CH_2{=}CH_2$ Propagation step;

$CH_3(CH_2)_3\dot{C}H_2$ -----> $CH_3CH_2\dot{C}H_2 + CH_2{=}CH_2$ Propagation step;

$CH_3(CH_2)_5\dot{C}H_2 + CH_3(CH_2)_5CH_2CH_2(CH_2)_5CH_3$ --->

$CH_3(CH_2)_5CH_3 + CH_3(CH_2)_5CH_2\dot{C}H(CH_2)_5CH_3$ Propagation step;

$2CH_3CH_2\dot{C}H_2$ -----> $CH_3(CH_2)_4CH_3$ Termination step.

1.4.2 Hydrogenation Reactions in the Absence of a Catalyst

In the absence of a catalyst, hydrogenation reactions consist of mainly saturation of free radicals. Fixari and Perchec (1989) studied hydrogenation of polyaromatics in a hydrogen-hydrogen sulphide system. They suggested that free radical hydrogenation occurs by thermal dismutation or radical H-transfer. Addition of H_2S in the system acted as a free radical initiator and promoted hydrogenation. Miki **et al** (1983) suggested that, in the absence of a catalyst, the amount of hydrogenating hydrogen transferred from the heavier fraction was 1½ times that supplied from the gaseous phase. Formation of free radicals occurs through thermal decomposition. The free radicals can be saturated by abstracting hydrogen from heavier molecules or by reacting with molecular hydrogen or a hydrogen free radical.

1.4.3 Catalytic Cracking Reactions

The cracking reaction in the presence of a catalyst is different from thermal cracking. The latter is a free radical process. The former is an ionic process involving carbocations (positively charged organic species) with the positive charge on a carbon atom:

e.g.,

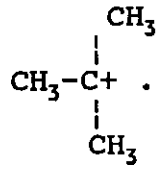

The use of a catalyst provides alternate routes for cracking reactions, that have lower activation energies. The formation of a carbenium ion (trivalent cation) can occur in either of two ways.

1. Addition of a proton (H^+) from a Brønsted acid catalyst site to an olefin:

$$R\text{-}CH{=}CH\text{-}R + H^+ \text{-------}> R\text{-}CH_2\text{-}C^+H\text{-}R.$$

2. Abstraction of a hydride ion (H^-) from a hydrocarbon by a Lewis acid catalyst site or by another carbenium ion:

$$RH + L \text{ -------}> R^+ + LH^- \quad \text{(abstraction by Lewis acid site),}$$

$$RH + R'^+ \text{ -----}> R^+ + R'H \quad \text{(Abstraction by carbenium ion).}$$

Once the carbenium ions are formed, cracking of C-C bonds proceeds with the formation of smaller carbocations adsorbed on

the catalyst and a gas phase olefin. Products of catalytic cracking depend on the carbocations formed. The cations desorb by rearranging through hydride ion shifts, methyl group shifts, or isomerization (Speight, 1980 and Wojciechowski and Corma, 1986).

1.4.4 Hydrogenation Reactions in the Presence of a Catalyst

In resid hydrocracking the presence of a hydrogenation catalyst leads primarily to the saturation of olefins and to a lesser extent the saturation of some polyaromatics. The hydrogenated compounds can be cracked. Essentially all the initial reactions of catalytic cracking occur but some of the secondary reactions are inhibited, or stopped, by hydrogenation. For example, alkenes are saturated while branched chain paraffins undergo demethanation. Naphthenic hydrocarbons undergo ring scission followed by immediate saturation of each fragment produced. On the other hand, aromatic hydrocarbons are more resistant to hydrogenation. Under severe conditions, aromatics are converted to naphthenic rings followed by scission of the alkyl side chains. Polynuclear aromatics are more readily attacked than the single-ring aromatic compounds. The reactions occur in a stepwise process in which one ring at a time is saturated and opened (Speight, 1980). Miki et al (1983) found that, in presence of a catalyst, hydrogen consumption from the gas phase was higher than hydrogen abstracted from the heavy oil fraction. Therefore carbonization of the heavy oil fraction was prevented.

1.5 Hydrocracking Catalysts for Heavy Oils and Residua

1.5.1 Historical Background

The development of hydrocracking catalysts began when high pressure coal hydrogenation was investigated. Donath (1983) has provided an historical account of this subject. In 1869 Berthelot reported the first catalytic coal liquefaction experiment. Further experiments done by Dafert and Niklausz in 1911 showed that bituminous coal could be converted to semiliquid material with a 60 % oil content. Not much was achieved before 1924, when extensive research on hydrogenation catalysts started.

In 1924, experiments in Ludwigshafen (Germany) led to the discovery of modern coal liquefaction catalysts. In the same year it was realized that sulphides and oxides of molybdenum, tungsten, and cobalt were active hydrogenation catalysts at 200 bar hydrogen pressure. By 1926, tests on most of the elements of the periodic table showed that molybdenum and tungsten had the best hydrogenation activity.

International cooperation in the development of hydrocracking (or hydrotreating) catalysts started between the years 1929 and 1931. It involved European Countries and the USA. By the year 1943, twelve commercial plants hydrogenating bituminous coal and tar oils had been built.

Many catalysts (about 5000 by 1930 and 8400 by 1940) were tested for their hydrodesulphurization (HDS) and hydrodeni-

trogenation (HDN) properties. In 1940 the first catalysts for hydrotreating coal oil were prepared from MoO_3 and NiO or from WS_2 and NiS supported on alumina.

1.5.2 Composition of Resid Hydrocracking Catalysts

Despite the fact that other support materials (e.g. carbon) rather than alumina have been tried, alumina is still the conventional support material used. Since the 1970s, research has intensified on the study of the structure of catalysts containing molybdenum and cobalt/nickel supported on alumina. Catalysts prepared in different ways with varying concentration of MoO_3 and CoO/NiO on alumina support were investigated (Ripperger and Saum, 1977; Topsøe and Clausen, 1984; Chianelli, 1984; Knözinger, 1988; and Prins **et al**, 1989). The following sections describe the solid state catalyst components which have been suggested in these studies.

1.5.3 Alumina Support

Alumina is used as a support (carrier) because of its favourable physical and chemical properties. On calcination, alpha alumina monohydrate is transformed to a thermally and mechanically stable gamma alumina. Gamma alumina has a large surface area which is important for the dispersion of the active species (molybdenum and cobalt/nickel).

1.5.4 Molybdenum and its Role in Catalysts

Most resid hydrocracking catalysts contain molybdenum supported on alumina. Formation of MoS_2 is achieved by sulphiding the calcined catalysts by a mixture of H_2S and H_2, CS_2 and H_2, thiophene and H_2, or a feedstock containing high sulphur content and H_2. Studies (Ripperger and Saum, 1977; Topsøe and Clausen, 1984; Chianelli, 1984; Knözinger, 1988; and Prins **et al**, 1989) on sulphided Mo-Al_2O_3 catalysts have agreed that MoS_2 is formed and that it constitutes the active HDS phase of the catalysts.

1.5.5 Cobalt and Nickel Promoters

The addition of a small amount of Co or Ni in molybdenum-alumina catalysts has been found (Ripperger and Saum, 1977; Topsøe and Clausen, 1984; Chianelli, 1984; Knözinger, 1988; and Prins **et al**, 1989) to promote HDN and HDS. When catalysts containing Co or Ni are sulphided, an active phase referred to as the Co-Mo-S or Ni-Mo-S phase is formed on the surface of the catalyst support (γ-Al_2O_3). Topsøe and Clausen (1984) found that increasing the amount of Co in the Co-Mo-S phase increased the catalyst's activity. The amount of molybdenum in the catalyst dictates the amount of cobalt required. Studies (Ripperger and Saum, 1977; Topsøe and Clausen, 1984; Chianelli, 1984; Knözinger, 1988; and Prins **et al**, 1989) found that increasing the amount of cobalt in catalysts can also lead to the formation of a cobalt

sulphide crystalline phase (Co_9S_8). The Co_9S_8 phase does not promote HDS activity of catalysts.

1.5.6 Other Catalyst Additives (Components)

Effect of Alkali and Alkaline Earth Metals

The effect of alkali metals (lithium, sodium, and potassium) and alkaline earth metals (calcium and magnesium) on Co-Mo-Al_2O_3 or Mo-Al_2O_3 catalysts have been studied (Kelly and Ternan, 1979; Ternan and Kriz, 1980; and Papaioannou and Haynes,Jr., 1989). Addition of these metals to the catalyst was aimed at reducing catalyst coking. The results had shown that, although initial coke deposition decreased, longer term coke deactivation (deposition) remained almost the same. Other workers (Papaioannou and Haynes, Jr., 1989) showed that the addition of calcium and magnesium in Co-Mo-Al_2O_3 decreased the catalyst's acidity, specific surface area, and HDN activity.

Effect of Phosphorous

Studies on the effect of phosphorous on Co-Mo-Al_2O_3 or Ni-Mo-Al_2O_3 have been reported (Fitz, Jr. and Rase, 1983; Atanasova **et al**, 1988; and Kang **et al**, 1988). The results obtained had shown that a small concentration (less than 2 wt %) of P_2O_5 in the

catalyst improved HDS, HDN, hydrodemetallization (HDM), and MCR removal. It was suggested that the function of phosphorous was to prevent formation of aluminates of nickel or cobalt. Phosphorous was also found to increase the mechanical strength and heat stability of the catalysts (Fitz, Jr. and Rase, 1983).

Effect of Fluoride Ion

The addition of fluoride ion to Co-Mo/Al_2O_3 hydrocracking catalysts has been found to promote HDS and HDN of bitumen (Boorman **et al**, 1984). Hydrocracking experiments performed at 13.9 MPa pressure and at temperatures between 400-450°C showed that HDS and HDN were enhanced when fluoride ion was impregnated after the catalysts containing molybdenum and cobalt had been calcined. More studies (Matralis **et al**, 1988 and Miciukiewicz **et al**, 1989) were done on HDS of thiophene with F-Co-Mo/Al_2O_3 and F-Mo/Al_2O_3 at atmospheric pressure and temperatures of 250-350°C. Matralis **et al** (1988) found increased thiophene HDS with F-Co-Mo/Al_2O_3 catalysts containing less than 0.8 wt % fluoride. Thiophene HDS decreased when catalysts contained between 0.8-2.0 wt % fluoride. Miciukiewicz **et al** (1989) found that there was a decrease in thiophene HDS as the fluoride ion content was increased in the F-Mo/Al_2O_3 catalysts. It was suggested that addition of a small amount of fluoride ion enhanced the dispersion of cobalt and molybdenum on the support. The increased dispersion was probably caused by a change in the surface properties of the support.

1.5.7 Use of Zeolite in Catalysts

Zeolites are porous crystalline aluminosilicates. The zeolite framework consists of an assemblage of SiO_4 and AlO_4 tetrahedra with oxygen being shared between two tetrahedral Al or Si atoms. The tetrahedral units are joined together in various regular arrangements through shared oxygen atoms, to form an open crystal lattice containing micro pores of about 0.3 to 1 nm. The micropore structure is determined by the crystal lattice, hence, it is precisely uniform with no distribution of pore size.

Studies (Meier and Olson, 1987) indicated that 64 different zeolite framework structures had been identified, including both natural and synthetic forms. The structural formula of a crystallographic unit cell of a zeolite is as follows (Bolton, 1976):

$$M_{x/n}\,[(AlO_2)_x.(SiO_2)_y].\ mH_2O.$$

Where M is a cation of valence n, m is the number of water molecules, and the sum of x and y is the total number of tetrahedra in a unit cell. Each aluminium atom introduces one negative charge on the framework which must be balanced by an exchangeable cation.

The silica aluminium ratio (Si/Al) in zeolite is never less than 1.0 and can be infinity. For example, pure silica structures have been synthesized. Aluminium rich zeolites have very high affinities for water and other polar molecules, while

silica rich zeolites are essentially hydrophobic, i.e., adsorb n-paraffins in preference to water. The transition from hydrophillic to hydrophobic occurs at a Si/Al ratio of 8 to 10 (Rabo, 1976; Meier and Olson, 1987 and Ruthven, 1984).

Reviews (Barthomeuf, 1983 and Wojciechowski and Corma, 1986) on zeolites have documented that, by replacing the exchangeable cations (e.g. sodium ion) in zeolites by ammonium ion and calcining at high temperature, Brønsted acid sites can be created. Several improvements were obtained by using zeolites in FCC catalysts. These are listed below.

1. Conversion: The more active a catalyst, the lower is the temperature required for a given conversion and the longer it can be used before regeneration. Increased conversion will allow processing of more severe feedstocks or at increased space velocity (Jacobs, 1977).

2. Slow deactivation rate: Because of higher activity, cracking reactions occur at relatively low temperature. Operation at lower temperatures decreases the deactivation rate of the catalysts (Jacobs, 1977).

3. Resistance to ammonia poisoning: Feedstocks containing nitrogen form ammonia and decrease the cracking activity of the catalyst. However, zeolite catalysts can operate in the presence of substantial concentrations of ammonia. Silica-alumina catalysts are strongly poisoned by ammonia. The greater ability of the zeolites to tolerate either basic nitrogen compounds or ammonia has been attributed to their greater acidity. A study

(Rabo, 1976) to find the effect of ammonia on the cracking activity of catalysts suggested that the cracking activity of a catalyst was controlled by both the quantity of zeolite (or number of acid site) in the catalyst and the nitrogen content of the feed.

1.5.8 Effect of Zeolite in Hydrocracking Catalysts

Although zeolites have been used in FCC catalysts since 1962 (Venuto and Habib, 1979; Wojciechowski and Corma, 1986 and Shaheen, 1980), their application in resid hydrocracking catalysts is still in the preliminary stages. The few studies of catalysts with zeolite used for hydrocracking resid are described in this section.

Radchenko et al (1983) studied the stability of the crystal lattice in 5-30 wt % Ni-Y zeolite contained in nickel-molybdenum-alumina hydrocracking catalysts. The catalysts were used for 320 h at 360-500°C, hydrocracking a vacuum residuum with an initial sulphur content of 1.5 wt %.

The presence of Brønsted acid centres in the Ni-Y containing catalysts was determined by pyridine adsorption. The number of Brønsted acid sites was found to increase with increasing zeolite content of the catalysts. The catalyst with 20 wt % Ni-Y zeolite was tested for acidity after 320 h of use, and it was found that coke deposits blocked the strong Brønsted acid centres. Regeneration of the catalysts in air at 400°C restored the Brønsted acid centres of the catalysts.

Sidel'kovskaya **et al** (1988) studied the effect of 5 wt % HY zeolite in Ni-Mo-/alumina catalysts. Catalysts were analyzed by diffuse reflection electron spectroscopy (DRES), thermogravimetry, X-ray photoelectron spectroscopy (XPS), and Raman spectroscopy. The results showed that the presence of HY zeolite caused the nickel interaction with the alumina to decrease. A more active and dispersed nickel-molybdenum surface phase was formed.

HDS and HDN of heavy gas oil has been reported (Sambi and Mann, 1989) using rare exchanged Y (REY) zeolite in Ni-Mo-Silica-alumina catalysts. Catalysts with various amounts of REY zeolite were tested. A catalyst containing 25 wt % REY zeolite was found to be the optimum. Krichko **et al** (1984) studied the HDS, HDN, and hydrodeoxygenation (HDO) of coal liquefaction products using zeolitic catalysts. Catalysts prepared by co-impregnation of HY zeolite with molybdenum and nickel solutions and then supported on alumina were found preferable.

A physical mixture (1:1 by weight) of a commercial catalyst, $NiO-MoO_3/Al_2O_3$ (BASF M8-21), and Ru/HY (MS-83) catalyst had a better quinoline HDN than either of the two catalysts alone (Harvey and Pratt, 1985). Pelleted catalysts were prepared from physical mixtures containing 0-100 wt % of Y-zeolite and then were evaluated for HDN of shale oil. The best HDN was obtained with the 1:1 physical mixture. Continuous processing tests with shale oil at 13.8 MPa pressure and 450°C over BASF M8-21 and MS-83 were also performed. The liquid product from the BASF M8-21

commercial catalyst was found to be waxy, yellow-coloured and solid at room temperature. The liquid product from the MS-83 catalyst was clear and had high volatility.

Ni/W/H-Y catalysts are known to have a higher gasoline selectivity than Ni/W/SiO.Al_2O_3 catalysts (Maxwell, 1987). The selectivity of zeolites is useful for maximizing a preferred product.

These few studies show that zeolites can be used to improve resid hydrocracking catalysts. The addition of zeolite to resid hydrocracking catalysts increases their Brønsted acidity.

1.5.9 Zeolites Used in This Study

A. Mordenite

The framework structure of mordenite consists of chains of tetrahedra cross-linked by the sharing of oxygen atoms (Meier and Oslon, 1987 and Bolton, 1976). In mordenite each tetrahedra belongs to one or more five membered rings in the framework. The Si/Al ratio is about 5.0. The aluminium content of the framework may be decreased by acid leaching without loss of crystallinity (Bolton, 1976). The channel structure of mordenite is unidimensional. The main channel, which is formed from twelve-membered oxygen rings, has a free diameter of 0.67-0.70 nm. The structural formula of a crystallographic unit of a Na-mordenite is as follows:

$Na_8[Al_8Si_{40}O_{96}] \cdot 24H_2O$.

To obtain H-mordenite zeolite, the sodium cation in Na-mordenite is exchanged with ammonium (NH_4^+) cation. Then it is calcined to decompose the ammonium ion into ammonia gas, which vaporizes, and a proton which stays in the solid. H-mordenite zeolite was the type used in this study.

B. Zeolite Y

The framework structure of type Y zeolite is the same as the framework structure of the mineral faujasite. The unit cells are cubic containing 192 total SiO_4 and AlO_4 tetrahedra (Meier and Olson, 1987; Ruthven, 1984 and Bolton, 1977). The framework is made of a tetrahedral arrangement of double six-ring units. The three dimensional channel structure is composed of twelve-membered oxygen rings which are connected by openings of about 0.74 nm. Large molecules such as neopentane and tertiary butyl amine can penetrate these pores (Ruthven, 1984). The Si/Al ratio of Y type zeolite is within the range 1.5-3.0. In natural zeolite Y, the charge balancing cation present in the alumino-silicate framework is sodium, calcium, or magnesium. In synthetic zeolite Y the charge balancing cation is generally an alkali metal ion, most frequently sodium. The presence of an alkali metal ion in zeolites results in poor activity of the zeolites as catalysts. Thus, sodium Y (Na-Y) zeolite is cation exchanged by other ions such as ammonium and calcined to form a

hydrogen zeolite, in order to improve its activity as a catalyst. The Y zeolite used in this study was a cation exchanged H-Y zeolite.

1.5.10 Catalyst Particle Size

The size of catalyst particles used in resid hydrocracking affects the conversion. Small catalyst particles have larger external surface areas, and a shorter diffusion path. This increases the effectiveness of the catalyst. In resid HDS, sulphur removal has been shown to increase with decreasing catalyst particle size (Green and Broderick, 1981). It has been shown (Quann **et al,** 1988 and Green and Broderick, 1981) that the concentrations of the metals deposit is greatest on the outer surface of the catalysts and decreases towards the centre. In extreme cases, sufficient metals can deposit in the pores near the external catalyst surface to cause pore mouth plugging. This will make the inner surface area in catalyst particles inaccessible. Though smaller particles are more effective, reactor hydrodynamics (pressure drop in fixed beds, catalyst separation from the liquid product in fluidized beds) are impractical for catalysts with particle sizes less than 0.8 mm (1/32 in) (Quann **et al**, 1988).

1.5.11 Pore Diffusion

In hydrocracking resid using porous catalysts, the larger asphaltene molecules must diffuse through the catalyst pores to the reaction sites within the catalyst particles. Pores in catalysts are classified in three categories (Gregg and Sing, 1982) according to their width (diameter) using the International Union of Pure and Applied Chemistry (IUPAC) classification. The three classes are: micropores with pore width less than 2 nm, mesopores with pore width between 2 and 50 nm, and macropores with pore width greater than 50 nm. Resid asphaltene molecules are too large (section 1.2) to diffuse through the micropores. Measurement of effective diffusivity of resid molecules in catalyst pores is difficult because of their complex composition and wide size range. Some of the few correlations which have been used or developed to determine liquid pore diffusion are discussed here.

Thrash and Pildes (1981) measured asphaltene diffusion coefficients through Track-etched membranes. The asphaltenes were obtained from a vacuum residuum by hexane Soxhlet extraction followed by chromatographic separation. Using very dilute solutions of asphaltenes in toluene (10^{-5} g/cm^3), diffusion coefficients through membranes having pores of about 100 nm were determined. By using Fick's first law and the rate of mass transfer given by Equation 1 the value of D was determined. Equation 1 is as follows:

$$J = \frac{DA\Delta c}{L}, \quad (1)$$

where J is diffusivity flux, D is the measured diffusion coefficient, A is the total pore area, Δc is the concentration difference across the membrane, and L is the length of the pore. Using the value of D which they obtained (4.5×10^{-6} cm^2/s) the hydrodynamic radius, r_m, of the diffusing asphaltene molecules was calculated using the Stokes-Einstein relation:

$$D = \frac{kT}{6\Pi\eta r_m}, \quad (2)$$

Where k is the Boltzmann's constant, T is the absolute temperature, η is the solvent viscosity, and r_m is the molecular radius. Their overall finding was that molecular association with increasing solution concentration decreased the diffusion coefficient. It was suggested that free diffusion in pores occurs when the ratio of molecular radius to pore radius (r_m/r_p) is less than 0.1. The diameter of the asphaltenes obtained using equation 2 was 1.6 nm. Other calculations (Baltus and Anderson, 1983) based on diffusion had obtained asphaltene diameters ranging from 4 to 30 nm.

Using the membrane pore diameter, the ratio of r_m/r_p in this case was about 0.02. Considering the size of asphaltene molecules obtained in this case, it was suggested that, for molecules to diffuse freely in catalyst pores, their pore

diameters must be greater than 20 nm. It should also be born in mind that the size of asphaltenes varies according to the solvent used (Kyriacou **et al**, 1988b). The extent of asphaltene association during the actual hydrocracking process may be quite different from their association at the conditions used for the experiments which were performed to determine their molecular sizes.

Although it is difficult to measure the effective diffusivities of molecules in catalyst pores, a correlation between bulk diffusion and pore diffusion in terms of molecular size and pore size is vital. Ternan (1987) developed an empirical equation requiring one parameter, which correlates effective diffusivity of a solute molecule in a pore (D_{eff}) with diffusivity of a solute molecule in a bulk phase solution (D_B). The equation is as follows:

$$\frac{D_{eff}}{D_B} = \frac{(1-\lambda)^2}{(1+P\lambda)}, \qquad (3)$$

where $\lambda=r_m/r_p$, r_m is the radius of the solute resid molecule, r_p is the radius of the pore, and P is a constant parameter. The equation was found to fit experimental data quite well. Data by Baltus and Anderson (1983) for Kuwait petroleum asphaltene fractions diffusing through pores of uniform size showed a best fit when the value of the P was 2.017. Equation 3 was considered more useful than earlier existing empirical equations

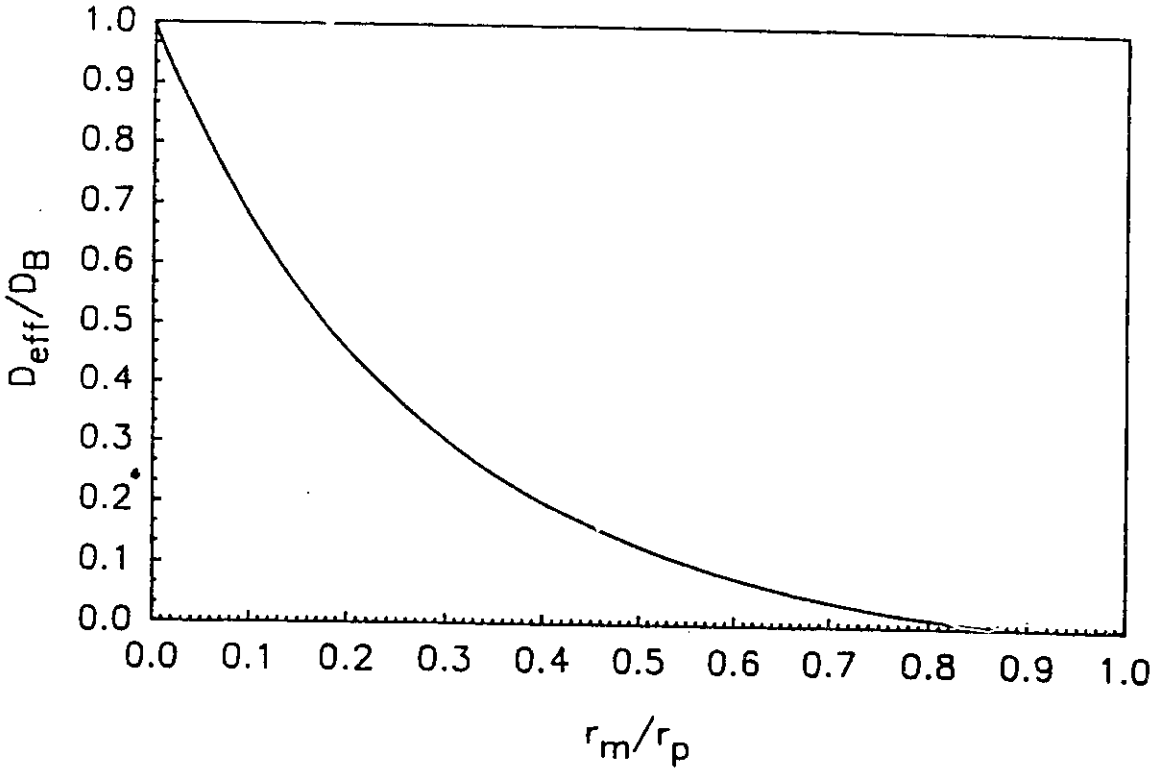

Figure 5: Correlation between the ratio of effective diffusivity of a petroleum molecule in a pore to the bulk diffusivity of the same molecule in the bulk (D_{eff}/D_B) and the ratio of the molecule size to the pore size (r_m/r_p), assuming a P value of 2.

because it required only one parameter and it accurately predicted D_{eff} at both physical limits. In a real system, for smaller pores, when $r_p \rightarrow r_m$ ($\lambda \rightarrow 1$) then $D_{eff} \rightarrow 0$ and for very large pores ($r_p > r_m$) $\lambda \rightarrow 0$ and $D_{eff} \rightarrow D_B$. The equation satisfies these conditions.

Equation 3 can be used easily to estimate the ratio of effective diffusivities in catalyst pores. For example, if the P value of 2 for asphaltenes is used (Ternan, 1987) Figure 5 can be plotted. When there is a change in the resid hydrocracking catalyst pore size, the diffusional effect of that change can be predicted from Figure 5. In other words, if the size of the resid molecule, r_m, is known from section 1.2, then Figure 5 can be used to choose the size of the catalyst pores, r_p, to give whatever value of D_{eff}/D_B that is desired.

1.5.12 Catalyst Pore Size and Surface Area

While increasing the pore size of a catalyst is desirable for diffusion, in unimodal catalysts it has a consequent effect of decreasing catalyst specific surface area. Ternan (1983) studied catalytic hydrocracking of Athabasca bitumen on catalysts with different median pore diameters. The results showed that there was an increase in sulphur and asphaltene conversion per unit area per unit time with increasing catalyst pore diameter. On the other hand overall sulphur and asphaltene conversion decreased with increasing pore diameter. This was because the

decrease in the total surface area had a greater influence than the increase in diffusion rate.

The pore sizes of unimodal catalysts can be increased by sintering, i.e., fusion of small particles to form larger particles, and therefore larger pore spaces between the particles. Enlarging catalyst pores through sintering causes a lower catalyst specific surface area. In hydrotreating coal derived oils, more efficient sulphur removal was found (Gravin, 1984) over a catalyst with pore diameter of 6.6 nm than over a catalyst with pore diameter of 9 nm. When sintering was used to incorporate macropores (>200 nm), the Ni-Mo-Al_2O_3 catalyst only appeared to be more active if the comparison was made on a unit catalyst surface area basis. Hardin **et al** (1978) studied hydroprocessing of oil sands bitumen with unimodal catalysts with pore diameter changing from 7.5 to 1000 nm. The results showed constant HDS, HDN, and HDM conversions with catalysts having pores between 7.5 to 50 nm. The beneficial increase in mass transfer rates did not produce greater conversions because of the accompanying decrease in the catalyst surface area.

Studies on bimodal catalysts (Suzuki and Onuma, 1984) have shown that the catalyst performance can be improved if both smaller and larger pores are present. The larger pores provide more volume for mass transfer and metal deposition without pore mouth plugging, while smaller pores provide more surface area on which the reactions can occur. Suzuki and Onuma (1984) found that bimodal catalysts had greater metal tolerance than smaller

pore unimodal catalysts and had more catalytic activity than a larger pore unimodal catalyst. The bimodal catalysts were found to maintain a good catalytic activity even after 1400 h of use.

1.6 Catalyst Characterization Techniques

The nature of the solid catalysts and the number of the particular types of sites govern the rate of reaction. Methods have been developed to determine the structure of the catalysts surface (morphology) and the number of sites.

1.6.1 Correlation between Catalyst Solid Structure and Catalytic Activity

Parham and Merrill (1984) studied the oxides and sulphides of commercial Co-Mo/Al_2O_3 with Extended X-ray Absorption Fine Structure (EXAFS). EXAFS is a technique which is used to obtain structural information of solids. It is used to measure the coordination number of elements and bond lengths between elements of a solid structure. The information obtained is used to deduce the type of chemical species which are present in the structure and the manner in which they are coordinated. Catalysts were sulphided at temperatures from 25-600°C. The spectra of the oxides and sulphides along with some model compounds were measured. The results showed that no MoS_2 was formed when the

sulphiding temperature was below 200°C. Above 200°C crystals of MoS_2 were formed. The MoS_2 crystalline sizes were observed to increase with sulphiding temperature.

The correlation between thiophene HDS and structural parameters determined by EXAFS have been studied (Boudart **et al**, 1983) over Co-Mo/Al_2O_3 catalysts. Thiophene HDS experiments were carried at 300°C and atmospheric pressure. The results showed that HDS activity increases with the Co/(Co + Mo) atomic ratio to 0.33. Catalysts with Co/(Co + Mo) atomic ratios greater than 0.33 had diminished HDS activity. The correlation between the number of sulphur first neighbours of molybdenum determined by EXAFS and the Co/(Co + Mo) atomic ratio had a similar trend.

Another technique which has been used to correlate the HDS activity to the chemical species present in the catalysts is *in situ* Mössbauer Emission Spectroscopy (MES). Wivel **et al** (1981) showed that there is a direct relationship between the HDS activity and the presence of a Co-Mo-S surface phase in the catalysts. Catalysts were prepared with various proportions of Co but a constant concentration of Mo on the alumina support. The thiophene HDS activity of the catalysts was determined at 350°C and at atmospheric pressure. Three forms of cobalt existing in the Co-Mo/Al_2O_3 sulphided catalysts were cobalt located in the alumina, cobalt in Co_9S_8, and cobalt located in a Co-Mo-S surface phase. These results distinguished between the amount of the cobalt in the catalyst and the amount which forms the Co-Mo-S phase. A correlation between the amount of cobalt in

the catalyst and the catalyst thiophene activity showed a maximum in catalytic activity with catalysts containing Co/(Co + Mo) atomic ratio of 0.5 (i.e., Co/Mo = 1.0). At low concentrations of cobalt (Co/Mo < 0.4) no Co_9S_8 was formed. There was a linear increase in the amount of cobalt in the Co-Mo-S phase between 0 < Co/Mo ≤ 0.4. Above Co/Mo = 0.5, Co_9S_8 was observed with a sharp decrease of cobalt in the Co-Mo-S surface phase. A plot of the thiophene activity parameter versus the $Co_{Co\text{-}Mo\text{-}S}/Mo_{Total}$ ratio showed a linear correlation up to a $Co_{Co\text{-}Mo\text{-}S}/Mo_{Total}$ ratio of 0.5. Catalysts with Co/Mo ≤ 1.0 were found to have the Co-Mo-S phase as the most abundant phase.

Boorman **et al** (1984) used X-ray Photoelectron Spectroscopy (XPS) to study the binding energy of molybdenum in catalysts used in hydrocracking bitumen. The effect of the impregnation sequence on the molybdenum species on the surface was examined. Catalysts impregnated with fluoride ions or sodium ions after having been impregnated with Mo and Co first had a higher ratio of Mo-O bonding to Mo-S bonding than catalysts in which fluoride ions or sodium ions were impregnated first. A greater ratio of Mo-O bonding to Mo-S bonding suggests a greater dispersion of molybdenum on the Al_2O_3 support. A greater dispersion of cobalt and molybdenum would explain the increased HDS activity of the catalysts that was observed.

1.6.2 Correlation of Sites and Activity of Catalysts

The number of sites available for adsorption of certain probe molecules is often thought to measure the dispersion of the chemically active species (reaction sites) on the catalysts. Adsorption of molecules such as NH_3, CO, CO_2, NO, O_2 and others have been used to study the concentration of sites in catalysts.

Laine et al (1984) studied acid strength distribution on catalysts by ammonia adsorption. The ammonia adsorption isotherms at 200°C of MoAlSi and NiMoAl catalysts were measured. The results indicated that the total acidity (Lewis and Brønsted) of the catalysts was higher in MoAlSi catalysts than in NiMoAl catalysts. MoAlSi catalyst also had stronger acid sites than the NiMoAl catalyst.

Moon and Ihm (1988) found a correlation between the amount of NO chemisorbed in Co/C, Mo/C, Co/Al_2O_3, and Mo/Al_2O_3 catalysts and their thiophene HDS activities. Chemisorption and Temperature Programmed Desorption (TPD) of NO and O_2 probe molecules were used to correlate adsorption sites with thiophene HDS catalytic activity. Oxygen was found to occupy only a fraction of the sites occupied by NO. Thiophene HDS activities of the catalysts were found to correspond to NO adsorption.

Several studies have correlated oxygen chemisorption and catalyst HDS, HDN and hydrogenation activities. Burch and Collins (1985) found no correlation between oxygen chemisorption and HDS activities of commercially available HDS catalysts.

Brunet et al (1988) studied the correlation between nickel loading and oxygen chemisorption on HDN catalysts. Oxygen chemisorption was found to correlate well with nickel loading and its interaction in Ni-Mo/alumina catalysts. On the other hand the catalysts without the nickel promoter were found to chemisorb more oxygen than the nickel promoted catalysts. Thus, correlating oxygen chemisorbed with HDN activity was not successful. Another study by Nag et al (1988) found that both thiophene HDS and cyclohexene hydrogenation (HYD) could be correlated with the amount of oxygen chemisorbed in the catalysts. Lower temperature chemisorption of oxygen on W/alumina catalysts showed increased oxygen adsorption with increasing metal (W) loading. The thiophene HDS and cyclohexene HYD activities of the catalysts were found to increase with the catalyst metal loading.

1.7 Catalyst Deactivation in Resid Hydrocracking

In hydrocracking processes bulk coke is not formed because cracked products are hydrogenated before they condense. At higher temperatures the rate of hydrogenation may be lower than the rate at which the cracked products are formed. If such a situation occurs some cracked products may condense and form coke on the surface of the catalysts. The rate of hydrogenation can be increased by increasing hydrogen partial pressure. On the other hand, the equipment used has a pressure limit beyond which operation is not safe. Coke deposits cover the active sites of

the catalysts and hence lower their catalytic activities. Several studies which describe the phenomena of catalyst deactivation, including coke formation, are discussed.

A study on resid hydrocracking (Kriz and Ternan, 1984) showed that coking tendency is a function of feedstock properties and operating conditions. The coking tendency of Boscan heavy oil was found to increase with increasing temperature and decreasing hydrogen pressure. Although coking differed from catalyst to catalyst, it was shown that the trend at high severity (high temperature-low pressure) was the same. Coking tendency during hydrocracking without a catalyst was similar.

Nita **et al** (1987) studied deactivation of zeolitic catalysts used in resid hydrocracking. The catalyst they studied had molybdenum on an FeHY zeolite-alumina support, promoted with cobalt. The catalyst was tested for a period of 1500 h. During the first 400 h the operating temperature was raised from 380 to 410°C and maintained at 410°C for the rest of the time. The results showed that HDS activity increased with increasing temperature and decreased slowly with time at constant temperature. The hydrocracking activity (conversion of +343°C) was found to behave differently. It increased rapidly with increasing reaction temperature and continued to increase slowly at constant temperature to about 1000 h. The hydrocracking activity remained constant from 1000 to 1500 h. They explained the increase in +343°C conversion by the carbonization and coalescence of the carbonaceous deposit on the catalyst. It was suggested that the

acid sites on the catalyst, which had been covered by carbon in the initial period, become exposed and available for reaction when coalescence of the carbonaceous deposit occur.

Initially, the rate of coke deposition was high, but it decreased as the time on stream increased. The amount of carbon deposited was found to increase steadily during the first 45 h and very slowly during the remaining period. The position of the catalyst in the reactor bed did not affect the amount of carbon deposited. It was also found that the amount of metals deposited in the catalyst increased steadily with time on stream. More metals were deposited at the top of reactor (inlet position) while the least deposition occurred at the bottom of the reactor.

The effect of HDS catalyst chemical composition on the amount of coke has been reported (Ternan **et al**, 1979). In this study, it was found that increasing MoO_3 in a molybdenum-alumina catalyst decreased coke deposition. An increase of MoO_3 in the catalyst content (0 to 6 wt %) caused a significant decrease in catalyst coking. Further increase of MoO_3 in the catalyst caused a slight additional decrease in coke deposition. When different promoters (e.g. Ni, Co, Fe and Cu) were added to a catalyst with 2.2 wt % MoO_3, the catalyst coke content was not affected. While coke content decreased with increasing MoO_3, HDS activity increased with MoO_3. It was also shown that both the HDS activity of the catalyst and amount of coke content increased with reaction temperature. The amount of coke formed

was found to be a function of the feedstock used. A greater amount of coke was formed from hydrocracking bitumen than that produced from hydrocracking gas oil.

There are two ways in which coke can be formed: deposition from the vapour phase to form pyrolytic carbon, or solidification from the liquid or plastic state to form coke. In resid hydrocracking, coke is probably formed by the latter route. Brooks and Taylor (1968) worked with coal derived materials and observed the formation of a mosaic structure which, in its final stage, forms a mesophase (intermediate phase). The process involves formation of microspheres which coalesce into large spheres as the temperature is increased. The spheres can solidify from their liquid or plastic phase and initially form a fine mosaic structure. Alternatively, the spheres can grow further and coalesce further to form laminar or flow structures until no more plastic-like material remains. In the final stage, the mesophase solidifies into a semicoke. It is important to avoid mesophase formation in resid hydrocracking since it can lead to the development of large coke particles which can cause reactor plugging.

Nandi **et al** (1975) investigated the removal of coke-forming compounds in resid and observed the same phenomenon reported by Brooks and Taylor for coal derived materials. In this study bitumen or a mixture of bitumen and pulverized semi-anthracite coal was thermally hydrocracked. The coke formed when bitumen was thermally hydrocracked (in the absence of coal) at 450°C had

structures which were similar to those described by Brooks and Taylor (1968). In the initial stages spheroidal microstructures were observed. In a later stage the microspheres grew to form laminar structures.

Nandi **et al** (1978) found that two different structural cokes were formed when hydrocracking Athabasca bitumen. In this study bitumen was deasphalted by precipitating asphaltenes in a mixture of forty volumes of pentane to one volume bitumen. A bottom fraction (BF) of the deasphalted heavy oil was obtained by a vacuum distillation (5.4 kPa) at 260°C. Carbonization studies of the asphaltenes and BF were carried out at a controlled heating rate. The results showed that the bulk coke deposits (not coke on the catalyst surface) from BF had a flow-type anisotropic structure. The bulk coke from asphaltenes had a grain-mosaic structure. It was suggested that the differences in the coking properties could be caused by the extent of cross-linkage during carbonization.

1.8 Processing Parameters

Hydrocracking reactions are affected by a number of process parameters. In this section the effect of several of them are discussed.

1.8.1 Hydrogen Pressure

In hydrocracking processes, many of the catalytic reactions which occur involve hydrogen. Increasing the partial pressure of hydrogen in the reactor may increase the fraction of the catalyst surface covered by hydrogen (Speight,1981). Thus, hydrogenation activity of the catalyst is increased. As discussed in section 1.6, in resid hydrocracking hydrogen pressure has a major role on coke formation on the catalyst. In the absence of sufficient hydrogen (low pressure) the amount of coke on the catalyst will increase. Hydrogen pressure and the reaction temperature can be changed according to the feedstock properties to achieve a desirable conversion while avoiding catalyst coking.

1.8.2 Reactor Temperature

Temperature is the primary means by which hydrocracking processes can be controlled (Speight, 1981). Below a certain temperature some reactions (e.g. cracking) will not occur. When the temperature is above the minimum required for conversion, a small change in temperature may substantially increase the reaction rate. Although increasing the temperature increases the reaction rate, there is a maximum to which the temperature should be increased. Increasing temperature leads to formation of undesirable gas and coke products and hence the liquid product

yield will be lowered. Excessively high temperatures lead to deactivation of catalyst much more quickly (section 1.6).

1.8.3 Liquid Hourly Space Velocity (LHSV)

An increase in feedstock flow rate through a given reactor volume means a decrease in residence time of the reacting species. Liquid hourly space velocity is defined as, the volume feedrate based on the properties of the feedstock divided by the volume of empty reactor. An increase in LHSV is accompanied by a decrease in conversion. Studies (Real, 1987 and Altajam and Ternan, 1989) on the hydrotreating of gas oil and hydrocracking of Athabasca bitumen have shown that conversion decreases with increasing LHSV at constant temperature and pressure. At a given reactor temperature one can regulate LHSV to obtain a desired conversion and vice versa.

1.9 Commercial Processes For Conversion of Heavy Oils and Residua Without the Use of Hydrogen

Several commercial processes have been used to convert resid to lighter oils for further refining processes. There are two types of these processes, thermal (non-catalytic) conversion without hydrogen, and catalytic conversion without hydrogen. These processes will be described in this section.

1.9.1 Thermal (Non-Catalytic) Conversion Processes

A. Thermal Cracking

In thermal cracking processes, the molecular structure of hydrocarbons is changed at temperatures above 400°C without using hydrogen or a catalyst. The products are lighter hydrocarbon molecules and either coke or pitch (vacuum resid). A variety of thermal cracking processes are currently used in heavy oil upgrading and in petroleum refineries.

Visbreaking

Visbreaking is an abbreviation for viscosity breaking. It is a mild cracking process which operates at low conversion. Residua are upgraded through thermal conversion to give middle distillates and a stable unconverted heavy oil. Visbreakers operate at temperatures of 450 to 510°C and at pressures of 0.4 to 3.5 MPa. The heavy residua are heated and the products leaving the heater are quenched immediately by gas oil to prevent unnecessary cracking (Speight, 1980 and Meyers, 1986).

Eureka Process

The Eureka process is one of the thermal cracking processes for upgrading heavy oils. The process was developed in Japan by

Kureha Chemicals Industry Company in cooperation with Chiyoda Chemical Engineering and Construction Company. Successful plant operation started in 1976. The Eureka process is similar to the delayed coking process (discussed below) but with the following main differences. Steam is injected at the bottom of the reactor, and pitch (a residue material) is continuously drawn off in the form of a liquid by a pump. Pitch can be pulverized, burnt or gasified more economically than coke. Since in this process the reaction temperature is relatively low, the distillate yield is high (Hirotani **et al**, 1981 and Meyers, 1986).

B. Coking Processes

Coking processes are similar to visbreaking, except that more severe conditions are used. In particular the feedstock residence times are substantially greater. In this case residua are completely converted to lighter oils and coke. The major product in this process is gas oil (60-70 vol %), along with gasoline (20 vol %), gas (5 wt %), and coke (10-15 wt %). The advantage of coking over visbreaking is that coking produces more distillates from a given feedstock (Speight, 1980 and Meyers, 1986).

Delayed Coking

Delayed coking is a semicontinuous process in which the heated charge is transferred to large coking drums that provide the long residence time required for cracking reactions. This process avoids coking in the heat exchangers and the heaters and thus reduces fouling. Volatile materials from the coking drum are continuously removed while coke progressively accumulates in the drum (Gary and Handwerk, 1975 and Speight, 1980).

Fluid Coking

Fluid coking is a continuous process that employs fluidized solids as a heat carrier for the conversion of heavier low grade feedstocks to lighter, more valuable products. The feedstock is preheated and sprayed onto hot coke particles which enter a reactor where they are fluidized by the gaseous products rising through the bed. The process employs two vessels: a reactor and a burner. Coke particles circulate between the two vessels, transferring heat (generated by burning some of the coke in the burner) required for the cracking reaction in the reactor. The reactor operates at near atmospheric pressure and temperatures of 480 to 565°C (Kett et al, 1974 and Speight, 1980).

1.9.2 Catalytic Conversion

Two major catalytic processes for conversion without hydrogen are described in this section: the catalytic cracking process and the asphalt residual treating process.

Catalytic Cracking

Of all the cracking processes, catalytic cracking is the most important. It has revolutionized the refining industry since the 1940's. Catalytic cracking is basically used to produce high-octane gasoline from paraffinic gas oils. The use of catalysts modified the mechanism of bond scission between the carbon molecules. The severity of the processing was decreased and thereby eliminated the majority of secondary reactions that contributed to the production of gas, coke and MCR. A continuous fluid catalytic cracking (FCC) process features rapid transport of catalyst particles between the reactor and the regenerator. The catalyst particle size is of the order of 50 μm.

Most modern catalytic cracking units are FCC processes. In 1940 synthetic silica-alumina became the dominant commercial cracking catalyst, and one year later, the first FCC unit was introduced. Synthetic zeolite Y was commercialized in approximately 1959 and was incorporated into the matrix of FCC catalysts in 1962. By 1969, over 90 % of the United States catalytic cracking units were employing zeolite catalysts (Shaheen, 1980, Venuto and Habib, 1979). In 1971 the short contact time riser

reactor was introduced in order to decrease the hold-up of the active zeolite catalyst in the reactor and thereby minimize over-cracking and coke formation. FCC process flow sheets have been described by Venuto and Habib (1979).

The oil crisis, which resulted from the OPEC's sharp increase of the crude oil prices in 1973, encouraged the development of FCC processes for heavy oil residua (Otterstedt et al, 1986). Recently small amounts of residua have been mixed with gas oils and processed in units which were originally designed for gas oils. The use of heavy oils in the normal FCC units results in more coke and metals being deposited on the catalyst. During catalyst regeneration, combustion of the additional coke will produce extra heat, and there is a possibility of exceeding unit design temperature. In addition more SO_x and NO_x products will be formed, thus increasing pollution. Some companies, such as Kellogg at Borger, Texas, have tried to overcome the above problems by developing FCC processes specifically for heavy oil cracking (HOC).

Asphalt Residual Treating

The asphalt residua treating (ART) process is a selective fluid vaporization process that uses a proprietary contact material, SMART, to remove heavy metals, carbon residue, nitrogen, and sulphur compounds from resid (Bartholic and Haseltine, 1981). In this process a resid is contacted with SMART in a fluid riser system for a short contact time. The hot

SMART material selectively vaporizes the high-hydrogen components contained in the feedstock. Only a little of the metal containing molecules and some of nitrogen containing compounds are vaporized. The hydrocarbon vapours and the contaminated SMART are separated, with the vapours being quenched quickly to a point below the coking temperature. The condensed hydrocarbon vapours, which are essentially free of metals, are used as a feed for a gas oil FCC unit. The spent SMART material is regenerated with air and returned to the riser reactor.

1.10 Commercial Resid Hydrocracking Processes

There are several hydrocracking processes available for licence, e.g. the H-Oil, LC-Fining, VEBA, and CANMET processes.

1.10.1 H-Oil Process

The H-Oil process was designed to process resid using an alumina supported catalyst containing cobalt and molybdenum. The process employs an ebullated bed reactor. H-Oil units have been operated at the Cities Services refinery at Lake Charles, La., Shuaiba, Kuwait, Salamanca Mexico, and the Texaco Refinery at Covent La. At present time another unit is being constructed at Lloydminster Saskatchewan. Preheated recycle and make-up

hydrogen are mixed with the reedstock and charged to the reactor. The liquid passes upward through the catalyst maintained as an ebullated bed. A significant fraction of the liquid is recycled to keep the catalyst in an ebullated state. The products from the reactor are passed through a heat-exchanger to a high-pressure gas separator to remove the recycle gas. The liquid is sent to a low-pressure flash drum for removal of additional gases. The liquid stream proceeds to a distillation unit for separation into products. The operating pressure depends on the feed boiling point and can go as high as 21 MPa for a vacuum residuum. The operating temperature is between 425-455°C, depending on the feed properties(Gary and Handwerk, 1975; Driesen and Stewart, 1964; and Eccles **et al**, 1982). The H-Oil reactor system allows catalyst addition and withdrawal during operation.

1.10.2 LC-Fining

LC-fining is a resid upgrading process which appears to operate on the same principles as the H-Oil process. Differences in engineering design are offered by the process licensors. It has been practised commercially in Amoco's Texas City refinery. The process has also been operated at Syncrude Canada's Mildred Lake facility for over a year.

The process uses an expanded bed reactor which allows catalyst removal and addition during operation. Resid feedstock and hydrogen enter at the bottom of the reactor and pass up

through the catalyst bed, which is somewhat expanded. To maintain the required bed expansion some of liquid from the reactor top is pumped back into the reactor. The recycled hot liquid heats up the incoming fresh feed. Catalyst addition and withdrawal are done at rates and frequencies as may be required. Expanded bed operation allows processing of extra heavy oil feedstocks along with entrained sediment. Catalyst addition and withdrawal prevents accumulation of sediment, and hence, neither plugging nor pressure drop increase occurs with time.

To obtain the product quality requirements, the liquid and vapour effluent from the first reactor flow into one or two additional reactors. Liquid and vapour from the last reactor flow into a hot high-pressure separator, where hot liquid is drawn off and flows through a pressure reducer before going into a low-pressure/high-temperature stripper. Vapour from the high-pressure separator is pressure reduced and mixed with vapour from low-pressure/high-temperature stripper. The vapours then flow through a heat recovery system to a medium-temperature stripper where some more distillate is recovered. Vapours are desulphurized by passing them through an amine absorber. A pressure swing absorption (PSA) unit removes hydrocarbons and produces pure hydrogen for recirculation. Liquids from the strippers and low-temperature separator are sent to atmospheric fractionation (Driesen and Fornoff, 1989).

1.10.3 VEBA-Combi-Cracking.

The VEBA-Combi-Cracking (VCC) process was developed by VEBA OEL of West Germany. In this process the normal vacuum residuum feedstock with fine ground additive (optional) is compressed and mixed with compressed hydrogen and recycle gas. The compressed mixture is then preheated and fed to a liquid phase (LPH) reactor system. In this process three serially connected vertical reactors are used. The reactors with empty tubes are operated in an up flow mode. The conversion takes place at temperatures of 440-490°C and a pressure of 15-25 MPa.

The products from the reactor are discharged into a hot separator operating around the reactor temperature. The non-converted portion of the feed plus solid material are separated from the gaseous reaction products. A multistage flash unit is used to depressurized the bottom products of the hot separator. The gaseous product of the hot separator is mixed with the flash distillates and sometimes with the straight run distillate fraction and then fed to a gas phase (GPH) reactor. A mild hydrocracking is applied in the GPH reactor at the same total pressure as in the LPH reactors. Trickle-flow conditions on catalyst packing are applied (Döhler **et al**, 1987).

1.10.4 CANMET Hydrocracking Process

The CANMET hydrocracking process was developed by the Canada Centre for Mineral, Energy and Technology (CANMET) and was acquired by Petro-Canada in 1979. A demonstration plant of nominal capacity of 5,000 barrels/day (790,000 litres/day) was constructed by Lavalin Inc. for Petro-Canada's Montreal refinery. The construction was completed in 1985. The process employs an inexpensive throw-away additive which serves as a processing aid, by suppressing coke formation and acting as a site for metal and coke deposition.

The process operates at low temperature and low pressure because of the mild catalytic activity of the CANMET additives. Heavy oils can be processed at pitch conversion levels in excess of 85 % for test periods in excess of 30 days without problems caused by solid deposition on the reactor wall or within lines.

Studies on this process showed that pitch conversion was almost directly proportional to temperature at equal LHSV. Sulphur and pitch conversion increased with hydrogen consumption. The total liquid yield, and the light and heavy oil products' °API gravity remained almost constant for 30 day test periods with the additive on stream. The yields and properties of the naphtha fraction from different feedstocks from runs of 90 % pitch conversion were similar. Hence, the process is flexible and can be used for different resids (Patmore **et al**, 1981 and Pruden **et al**, 1988).

CHAPTER TWO

2.0 METHODOLOGY

This chapter describes the methods used both to characterize the catalysts which were prepared, and to characterize the liquid products obtained from the hydrocracking reaction experiments using the catalysts. The catalyst properties measured by these characterization techniques are given in Tables 4 and 5.

2.1 Characterization of the Catalysts Made

2.1.1 Elemental Composition

The elemental composition of the different species in the catalysts were determined by Inductively Coupled Argon Plasma (ICAP) spectroscopy. 0.1 g of catalyst was mixed with 0.4 g of lithium metaborate/tetraborate (50:50) and fused at 1000°C for 1 hour. Subsequently, the fused solid was dissolved in 100 mL of 5 % nitric acid at 90°C for 1 hour. The resulting solution was analyzed by ICAP for aluminium, molybdenum, cobalt, and silicon. The percentage oxide compositions shown in Tables 4 and 5 were calculated from the elemental composition.

2.1.2 Mercury Porosimetry

All catalysts were characterized by mercury intrusion porosimetry using a Micromeritics Autopore II 9220 Porosimeter. The catalyst characteristics are given in Tables 4 and 5. The surface area, S_{Hg}, was determined by assuming the pores penetrated by mercury had a cylindrical shape. The measured pressure at which a particular pore is penetrated is substituted into the equation of Young and LaPlace to obtain the pore radius (Gregg and Sing, 1982). The median pore diameter, d_p, is the diameter at which 50 % of the pore volume, V_p, had been filled with mercury. The particle density, is the weight of the particle divided by the exterior volume of the particle. The volume of the particle is obtained by subtracting the volume of mercury surrounding the particle before pore penetration from the total volume of the empty penetrometer.

2.1.3 BET Surface Area

The Brunauer, Emmett, and Teller (BET) standard method was also used to determine the specific surface area of the catalysts. A Carlo-Erba "Sorptomatic 1800 series" nitrogen adsorption apparatus was used. The BET method is based on the adsorption of N_2 gas on the surface of a catalyst at liquid nitrogen boiling temperature (-196°C or 77 K). The number of molecules of N_2 adsorbed to form a monolayer on the surface is measured. By multiplying the number of N_2 molecules adsorbed by the cross-sectional area of a single molecule (0.162 nm^2/molecule), the

surface area is obtained. Since N_2 is a small molecule, the surface area measured by BET includes the micropores which are not penetrated by mercury during mercury porosimetry. The surface areas obtained by BET method are also given in Tables 4, and 5.

2.1.4 X-ray Diffraction

X-ray diffraction (XRD) is a technique which is used to determine the lattice spacing of crystalline phases of a solid. If the solid is amorphous (not crystalline) then there is no characteristic diffraction pattern. By comparing the diffraction pattern of a catalyst with the standard pattern for a pure compound, one can identify the type of compounds in the catalyst. The method is a semi-quantitative, i.e., it can give an approximate amount of the compound in the catalyst.

Two samples of the catalysts with H-mordenite zeolite component (1 and 20 wt %) were examined by XRD. The main purpose was to see whether the crystalline structure of the H-mordenite zeolite was retained during catalyst preparation. The patterns obtained from the two catalysts are shown in Figure 6. The lower pattern of Figure 6 is for the catalyst with 1 wt % H-mordenite while the upper pattern is for the catalyst with 20 wt % H-mordenite. Figure 6 shows that the catalyst with 20 wt % H-mordenite had increased crystallinity as compared to the catalyst with 1 wt % H-mordenite. This is shown by the formation of peaks

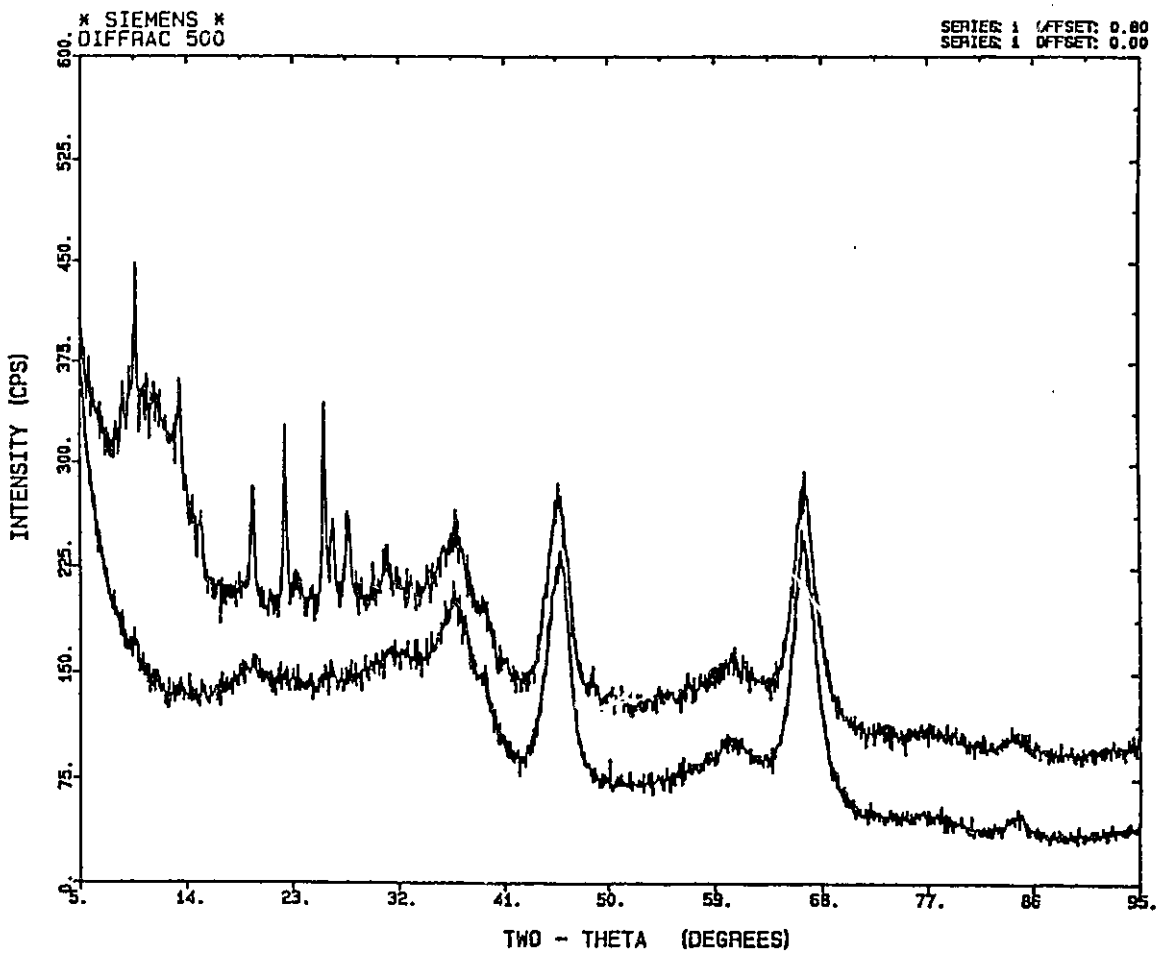

Figure 6: X-ray Diffraction patterns for catalysts containing 1 wt % (lower pattern) and 20 wt % (upper pattern) H-mordenite respectively. Intensity (CPS) versus Two-theta (degrees).

between 5 and 32 "two-theta" degrees. The peaks were intensified by addition of more zeolite in the catalyst. This indicated that the catalyst preparation procedure did not damage the crystalline structure of the zeolite used.

2.1.5 Benzofuran Temperature Programmed Desorption

Benzofuran temperature programmed desorption (TPD) was used to measure the effect of the zeolite on the acidity of the catalysts. The amount of benzofuran adsorbed was expected to be proportional to the number of acid sites available. Samples of the catalysts made were pre-dried for 3 h at 200°C and then saturated with the benzofuran. The samples were then used in benzofuran TPD.

The benzofuran TPD plots for selected representative catalysts are given in Appendix C. The wt % of benzofuran desorbed per minute between 80-150°C indicated the total number of acid sites. The effect of zeolite was obtained by comparing the catalysts. Figure 7 compares three of the curves from Appendix C showing the wt %/min of benzofuran desorbed as temperature was increased from 50-150°C. There is a curve for a catalyst without zeolite and two others for catalysts with 10 and 20 wt % H-mordenite zeolite. As the amount of zeolite in the catalyst increased the rate of benzofuran desorption increased and the desorption was at a slightly higher temperature. This

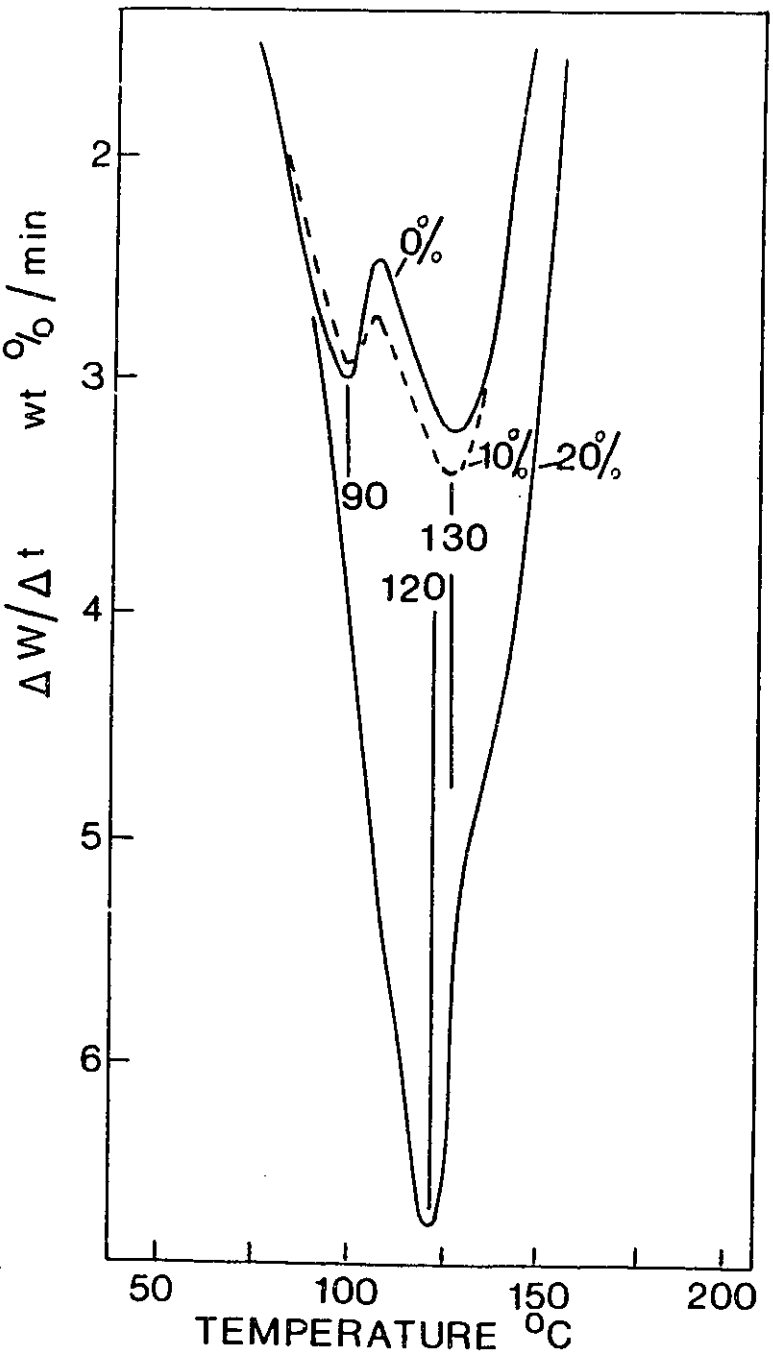

Figure 7: Benzofuran Temperature Programmed Desorption. Change in weight per unit time (wt % of sample per minute) versus temperature (°C). The curves are labelled by H-mordenite content, 0 wt %, 10 wt % and 20 wt % respectively. Peaks at 90, 120, and 130°C are indicated.

was an indication that the number of stronger acid sites increased with increasing zeolite content in the catalyst.

2.2 Analysis of the Liquid Product Samples

All the liquid product samples from the hydrocracking reaction experiments were analyzed for carbon, hydrogen, sulphur, nitrogen, and micro carbon residue % mass content. The specific gravity and the metal contents of the liquid product samples were also measured.

2.2.1 Carbon and Hydrogen Determination

The carbon and hydrogen content of the products were determined using a Perkin-Elmer Model 240C Elemental Analyzer. This equipment can be used to measure the amount of carbon and hydrogen in a sample over a range of 0.5 to 100 wt %. A sample is combusted in a pure oxygen under static conditions. The combustion products CO_2 and H_2O are detected by a self integrating, steady state thermal conductivity analyzer.

2.2.2 Sulphur Determination

The sulphur content of the samples was determined by either a Princeton Gamma-Tech model 100 chemical analyzer (an X-ray fluorescence ASTM D 4294 method) or a Leco Sulphur Determinator,

Sc-32. The X-Ray method is used to analyze samples with sulphur contents from 0.1 to 6 wt % while the Leco Sulphur Analyzer is used for samples with sulphur contents of 0.5 to 100 wt % sulphur. In the X-ray method, a sample is irradiated with a Fe^{55} source, causing fluorescent X-rays to be produced. The instrument detects the X-rays and is calibrated to give wt % sulphur content of the sample. With Leco Sulphur Analyzer, a sample is combusted in an oxygen atmosphere where sulphur oxidizes to SO_2. Moisture and dust are removed and the SO_2 gas is then measured by a solid state infrared detector. The instrument is calibrated to give wt % sulphur in the sample.

2.2.3 Nitrogen Determination

The nitrogen content of the samples was determined by a Dohrmann N-100 Total Nitrogen Analyzer. The method is applicable to samples containing 0.3 to 100 ppm total nitrogen. This method works by injecting a liquid sample into a stream of inert gas (He or Ar). The sample is vaporized and carried to a high temperature zone where oxygen is introduced and reacted with organic and bound nitrogen to form NO. The NO contacts ozone and is converted to excited NO_2. The light emitted as the excited NO_2 decays is detected by a photomultiplier tube and the resulting signal is a measure of the nitrogen in the sample.

2.3.4 Micro Carbon Residue (MCR) Determination

Determination of the MCR requires evaporation and pyrolysis of a petroleum product to provide some indication of its relative coke forming tendency. A weighed sample in a special metal container is placed in a metal furnace maintained at 550°C. The sample is heated quickly and the volatile matter is vented. The heavier residue remaining in the sample container undergoes cracking and coking reactions. After a specified heating period, the sample container is removed from the furnace, cooled and weighed. The residue weight is calculated as a percentage of the original sample (wt % MCR), and is a measurement of the coke forming tendency of the sample. The analysis, adhered to the Standard ASTM D524 Test Method.

2.2.5 Measurement of Specific Gravity

The specific gravity of the samples was measured using a hydrometer. A sample at ambient temperature was transferred to a measuring cylinder. The appropriate hydrometer was lowered into the sample and allowed to sink freely in the centre of the cylinder. After the hydrometer scale reading remained constant, the temperature of the sample was measured. The specific gravity reading obtained was converted to 15°C from the temperature at which it was measured, using ASTM specific gravity reduction to 15°C tables.

2.3 Characterization of the Used Catalysts.

All the catalysts from the hydrocracking reaction experiments were analyzed after they had been removed from the reactor. Their C, H, and N contents were analyzed after having been soxhlet extracted by toluene. Toluene soxhlet extraction was employed to remove hydrocarbon liquids that remained on the catalyst at the end of an experiment.

A Leco CHN-600 Carbon, Hydrogen, Nitrogen Analyzer 785-500 system was used to determine C, H, and N content of the spent catalysts. A weighed sample was burned in pure oxygen at 950°C to produce carbon dioxide, water vapour, oxides of nitrogen (NO_x), elemental nitrogen, and oxides of sulphur. The oxides of sulphur were removed with calcium oxide in a secondary combustion zone. The remaining combustion gases were collected in a ballast volume and allowed to mix thoroughly. For nitrogen determination, a 10 mL aliquot was taken and carried by helium into a reagent train consisting of (1) hot copper for the removal of oxygen and the reduction of NO_x to N_2, (2) N-catalyst, ascarite, for the removal of CO_2 and (3) magnesium perchlorate for the removal of H_2O. The remaining elemental nitrogen was measured by a thermal conductivity cell. Carbon and hydrogen were determined by infrared measurement of CO_2 and H_2O levels.

2.4 Calculation of PTOF

Pseudo turnover frequency (PTOF) is defined as the number of atoms (S, N, Ni, or V) removed per second per nm^2 of catalyst surface area. This is expected to be related to the turnover frequency (TOF), which is the number of reactions per second per reaction site. Many heterogeneous catalysts have more than one type of reaction site. Each type of site is expected to have a different TOF. The PTOF provides an average turnover frequency for the different reaction sites on a unit of catalyst surface area.

The PTOF of S, N, Ni, and V were calculated from the amount removed, (that is, the difference between the amount fed to the reactor and the amount in the liquid products), the total catalyst surface area in the reactor (SA), and the feedstock feed rate. Equation 4 below is a general equation in which X is either S, N, Ni, or V and Y is their corresponding atomic mass.

$$PTOF\left(\frac{X\,atoms\,removed}{nm^2\,s}\right) = \frac{g\,X\,removed}{g\,X\,fed} * \frac{g\,X\,fed}{h} * \frac{1\,h}{3600\,s} * \frac{1}{SA\,m^2} * \frac{1\,m^2}{10^{18}\,nm^2} * \frac{1\,g\,atom\,X}{Y\,g\,of\,X} * \frac{6.0224 * 10^{23}\,atoms\,X}{1\,g\,atom\,X} \quad (4)$$

Equation 4 can be simplified to equation 5 below:

$$PTOF\left(\frac{X\,atoms\,removed}{nm^2 s}\right) = \frac{\%\,XConv.}{100} * \frac{g\,Xfed}{h} * \frac{167.288}{Yg\,of X} * \frac{1}{SA} . \qquad (5)$$

By using the concentration of the removed species in the feedstock (Table 2), the feedstock feed rate (155 g/h), and the % conversions (Appendix A), the PTOF of the removed species were calculated using equation 5 above.

2.6 The Effect of Residence Time on the PTOF

Altajam and Ternan (1989) related PTOF to the LHSV and the conversion (χ) as shown in Equation 6 where C_1 is a constant:

$$PTOF = C_1 * LHSV * \chi . \qquad (6)$$

The χ can be replaced by the reaction rate constant (k) and residence or mean residence time (θ), as shown below.

The first order reaction for species X, with C_x as concentration of X at time (t), is written as

$$-\frac{dC_x}{dt} = kC_x . \qquad (7)$$

Integrating from the time t=0 to t=θ Equation 8 is obtained:

$$\ln \frac{C_o}{C_x} = k\theta . \qquad (8)$$

where C_o is the initial concentration of species X in the feedsock. Since $x = (C_o - C_x)/C_o$, equation 8 can be written as

$$\ln [1 - \chi] = k\theta . \tag{9}$$

Solving Equation 9 for x we obtain

$$\chi = 1 - \exp(-k\theta) . \tag{10}$$

Replacing LHSV in Equation 6 by C_2/θ, where C_2 is a constant, and x from Equation 10, Equation 11 can be obtained with $C = C_1C_2$

$$PTOF = \frac{C}{\theta} [1 - \frac{1}{\exp(k\theta)}] . \tag{11}$$

At a constant temperature, k is constant for a particular catalyst. The value of k will vary with temperature and the type of catalyst used. Figure 8 shows the variation of PTOF with θ for two different values of k (k = 1 for the lower curve and k = 5 for the upper curve) as calculated from Equation 11. An arbitrary value of 1 was assumed for the constant C. From the figure it is clear that PTOF decreases with increasing residence time and decreasing reaction rate constant.

If the overall reaction is second order, the PTOF also decreases with increasing residence time. Equation 12 can be derived in a manner similar to Equation 11 for a second order reaction. The κ in Equation 12 is equal to $C_o k$.

$$PTOF = \frac{C}{\theta} [\frac{\kappa\theta}{1 + \kappa\theta}] . \tag{12}$$

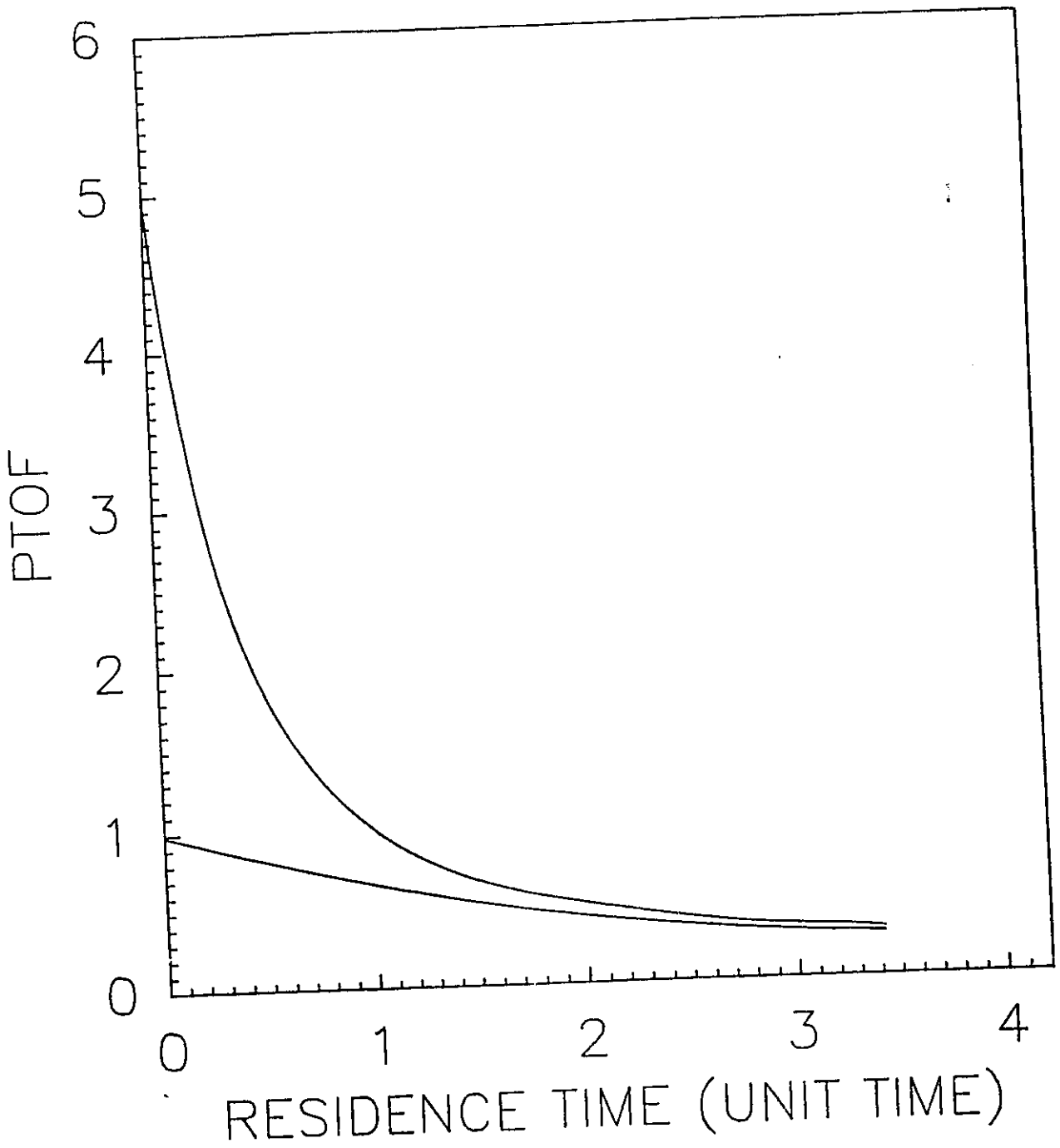

Figure 8: The effect of residence time on pseudo turnover frequency (PTOF). PTOF (atoms converted $(nm)^{-2}s^{-1}$) versus residence time (unit time). Upper and lower curves for k arbitrary values of 5 and 1 respectively in Equation 11.

CHAPTER 3

3.0 PROPERTIES OF MATERIAL

Two types of materials were used in these experiments: the Boscan heavy oil feedstock, and the solid catalysts. The solid catalysts were prepared by including different amounts and types of zeolites in the paste or gel which contained the various chemicals for standard Co-Mo-Al_2O_3 catalysts. The properties of the light hydrocarbon distillate oil that was mixed with the zeolite before including it in the paste are also described.

3.1 Properties of Boscan (Venezuela) Heavy Oil Used in This Study

Boscan heavy oil is one of the heavy crude oils shown in Table 1 (section 1.1). It has greater concentrations of hetero-atoms (sulphur and nitrogen) and metals (nickel and vanadium) than many of the heavy oils in Table 1. In particular, it has the greatest vanadium concentration of all the heavy crude oils in Table 1, and therefore it is an interesting feedstock for demetallization studies. Metals exist in petroleum as organo-metallic complexes, many of which are found in the asphaltene fraction. Table 2 shows the properties of the particular Boscan (Venezuela) heavy oil used as the feedstock in this study.

Table 2: Properties of Boscan (Venezuela) Heavy Oil

Specific gravity at 15°C	1.002
API gravity	9.7
Carbon (wt %)	81.8
Hydrogen (wt %)	10.4
Sulphur (wt %)	5.38
Nitrogen (wt %)	0.64
Pentane Insolubles (wt %)	20.1
Toluene Insolubles (wt %)	< 0.10
Micro Carbon Residue (wt %)	15.5
Ash (wt %)	0.22
+525°C Residue (wt %)	54.6
Vanadium (ppm)	1385
Nickel (ppm)	107
H/C Atomic Ratio	1.53

Table 3: Properties of Hydrocarbon Distillate Oil

Specific Gravity at 15°C	0.889
Carbon (wt %)	86.3
Hydrogen (wt %)	13.3
Nitrogen (ng/μL)	85.8
Boiling Range (°C)	245-553
Atomic H/C Ratio	1.85

3.2 Properties of Hydrocarbon Distillate Oil

A light hydrocarbon distillate oil (Imperial Oil, Zerice) was used in catalyst preparation. It filled the zeolite pores, preventing the aqueous alumina gel from penetrating the zeolite structure at the stage when the catalyst was in the form of paste. Furthermore, it prevented the paste from acting like a glue which would seal off the external surfaces of the zeolite crystals and prevent the reacting molecules from having access to the acidic sites on the zeolite exterior. The properties of the oil used are shown in Table 3.

3.3 Properties of the Catalysts Made

The properties of the catalysts containing H-mordenite and HY zeolite are given in Tables 4 and 5, respectively. A detailed description of the techniques used to determine these properties was given in section 2.1. Accounts were also given of the variations in compositions, specific surface areas, pore volumes, particle densities and the bulk densities of the catalysts as their zeolite content was increased.

The overall concentrations of the CoO, MoO_3, and Al_2O_3 in the catalysts were decreased slightly as the amount of the H-mordenite or HY zeolite was increased in the catalysts. Similarly the concentration of SiO_2 was increased with increasing catalyst zeolite content. Although the overall concentrations of

CoO, MoO_3 and Al_2O_3 appear to decrease slightly, in the actual catalysts the concentrations in the CoO-MoO_3-Al_2O_3 phase should be the same, i.e., equivalent to concentrations in the catalyst with no zeolite. The zeolite phase, on the other hand, would have no CoO or MoO_3.

The specific catalyst surface areas determined by the BET method (S_{BET}) increased with increasing catalyst zeolite content. Those determined by mercury porosimetry (S_{Hg}) decrease with increasing catalyst zeolite content. The BET method includes the area of micropores (d_p < 3 nm), i.e., the area in the zeolite pores, while the mercury porosimetry method does not. In this study the catalyst specific surface areas determined by mercury porosimetry were used because they represented catalyst surface areas likely to be reached by the asphaltene molecules.

The volume of the catalyst pores which were accessible to mercury was found to increase when zeolite was added to the catalyst. This could probably be explained by the different packing of the fine alumina particles when the zeolite crystals were present. In the case of the catalysts containing an H-mordenite component, the major increase in volume was in the medium sized pores (10 nm < d_p < 10 μm). On the other hand, the volume increase in catalysts containing an HY zeolite component was spread more evenly throughout the entire range of pore sizes. The change in pore volume caused a change in the median pore diameter. There was more change in the median pore diameter of the H-mordenite catalyst (5.3 to 8.4 nm) than in the catalysts containing an HY zeolite component (5.5 to 7.7 nm).

The catalyst particle densities determined by the mercury porosimetry method also decreased as the catalysts' zeolite content increased. The decrease in the catalysts' particle densities resulted in a decrease in the weights of the catalysts loaded into the reactor. The decrease in reactor catalyst loading was reflected in a decrease in the catalysts' bulk densities. Another feature which affected the bulk densities, especially with the catalyst containing an H-mordenite zeolite component, was the catalyst extrudate shapes. The extrudates were found to become more and more curved along the longitudinal direction, as their zeolite content was increased. This feature caused them to pack more loosely in the reactor. The greater apparent residence time of the feedstock in the reactor was also caused by the extrudate curvatures.

Table 4: Characteristics of Catalysts Having an H-mordenite Component

Composition						
H-mordenite (wt %)	0	1	3	5	10	20
Al_2O_3 (wt %)	81.5	81.2	80.0	78.9	76.5	72.4
MoO_3 (wt %)	15.4	15.3	15.1	14.9	14.4	13.5
CoO (wt %)	3.1	3.1	3.1	3.1	3.0	2.9
SiO_2 (wt %)	0.0	0.3	1.7	3.2	6.0	11.2
BET Specific Surface Area S_{BET} (m^2/g)	193	204	202	203	208	215
Mercury Porosimetry						
Specific Surface Area S_{Hg} (m^3/g)	194	195	191	196	184	169
Median Pore Diameter d_p (nm)	5.3	6.7	7.3	7.5	8.0	8.4
Total Pore Volume V_p (mL/g)	0.33	0.44	0.45	0.47	0.45	0.42
Volume of Larger Pores d_p>10 μm (mL/g)	0.0248	0.0412	0.0364	0.0468	0.0458	0.0417
Volume of Medium Pores 10 μm>d_p>10 nm (mL/g)	0.0795	0.1536	0.1572	0.1649	0.1484	0.1472
Volume of Smaller Pores 3 nm<d_p<10 nm (mL/g)	0.2245	0.2408	0.2545	0.2590	0.2567	0.2319
Particle Density (g/mL)	1.441	1.265	1.222	1.205	1.225	1.187
Catalyst weight per reactor volume (g)	93.9	86.7	75.8	67.8	76.8	57.0
Bulk Density (g/mL)	0.606	0.559	0.489	0.437	0.495	0.368
Residence Time (min)	25.6	24.7	26.5	28.0	26.1	30.4

Table 5: Characteristics of Catalysts Having an HY Component

Composition						
H-Y (wt %)	0	5	10	15	20	25
Al_2O_3 (wt %)	81.5	79.6	77.3	74.3	72.1	69.7
MoO_3 (wt %)	15.4	14.7	14.2	13.6	12.9	12.1
CoO (wt %)	3.1	3.0	2.8	2.7	2.6	2.4
SiO_2 (wt %)	0.0	2.6	5.8	9.2	12.4	15.7
BET Specific surface Area $S_{BET}(m^2/g)$	194	246	203	243	269	262
Mercury Porosimetry						
Specific Surface Area $S_{Hg}(m^2/g)$	183	209	175	187	177	158
Median Pore Diameter d_p (nm)	5.5	5.7	6.7	7.3	7.2	7.7
Total Pore Volume V_p (mL/g)	0.31	0.36	0.35	0.41	0.38	0.36
Volume of Larger Pores d_p>10 μm (mL/g)	0.0245	0.0251	0.0335	0.0419	0.0353	0.0417
Volume of Medium Pores 10 μm>d_p>10 nm (mL/g)	0.0606	0.0773	0.0703	0.0863	0.0929	0.0873
Volume of Smaller Pores 3 nm<d_p<10 nm (mL/g)	0.2253	0.2528	0.2434	0.2792	0.2513	0.2327
Particle Density (g/mL)	1.447	1.363	1.424	1.237	1.243	1.229
Catalyst weight per reactor volume (g)	85.4	75.4	79.5	77.6	78.4	73.1
Bulk Density (g/mL)	0.551	0.486	0.512	0.501	0.506	0.472
Residence Time (min)	27.4	28.6	28.3	26.3	26.2	26.7

CHAPTER 4

4.0 EXPERIMENTAL

A detailed account of catalyst preparation and the experimental procedures for hydrocracking reactions is described.

4.1 Catalyst Preparation

A series of two catalyst families having different types of zeolite components were prepared. The two types of zeolites used were H-mordenite and HY. In all cases an aqueous paste of cobalt nitrate, ammonium paramolybdate and alpha alumina monohydrate (CMA) was prepared and then a zeolite-oil paste was added to it. The CMA paste was prepared so that after calcining it would have a final composition of 3 wt % CoO, 15 wt % MoO_3 and 82 wt % Al_2O_3. The composition of CMA was typical of many commercial hydrocracking catalysts.

4.1.1 CMA Paste Preparation

All the quantities stated in the following description refer to the preparation of 1000 g of dry calcined $CoO-MoO_3-Al_2O_3$ catalyst. The solid materials used in the CMA paste preparation

are cobalt nitrate hexahydrate ($Co(NO_3)_2.6H_2O$) (Baker Chemicals), ammonium paramolybdate ($(NH_4)_6Mo_7O_{24}.4H_2O$) (Baker Chemicals), and alpha alumina monohydrate powder (Continental Oil Company, 100 mass % Catapal SB) as the support. A mass of 1094 g of alpha alumina monohydrate powder were weighed and poured into a mixer. A mass of 184 g of ammonium paramolybdate were dissolved in a mixture of 430 g of distilled water and 79 g of concentrated (29 wt % ammonia) aqueous ammonia. To enhance the solubility of the crystals of the ammonium paramolybdate, the mixture was heated and stirred. The solution was mixed with the alumina powder for about 15 minutes. Cobalt nitrate solution, prepared by dissolving 117 g of the salt in 88 g of distilled water, was then mixed slowly with the above paste for about 15 minutes, and 385 g of distilled water were also added to the paste. The CMA paste obtained at this stage was too soft to extrude. To make it stiffer, about 140 g of concentrated nitric acid (70 wt % acid) was added drop by drop with constant mixing until the paste was sufficiently stiff.

For the catalyst prepared without a zeolite component, the CMA paste was extruded through a stainless steel plate with holes of 1 mm diameter. The plate was placed at the bottom of an empty steel cylinder which was mounted vertically. The combined paste was placed on the top of the plate. A piston was moved down the cylinder, by a screw mechanism, until it contacted the paste and squeezed the extrudates through the holes in the plate. The extrudates were then dried and calcined.

4.1.2 Preparation of Catalysts with H-mordenite Zeolite Component

A zeolite-oil paste was prepared using H-mordenite powder (Union Carbide number, LZM-8) having a particle size less than 4 μm (supplier's information). This was verified by scanning electron microscopy (SEM) measurements. The zeolite-oil paste was prepared by adding a light hydrocarbon distillate oil (trade name Zerice from Imperial Oil Company). The properties of the oil are shown in Table 3 of Chapter 3. The amount of zeolite used varied according to the wt % zeolite required in the catalyst. For example, a catalyst containing 10 wt % zeolite required 11.1 g of zeolite powder to be mixed with 100 g of CMA paste to produce 111.1 g of final catalyst. The ratio of oil to zeolite used in preparation of the zeolite paste was 1.4 mL of oil per gram of zeolite. The oil was expected to fill the zeolite pores to prevent them from being filled with the CMA paste. The oil also acted like a lubricant in the process of extrudate preparation.

A series of five catalysts was prepared with H-mordenite zeolite as a component. The content of the H-mordenite in the series was 1, 3, 5, 10, and 20 wt %. For every catalyst containing a zeolite component, the appropriate quantity of zeolite-oil paste was prepared to match the required amount of CMA paste to obtain the final zeolite catalyst composition. The zeolite paste was mixed with the CMA paste for about 15 minutes. The properties of catalysts with H-mordenite are given in Table

4 of Chapter 3. Each of the catalysts was extruded as described at the end of section 4.1.1.

4.1.3 Preparation of Catalysts with HY Zeolite Component

The HY zeolite powder (Union Carbide number, LZY-82) had particle sizes similar to those of the H-mordenite zeolite. The same procedures were followed in the preparation of an HY zeolite paste as for the H-mordenite. A series of 5 catalysts with 5, 10, 15, 20, and 25 wt % HY was prepared. The physical properties of catalysts containing HY component are given in Table 5 of Chapter 3.

4.1.4 Catalyst Drying and Calcination

All the catalysts prepared were dried at 110°C for at least 10 hours. The drying was either carried out in a controlled fixed temperature oven or in a temperature programmable oven (TPO). All catalysts were calcined in the TPO, which was programmed to pre-dry for 30 min at 110°C and raise the temperature at a rate of 5°C/min to 450°C and calcine for 4½ h.

4.2 Hydrocracking Reaction Experiments

The hydrocracking reaction experiments were carried out in a fixed bed reactor operated in upward flow mode (bubble bed reactor). The experimental set-up, Figure 9, includes a Ruska constant feed metering pump, a preheater, a reactor, a three zone furnace, gas/liquid separators, a scrubber, and a wet test meter. The volume displacement pump had a flow controller with which the desired flow rate could be set. It had a scale with each division equivalent to 1 mL. The preheater for the pump had an on-off temperature controller and was used to preheat the feed. The reactor had a volume of 155 mL and a length to diameter ratio of 12. It had a thermowell positioned at the central axis with six thermocouples (at 5 cm intervals) connected to a temperature recorder. The three zone furnace, surrounding the reactor, had on-off temperature controllers and was used to maintain the reactor at the reaction temperature. The gas/liquid separators were used to collect the liquid product and allow the gaseous products to flow into the scrubber. One separator was used during unsteady state operation such as start-up and shut-down. The second separator was used to collect the product sample during the steady state reaction period. The scrubber had a potassium hydroxide solution to scrub the gases. The gas leaving the scrubber was passed through the wet test meter which registered the total volume.

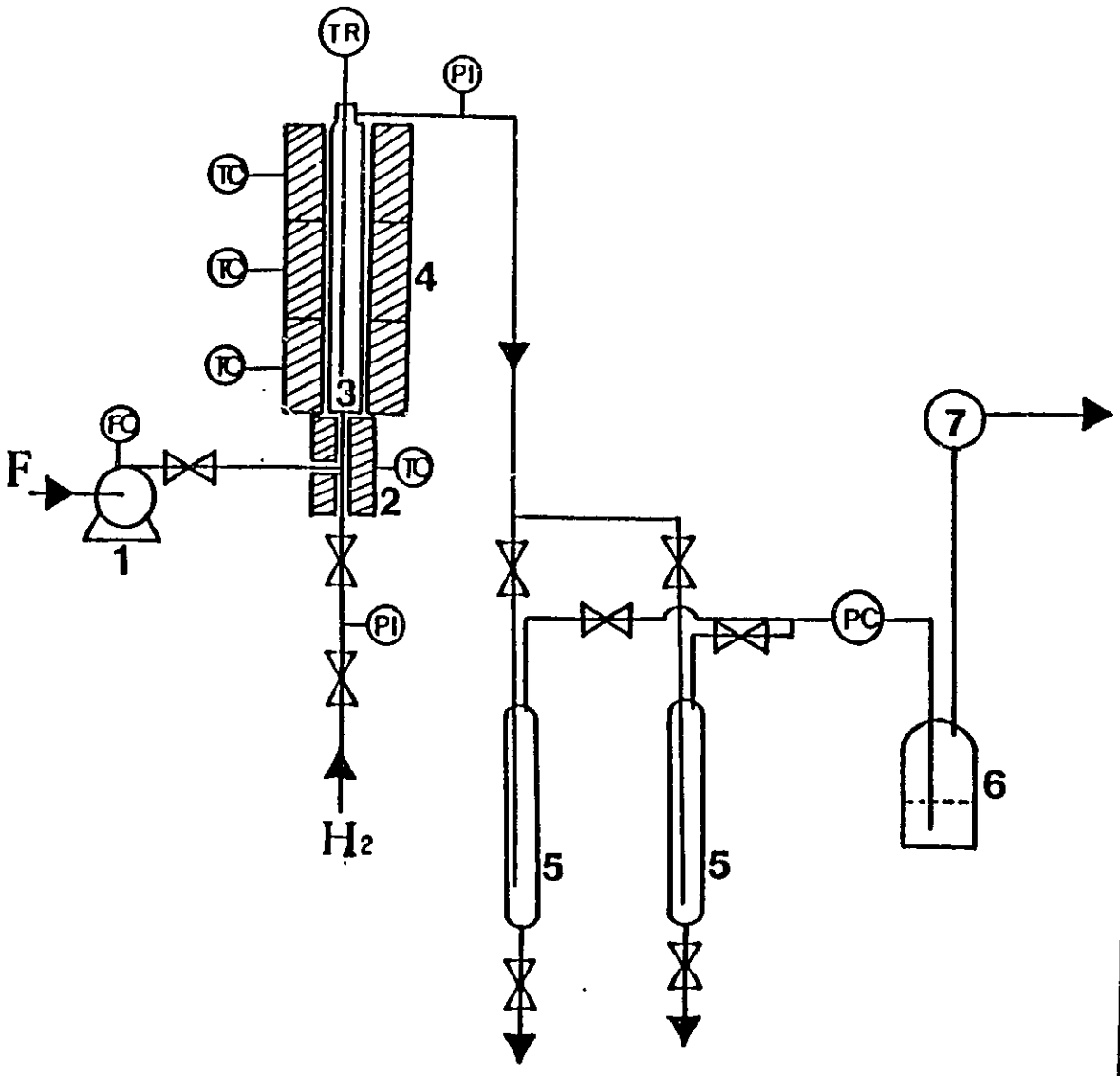

Figure 9: Experimental Set-up

1. Pump
2. Preheater
3. Reactor
4. Three Zone Furnace
5. Gas/Liquid Separator
6. Scrubber
7. Wet Test Meter

FC. Flow Controller
PC. Pressure Controller
PI. Pressure Indicator
TC. Temperature Controller
TR. Temperature Recorder
(For six thermocouples)

The following operating procedures were followed for every catalyst that was tested. The reactor fitted with the thermowell was completely filled with catalyst extrudates. Wire gauze with pores less than 1 mm was used to prevent catalyst particles from being carried away with the flowing fluid. The reactor was closed tightly and connected to the experimental system. Once all connections were properly tightened, the reactor was pressurized by hydrogen to 13.9 MPa (2000 psig). To check for leaks, the inlet and outlet valves to and from the reactor were closed while observing the reactor outlet pressure. If there were no leaks, the hydrogen feed was adjusted to flow at a rate of 36 mL/s at STP and maintained at a reactor pressure of 13.9 MPa. The heating was started while maintaining hydrogen flow. The pressure of the heavy oil was increased by the pump up to the reactor pressure before feeding was started, to prevent hydrogen from flowing back into the feedstock. When the reactor temperature reached about 200°C, the flow of Boscan heavy oil (Table 2) was started. The pump was set to deliver a feed rate of 160 mL/h (155 g/h), which was equivalent to a LHSV of 1.0 h^{-1}, calculated on the basis of the feedstock properties and the reactor empty volume. To reduce the viscosity of the heavy oil, the pump cylinder and its connections to the reactor were heated and insulated to maintain a temperature of about 100°C. The preheater at the entrance to the reactor was set to heat the flowing feed to around 300°C.

The only process variable which was varied in all the catalyst testings was the temperature. A reactor pressure of 13.9 MPa and a LHSV of 1.0 h^{-1} were used for all the experiments. Each catalyst was tested at two reaction temperatures as described in the following sections.

Several factors contribute to the final error in the reported results. These include the accuracy of the measurement of carbon, sulphur, nitrogen, nickel, vanadium, and MCR, as well as the reproducibility of the reaction experiments. The precision of the analytical results are generally within ±2 % of the reported results. However there could be some errors in the reaction experiments, resulting from the difficulty in the precise control of the process variables, such as temperature. Furthermore, slight variations in the process history of the catalysts would mean that the beginning of the steady state period would occur at different catalyst time-on-stream. This could result in differences in the extent of the catalysts deactivation. Considering all of the above, the results reported in the appendices are probably accurate to ±5 %.

4.2.1 Catalyst Presulphiding

Every catalyst was presulphided prior to its evaluation tests. Presulphiding was done by flowing a mixture of the Boscan heavy oil and hydrogen over each catalyst. The reactor and the flow conditions were set as described in the above section. The reactor temperature was allowed to rise from around 200°C to 400°C (in an interval of about 30 min) where it was maintained for at least 1 h. Considering the total amount of MoO_3 and CoO in the reactor (assuming 100 g of catalyst), at most 1 h was required to form MoS_2 and Co_8S_9 sulphides.

Presulphiding with heavy gas oil was studied by Ternan and Whalley (1976) and was found to be similar to the use of hydrogen sulphide. In their study, catalysts were presulphided with H_2S at a temperature of 400°C, a pressure of 0.102 MPa, and an H_2S flow rate of 57.2 mL/s for 2 h, in a bottom feed reactor filled with 100 mL of Ni-Mo-Al_2O_3 catalyst containing 2.1 wt % NiO and 5.4 wt % MoO_3. The same type of catalyst was presulphided at

similar conditions, except that in this case a pressure of 13.9 MPa and gas oil flow rate of 200 mL/h were used. The gas oil that was used had 3.64 wt % sulphur and a boiling range of 345-525°C. The presulphiding materials were found to have no influence on the HDS and HDN activities of the catalysts.

4.2.2 Evaluation of Catalysts with H-Mordenite Component

One catalyst without H-mordenite zeolite and five others with different amounts of H-mordenite were tested at 400°C and 450°C. The procedures described in section 4.2 and 4.2.1 were followed. After presulphiding the catalyst, the first test was done at 400°C by switching the flow of the reactor products to the sample collector vessel. A sample was collected for a 2 h period, during which the temperature was maintained constant. After the first test, the reactor temperature was raised to 450°C, and left to attain steady-state readings of temperature and gas flowrate before another 2 h sample was collected.

4.2.3 Evaluation of Catalysts with HY Component

Six catalysts were evaluated. Five of the catalysts had HY zeolite in various amounts, while one had no zeolite. For this set of catalysts, reactions were carried at 400°C and 370°C. Experiments were performed in a manner similar to those with the H-mordenite catalysts except for the difference in temperature used for the second experiment with each catalyst. The first test was performed at 400°C followed by the second test at 370°C.

CHAPTER 5

5.0 RESULTS AND DISCUSSION

The objective of this study was to investigate hydrocracking reactions with Boscan heavy oil using catalysts containing a zeolite component. Conventional hydroprocessing catalysts are supported on alumina which has predominately Lewis acid sites. It was expected that the Brønsted acid sites in the zeolite would enhance the acidity of the catalyst surface (Decroocq, 1984; Benesi, 1967; Haynes, Jr., 1978; and Mishin **et al**, 1988) and therefore enhance the cracking reactions. In this chapter the reaction results are discussed both for non-catalytic hydrocracking and for catalytic hydrocracking with catalysts containing a zeolite component.

5.1 Non-Catalytic Hydrocracking

Three experiments were carried out at different temperatures (400, 425, and 450°C) using the reactor filled with 4.7 mm stainless steel beads instead of a catalyst. Hydrogen pressure, hydrogen flow rate, and feedstock flow rate were maintained at the same conditions (section 4.2) for both catalytic hydrocracking and non-catalytic hydrocracking.

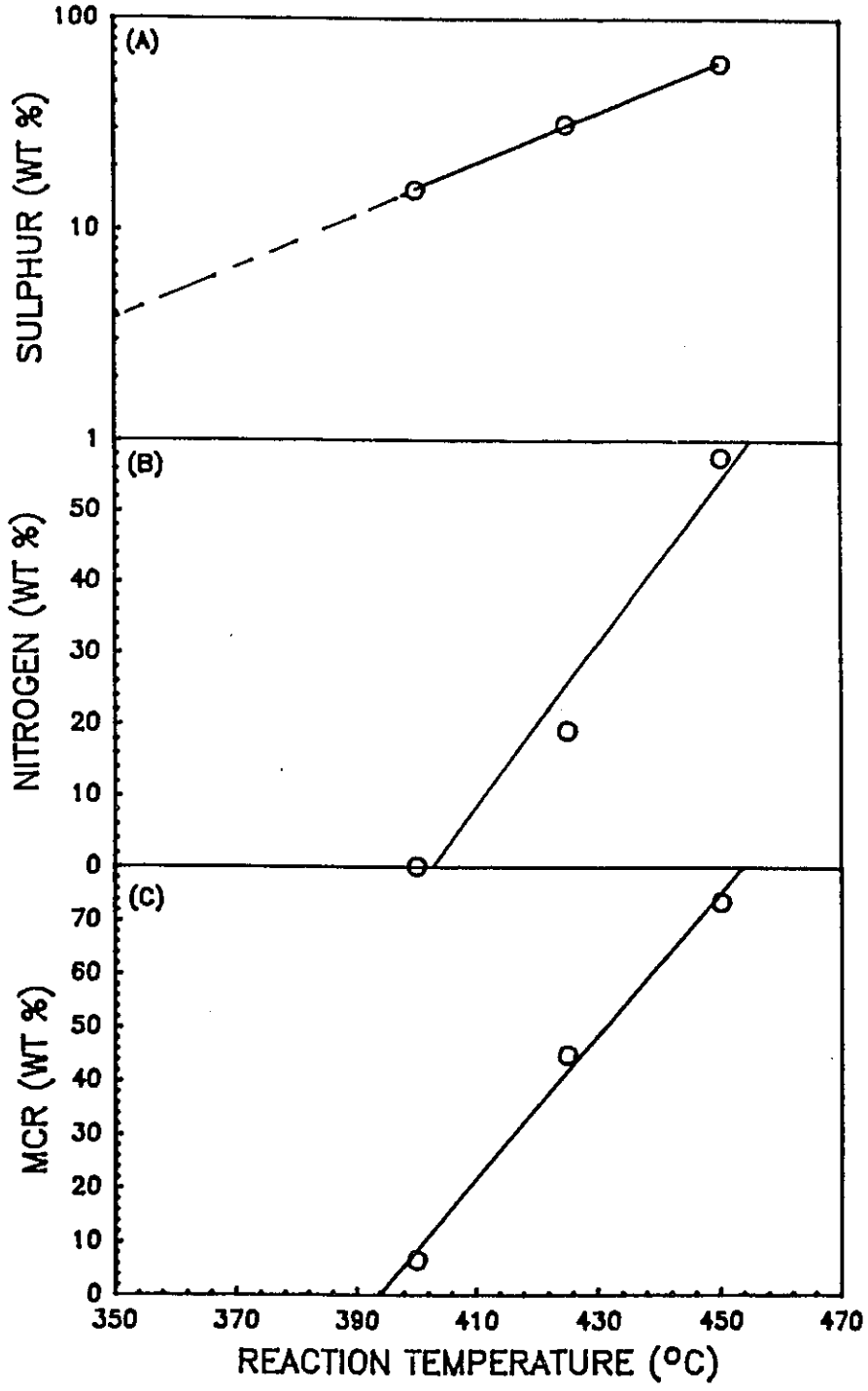

Figure 10: Conversion (wt %) versus reaction temperature (°C) for non-catalytic hydrocracking. Figure 10A sulphur, Figure 10B nitrogen, and Figure 10C micro carbon residue.

Figure 10 shows the removal of sulphur, MCR, and nitrogen in Boscan heavy oil as a function of temperature. The logarithm of sulphur conversion was found to be a linear function of temperature (see Figure 10A). Nitrogen and MCR conversion were linear functions of temperature, as shown in Figures 10B and 10C. At 400°C non-catalytic conversion of sulphur and MCR were small, about 15 and 7 wt % respectively, while there was no nitrogen conversion. At 450°C there was a significant removal of sulphur (61 wt %), MCR (74 wt %), and nitrogen (57 wt %) in the liquid product, though the liquid product yield was substantially lowered (about 58 wt %).

The conversions of sulphur, nitrogen, and MCR can be represented by α, β, and γ respectively. Then the following correlations between conversion and temperature can be obtained from the results in Figure 10:

$$\log \alpha = aT + b; \tag{13}$$

$$\beta = cT + d; \tag{14}$$

$$\gamma = eT + f; \tag{15}$$

where T is the reaction temperature and a,b,c,d,e, and f are constants. Since few data points were determined, the reliability of these predictions is subject to verification by more experimental data.

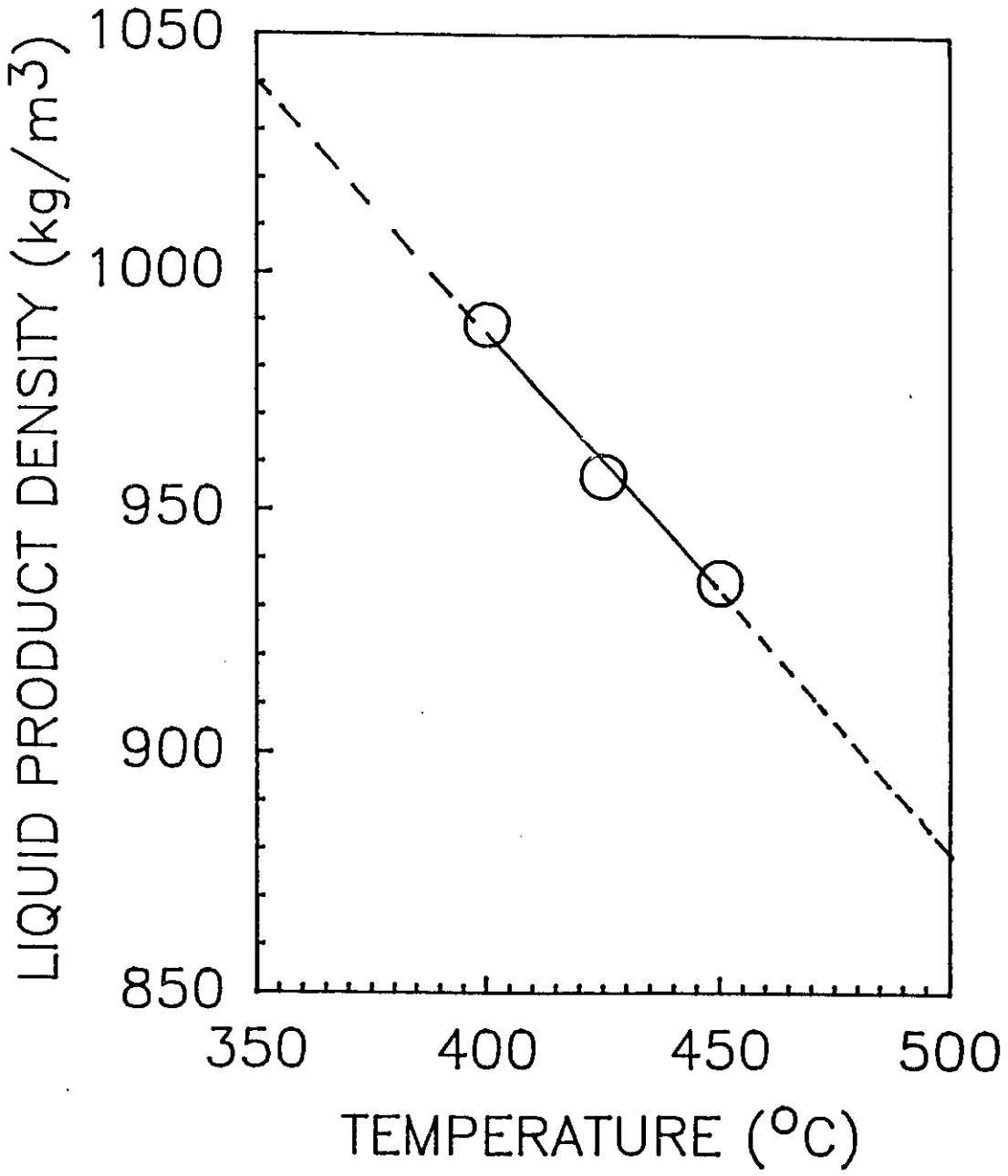

Figure 11: Liquid product density (kg/m^3) versus reaction temperature (°C) for non-catalytic hydrocracking reactions.

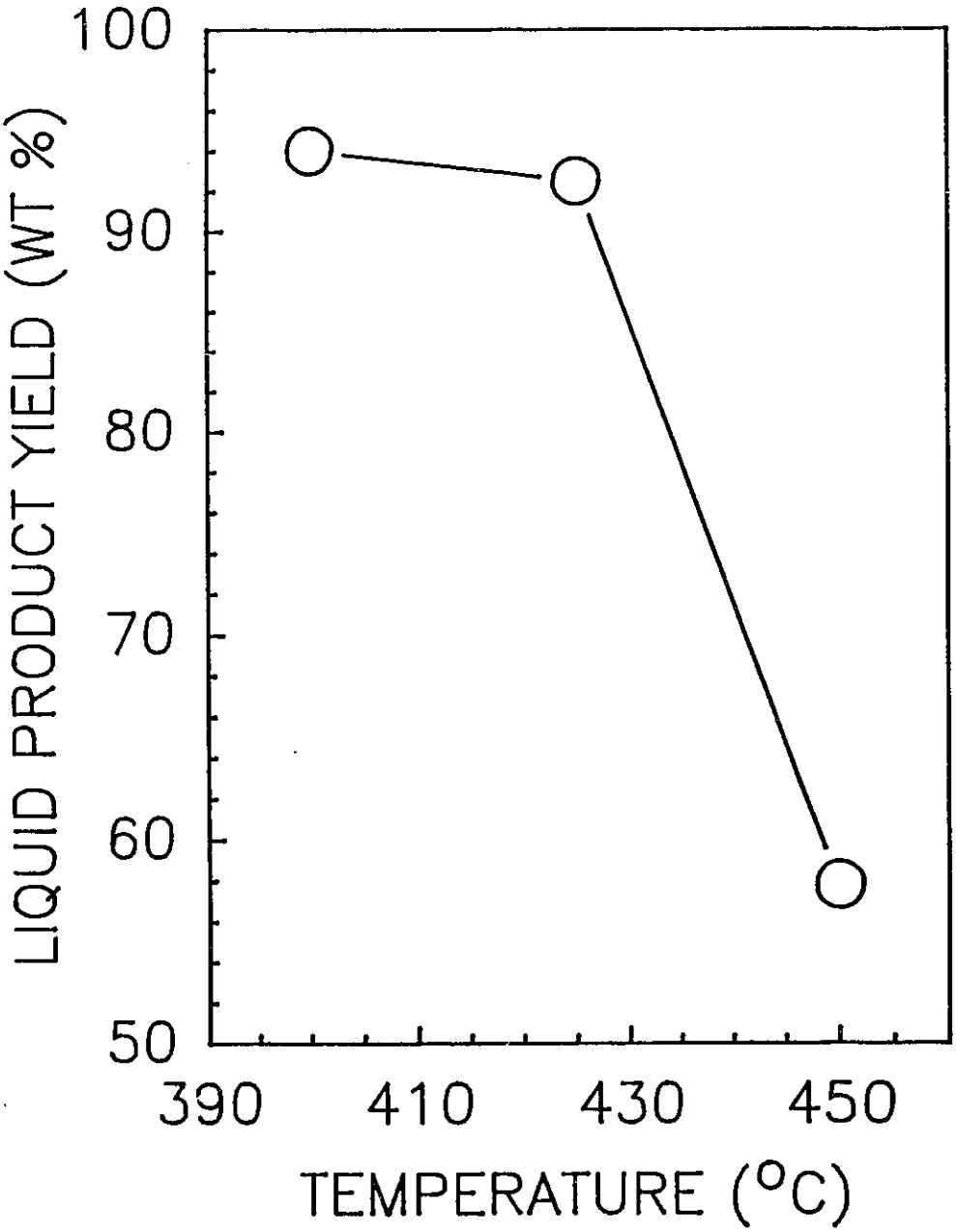

Figure 12: Liquid product yield (wt %) versus reaction temperature (°C) in non-catalytic hydrocracking reactions.

Figure 11 shows the liquid product density as a linear function of the reaction temperature. The results suggest that liquid product density decreases linearly with increasing temperature during non-catalytic hydrocracking of heavy oils. According to these results non-catalytic hydrocracking will have very little effect below 400°C. Previous studies (Soodhoo and Phillips, 1988) on non-catalytic hydrocracking of asphaltenes had shown that only a very small amount of gases (0-2 wt %) were produced below 400°C when the reaction time was less than ½ h. Other studies (Köseoglu and Phillips, 1988) on non-catalytic hydrocracking of Athabasca bitumen showed a total gas yield of less than 4 wt % at 375°C. The results of Figure 11 can be used to predict the temperature below which non-catalytic hydrocracking is ineffective. For this particular case extension of the correlation indicates that at 385°C the liquid product density would be the same as the feedstock density.

Figure 12 shows the liquid product yield as a function of temperature in non-catalytic hydrocracking. Between 400 and 425°C there was a very small decrease in liquid product yield. At 450°C the liquid product yield was 30 wt % lower than at 425°C. The decrease in liquid product yield was probably caused by increased cracking with more gases and coke being formed. Soodhoo and Phillips (1988) showed coke and gas formation increased very rapidly with temperature of the reaction when asphaltenes were non-catalytically hydrocracked. A substantial amount (about 30 g) of coke was observed in the reactor after the 3 non-catalytic reactions.

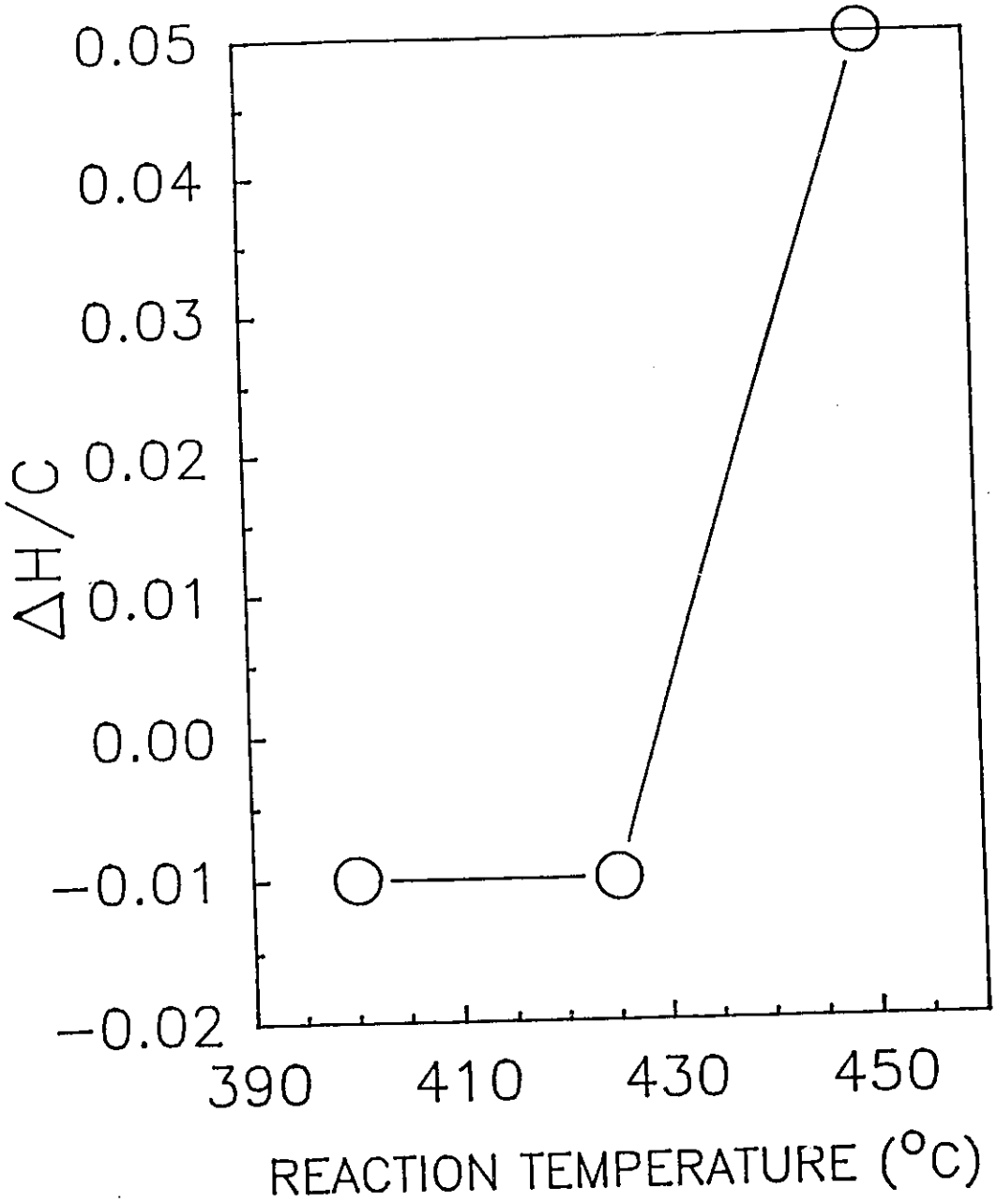

Figure 13: Change in hydrogen to carbon atomic ratio (Δ(H/C)) versus reaction temperature (°C) for non-catalytic reactions.

Figure 13 shows the change in hydrogen to carbon atomic ratio $\{\Delta(H/C) = (H/C_{out} - H/C_{in})\}$ between the liquid product and the Boscan heavy oil feedstock. After running the non-catalytic hydrocracking reactions at 400, 425, and 450°C the reactor had coke throughout the space between the stainless steel balls. Hydrogen transfer could occur from larger carbonaceous molecules (CM) to the cracked products. This could form liquids having an increased H/C atomic ratio and solid coke which would result in a decrease in liquid product yield. The decrease in $\Delta(H/C)$ at low temperature was presumably caused by cracking reactions which converted alkyl side chains to gaseous molecular fragments which were rich in hydrogen and liquid molecules poor in hydrogen. As the temperature was increased (from 425-450°C) there was more cracking, i.e., more larger CM were fragmented to form gas and lighter liquid molecules which were hydrogenated through hydrogen transfer reactions (higher H/C atomic ratio). Saturation of the products of the cracking reactions (free radicals) by hydrogen transfer from CM led to the condensation of some of the CM to form solid coke. Formation of gas and solid coke led to a decrease in the liquid product yield. Thermodynamically, the effect of temperature on the $\Delta(H/C)$ can be explained by the dehydrogenation-hydrogenation reaction equilibrium. In the absence of a catalyst most of the hydrogen consumption is through hydrogen transfer from the CM (Miki et al, 1983). When the temperature is increased there is more cracking and therefore more free radicals. The increase in hydrogen consumption by the free radicals shifts the equilibrium towards dehydrogenation of

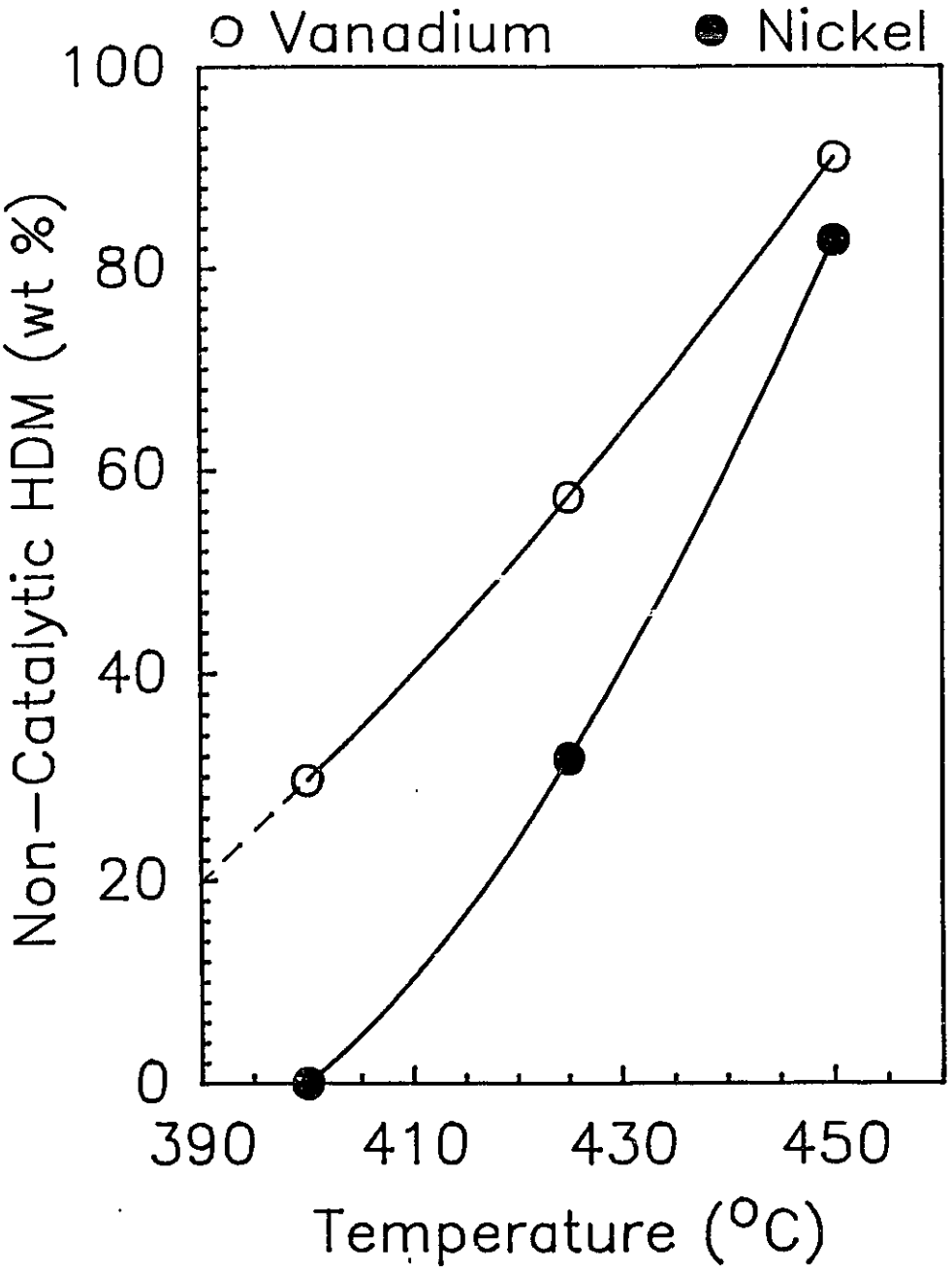

Figure 14: Metal conversion (wt %) versus reaction temperature (°C) in non-catalytic hydrocracking reactions. Open and solid circles represent vanadium and nickel respectively.

the CM, i.e., an increase in solid coke formation. A study by Wilson et al (1985) on the saturation of aromatics of a middle distillate fraction in the presence of a catalyst showed that the chemical equilibrium was shifted towards dehydrogenation with increasing temperature above 380°C. Although that was an entirely different system, the thermodynamics of this reaction are also expected to be affected by temperature in a similar way, given that other conditions remain equal.

There is no doubt about non-catalytic hydrocracking being different from thermal cracking. Results (Köseoglu and Phillips, 1988) on coke yield and asphaltene conversion showed that asphaltene conversion was much higher in thermal cracking than in non-catalytic hydrocracking. Furthermore, at the same asphaltene conversion, coke yield was much less in non-catalytic hydrocracking than in thermal cracking. The hydrogen gas participates by reacting with unsaturated products which can act as hydrogen acceptors. The coke yield decreases because hydrogen gas saturates the hydrogen deficient species (free radicals) that are produced by thermal cracking reactions. This hinders the condensation of hydrogen deficient species. In another words, hydrogen gas terminates reactions between free radicals, preventing them from forming coke.

Figure 14 shows the wt % of the nickel and vanadium removed as a function of the reaction temperature in non-catalytic hydrocracking. At 400°C no nickel was removed but about 30 wt % vanadium was removed. At 450°C the amounts removed were 91 wt % vanadium and 83 wt % nickel. Although a substantial amount of the metals can be removed at high temperature in non-catalytic hydrocracking, the liquid product yield is unacceptably low.

5.2 Catalytic Hydrocracking with Catalysts Containing an H-Mordenite Zeolite Component

The results obtained from the hydrocracking reaction experiments with catalysts containing an H-mordenite zeolite component are discussed in this section. The properties of the catalysts containing the H-mordenite zeolite component are given in Table 4. Each catalyst was tested at 400 and 450°C.

Figure 15 shows that the conversions of sulphur, nitrogen, and MCR decrease slightly as the H-mordenite content of the catalyst increases. The conversion results suggest that the zeolite has decreased the catalytic activity of the catalyst. It is known that surface acidity increases as the zeolite content of a catalyst increases (Barthomeuf, 1983; Benesi, 1967; Mishin **et al**, 1988; and Radchenko **et al**, 1983). It has also been reported that zeolite increases the interaction between Ni and Mo through the formation of surface aggregates (Sidel'kovskaya **et al**, 1988). The zeolite was expected to increase the acidity of the catalyst and consequently increase the conversions. Therefore some explanation for the results in Figure 15 was sought.

Figure 16 shows a substantial decrease in specific surface area of the catalysts (measured by mercury porosimetry) as the H-mordenite content is increased, especially above 5 wt %. Undoubtedly, the decreases in HDS, HDN, and MCR removal, shown in Figure 15, are related to the loss in the surface area available for the hydrocracking reactions and the decrease in the amount of the catalyst loaded in the reactor. The amount of the catalysts loaded in the reactor and the corresponding bulk densities are

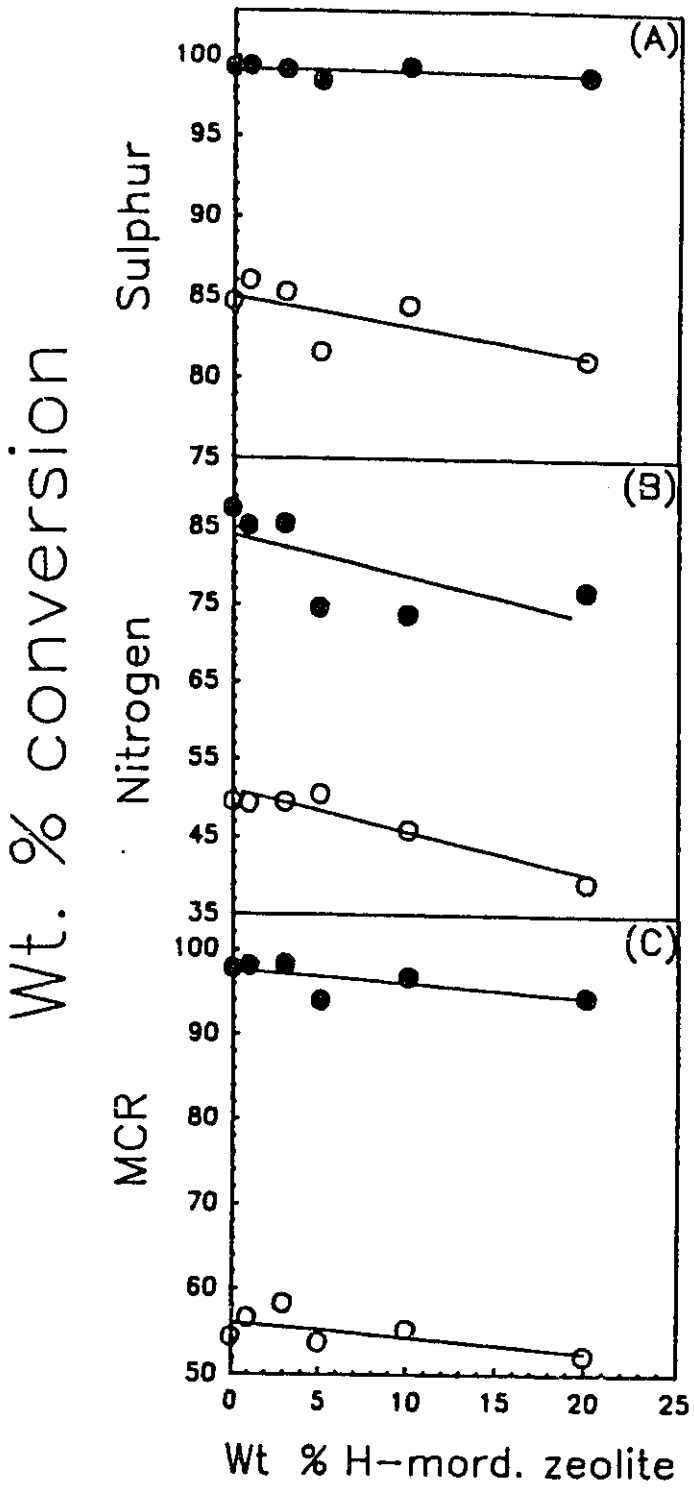

Figure 15: Conversion (wt %) versus H-mordenite zeolite content (wt %) of the catalyst. Figure 15A sulphur, Figure 15B nitrogen and Figure 15C micro carbon residue. Open and solid circles represent experiments at 400 and 450°C respectively.

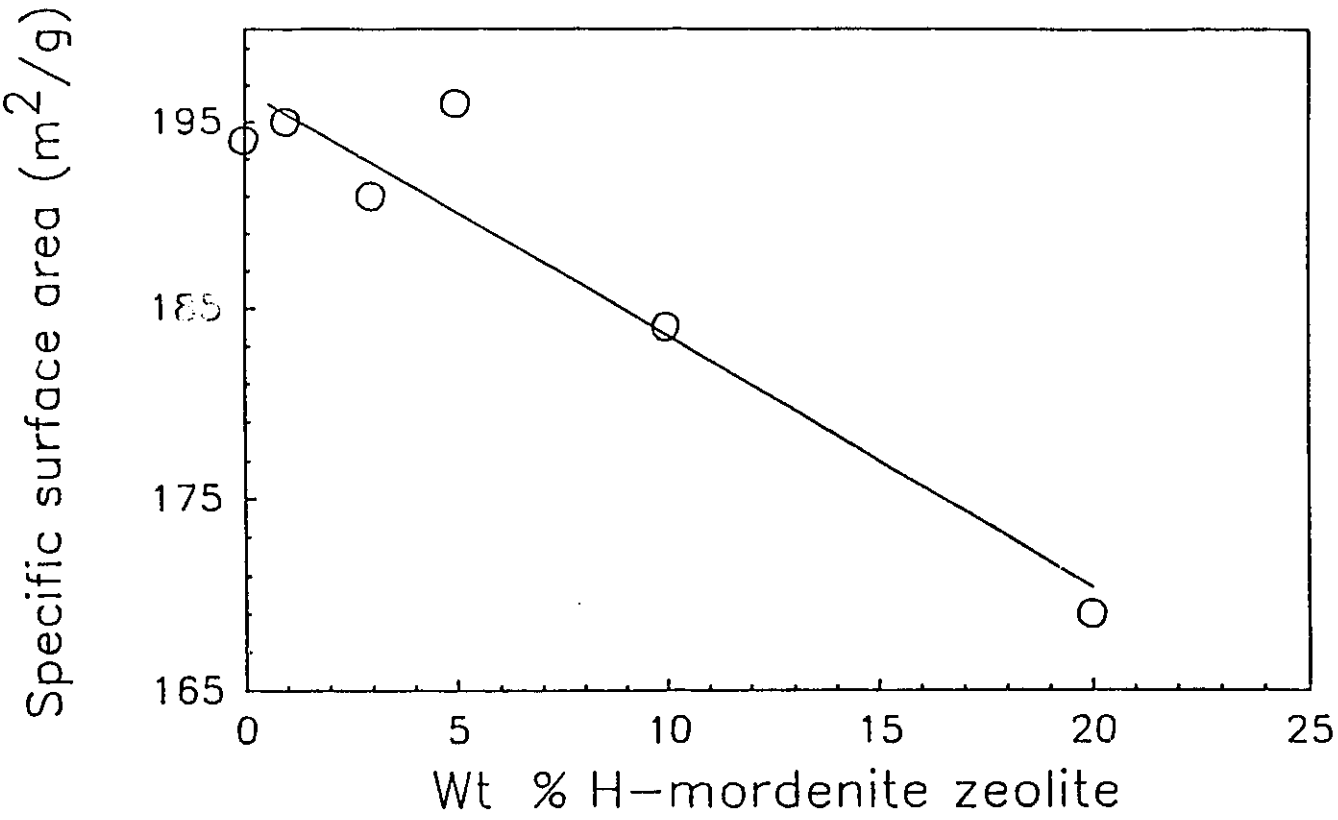

Figure 16: Specific surface area (m^2/g) versus catalyst H-mordenite zeolite content (wt %).

given in Table 4. The decrease in bulk density with the increasing catalyst H-mordenite zeolite content is also shown in Figure 19A.

Figures 17A and 17B show the mercury porosimetry curves for the catalyst with no H-mordenite and with 20 wt % H-mordenite respectively. At each pressure there are two curves. The smaller value of mercury volume corresponds to mercury penetrating the pore, whereas the greater value of mercury volume corresponds to mercury retracting from the pore. In all catalysts, the mercury could penetrate pores between 100 μm and 3 nm, at the pressures used with this equipment. From the mercury penetration curves, the pores can be divided into three regions of different sizes. The pore volumes in the regions of larger pores (d_p > 10 μm), medium pores (10 nm < d_p < 10 μm), and smaller pores (3 nm < d_p < 10 nm) are shown in Figure 18 and Table 4. Most of the pore volume in all cases is in the smaller range and it is almost the same in each case. For each region the catalysts with H-mordenite, Figure 19, have greater pore volume than the one without H-mordenite. The major difference between the catalysts with and without zeolite lies in the region of the medium pore range. The catalysts with H-mordenite have considerably more pore volume in this range. There is an increase in the total pore volume, caused by the increase in volume in the medium pores. The increase in medium pore volume occurred simultaneously with the decrease in the specific surface area of the catalysts shown in Figure 14, and with an increase in the median pore diameter shown in Table 4.

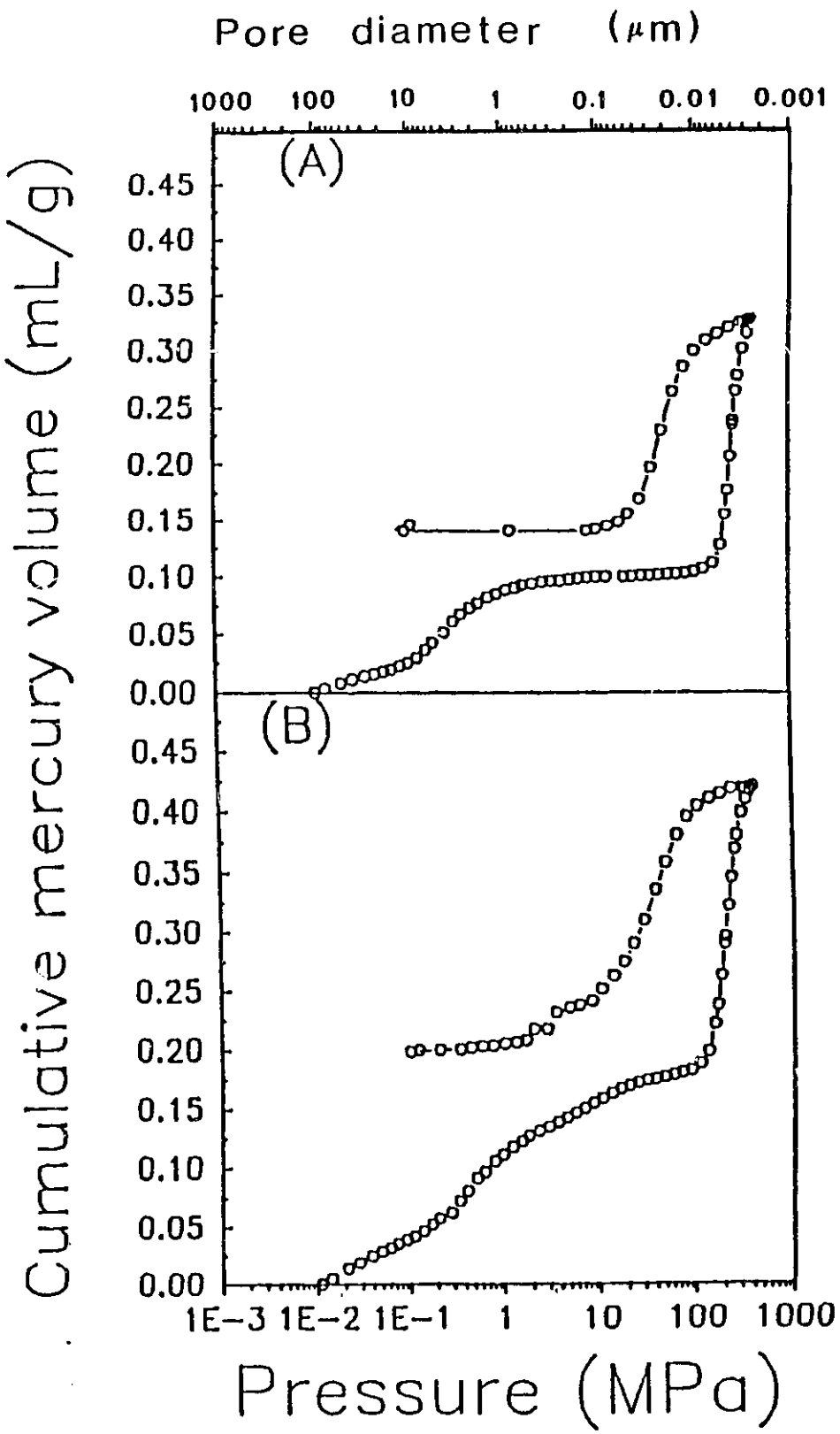

Figure 17: Cumulative mercury intrusion volume (mL/g) versus catalyst pore diameter (μm). A -a catalyst without zeolite and B -a catalyst with 20 wt % H-mordenite.

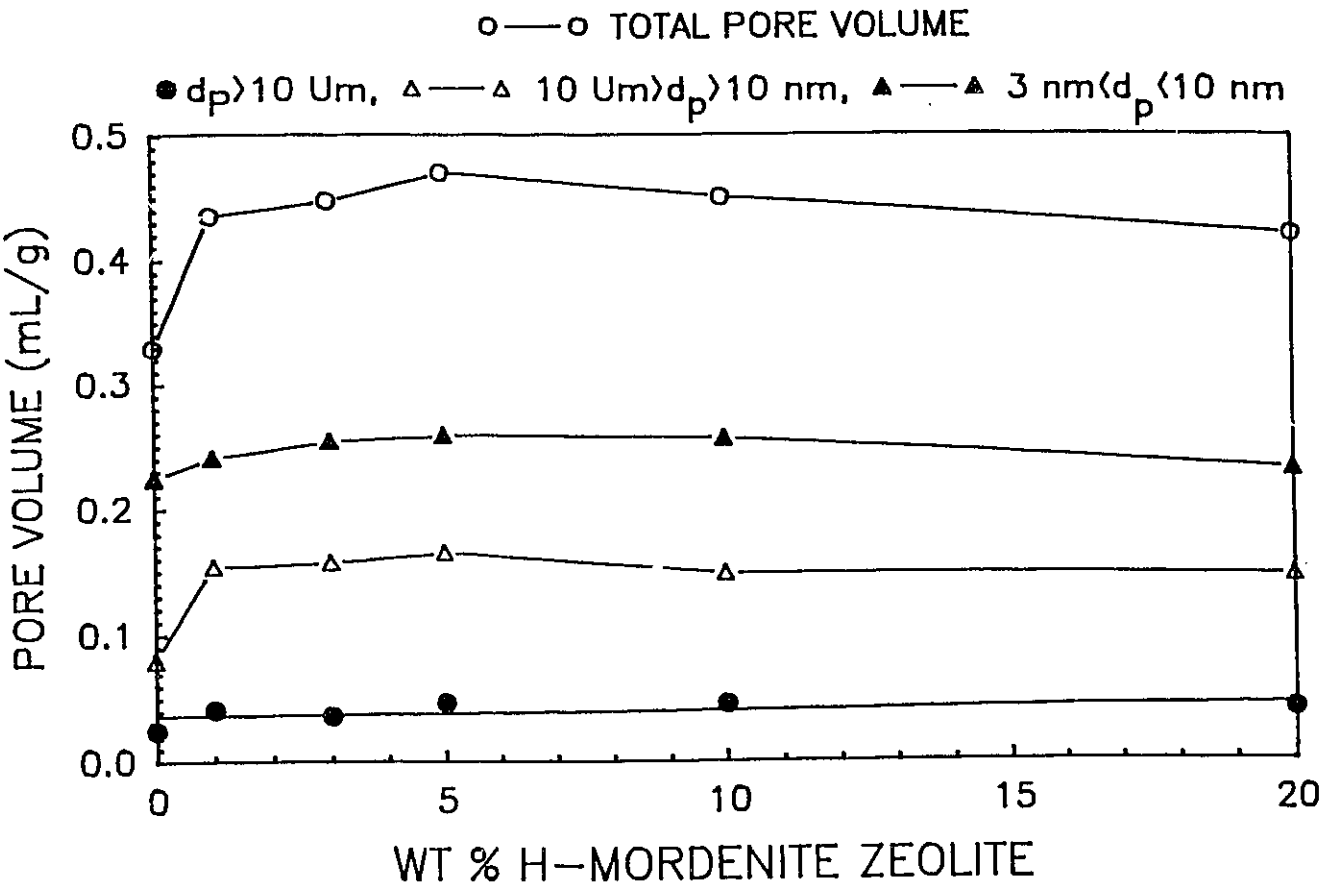

Figure 18: Pore volume (mL/g) versus H-mordenite zeolite content (wt %) of the catalyst. Open circles total pore volume, solid circles d_p > 10 μm, open triangles 10 μm>d_p>10 nm and solid triangles 3 nm<d_p<10 nm.

Figure 19A shows that the bulk density of the catalyst decreases as the H-mordenite content increases. The bulk density was obtained by measuring the weight of catalyst loaded into the 155 mL volume reactor. Thus, in addition to the decrease in specific surface area, there was also a decrease in amount of catalyst. The 10 wt % H-mordenite is an exception in that it deviates from the line in Figure 19A. The combined decrease in these two features, i.e., specific surface area (m^2/g) and the weight (g) of the catalyst loaded in the reactor, as the H-mordenite increased, caused a large decrease in the total catalyst surface area in the reactor. This undoubtedly contributed to the decrease in the overall conversion shown in Figure 15.

The decrease in the catalyst bulk density with increasing H-mordenite content was partially caused by the change in shape of catalyst extrudates. As the amount of H-mordenite in the catalyst increased, the cylindrical extrudate shapes became progressively rougher and particularly more curved in the longitudinal dimension. This caused a larger void space between the catalyst extrudates during packing, hence less catalyst was loaded into the reactor. Another contributing factor to the decrease in bulk density was the decrease in catalyst particle density with increasing catalyst H-mordenite content, as shown in Table 4 (section 3.5). This effect accounts for less than 20 % as compared to the 40 % decrease in bulk density shown in Figure 19A.

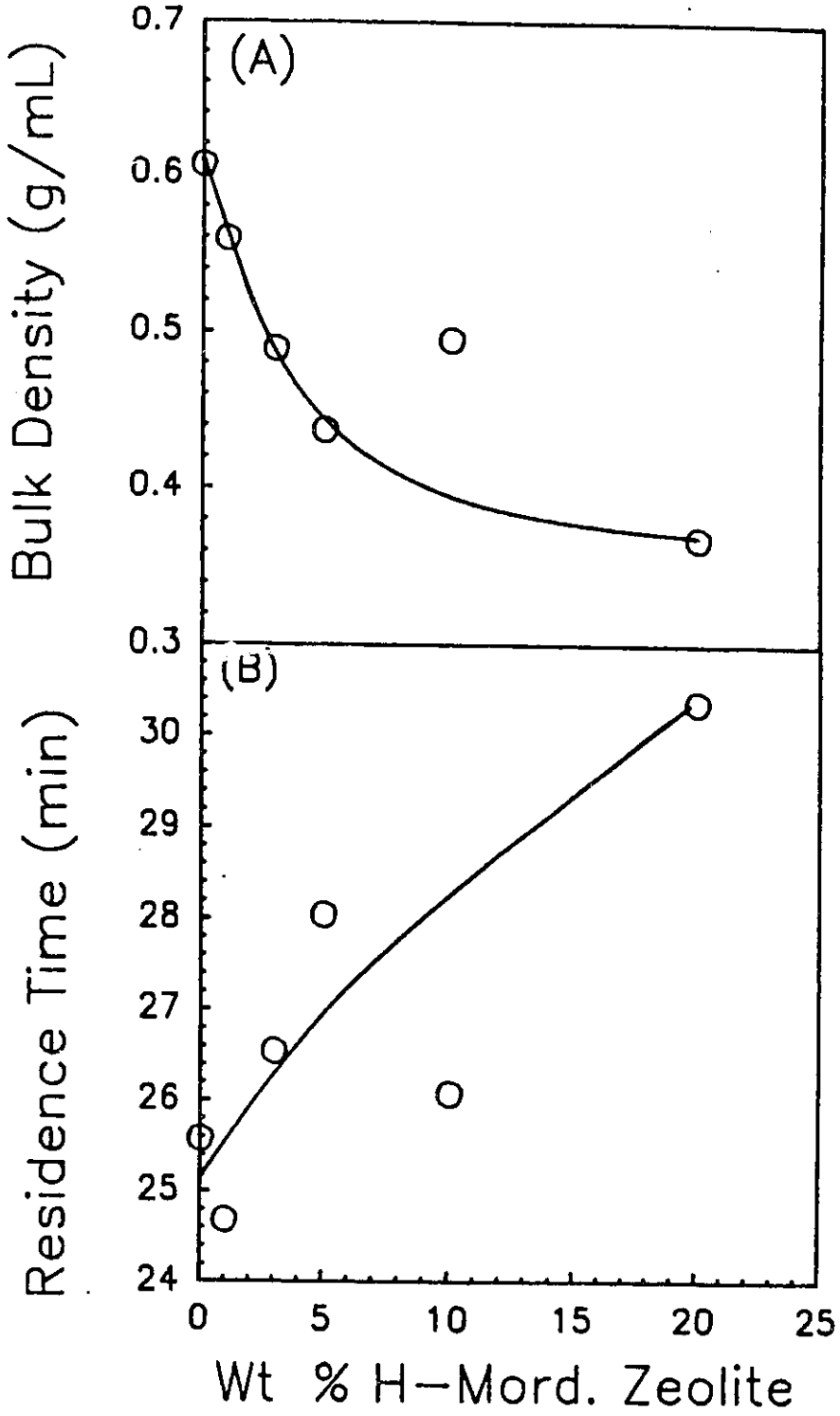

Figure 19: A -catalyst bulk density (g/mL) versus H-mordenite content (wt %) of the catalyst. B -apparent residence time in the reactor (min) versus H-mordenite content (wt %) of the catalyst.

The relative residence time of a molecule in the reactor was calculated from the void volume between the catalyst extrudates in the reactor. The space between the extrudates was calculated by dividing the catalyst weight in the reactor by the particle density of the extrudate given in Table 4. This value was subtracted from the total volume of the empty reactor to give the void volume in the reactor. Using the correlation of Reilly et al (1986) with the conditions in the reactor, a liquid hold-up of approximately 94 % was estimated (see Appendix-B). The void volume in the reactor was multiplied by the percent liquid hold-up to obtain the volume of liquid in the reactor. This was divided by the volumetric liquid flow rate (mass flow rate multiplied by liquid density) to obtain the relative residence time. The value used for density (0.78 g/mL) is typical of the average of the feedstock and liquid product densities at reaction conditions.

The relative residence times, shown in Figure 19B, increase with increasing H-mordenite content of the catalyst. In this case the 10 wt % H-mordenite catalyst also deviates from the curve. The increase in relative residence time is caused by the increase in void space between the catalyst extrudates in the reactor which results from the curvature of the extrudates mentioned earlier. Apparently the catalyst with 10 wt % H-mordenite packed more densely compared with the others. Since the nature of packing depends on the particle shape and size, the increase in void space between the catalyst extrudates is consistent with the difference in shape of the catalyst extru-

dates that was observed with increasing H-mordenite content.

To examine the effect of decrease in specific surface area and the amount of catalyst loaded in the reactor, the PTOF (section 2.5) was calculated for each catalyst. The results in Figure 20 show that the PTOF increases with increasing H-mordenite content. However, the 10 wt % H-mordenite points again deviate from the curves. Nevertheless, this general trend in Figure 20 indicates that when the results are compared on a unit catalyst surface area basis, the mordenite component enhances the reactions.

Figure 21 shows the increase in PTOF with increasing residence time. Of interest here is the 10 wt % H-mordenite catalyst (relative residence time = 26 min) which is much closer to the curve in Figure 21 than in Figures 19 and 20. Figure 21 suggests that the increase of PTOF might have been caused by the increase in residence time. However this suggestion is not correct because it has been shown theoretically in Section 2.6, by Equation 11 and Figure 7, that the PTOF must decrease with increasing residence time.

To eliminate the issue of residence time, the PTOF's were divided by their corresponding residence times. In Figure 22, the PTOF per unit residence time (PTOF/θ) increases with increasing H-mordenite content. Despite the theoretical decrease in PTOF caused by the increased residence time, a reasonable increase in PTOF/θ was obtained with the increasing H-mordenite content in the catalysts. This phenomenon suggests that H-mordenite had enhanced the activity of the catalysts.

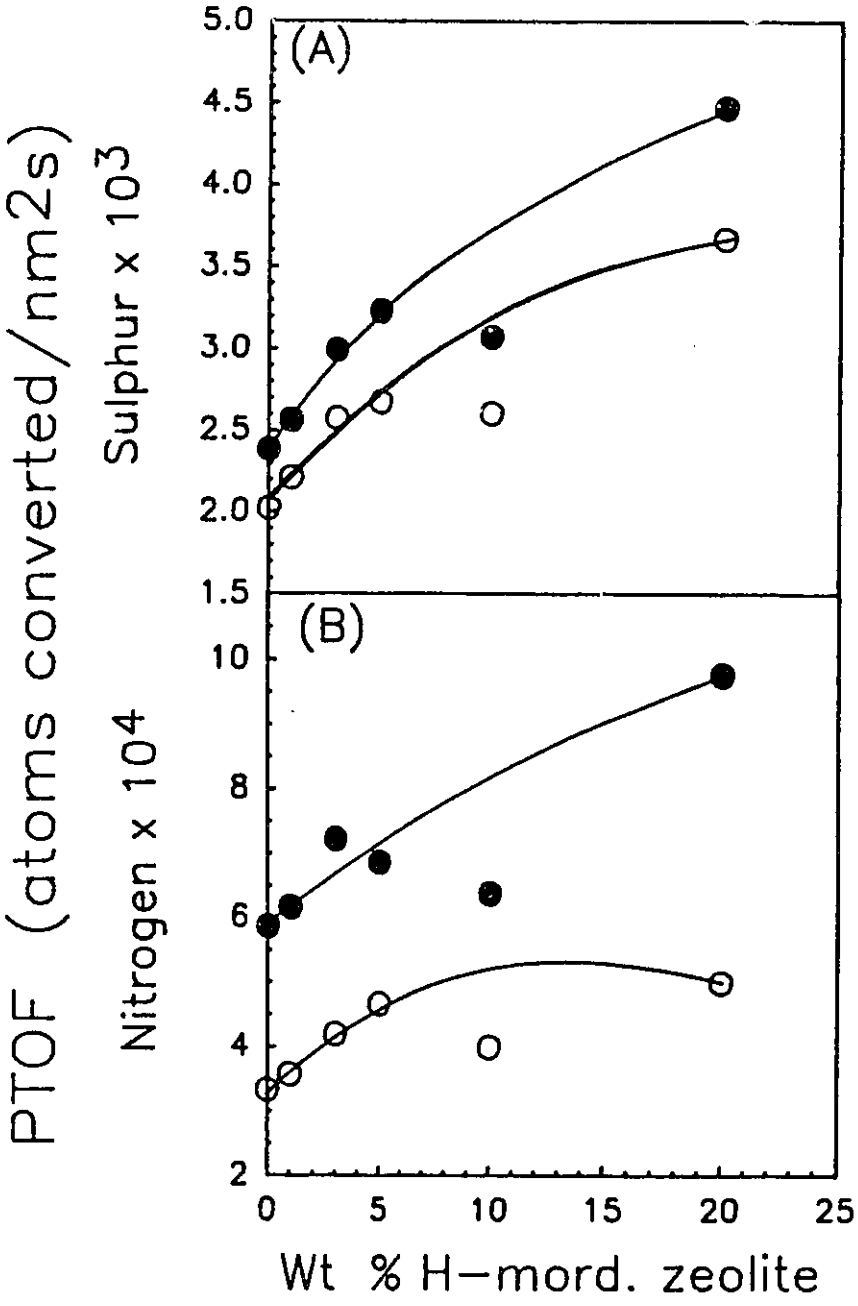

Figure 20: Pseudo turnover frequency (atoms S or N removed $nm^{-2}s^{-1}$) versus H-mordenite zeolite content (wt %) of the catalyst. Figure 17A sulphur and Figure 17B nitrogen. Open and solid circles are for the experiments at 400 and 450°C respectively.

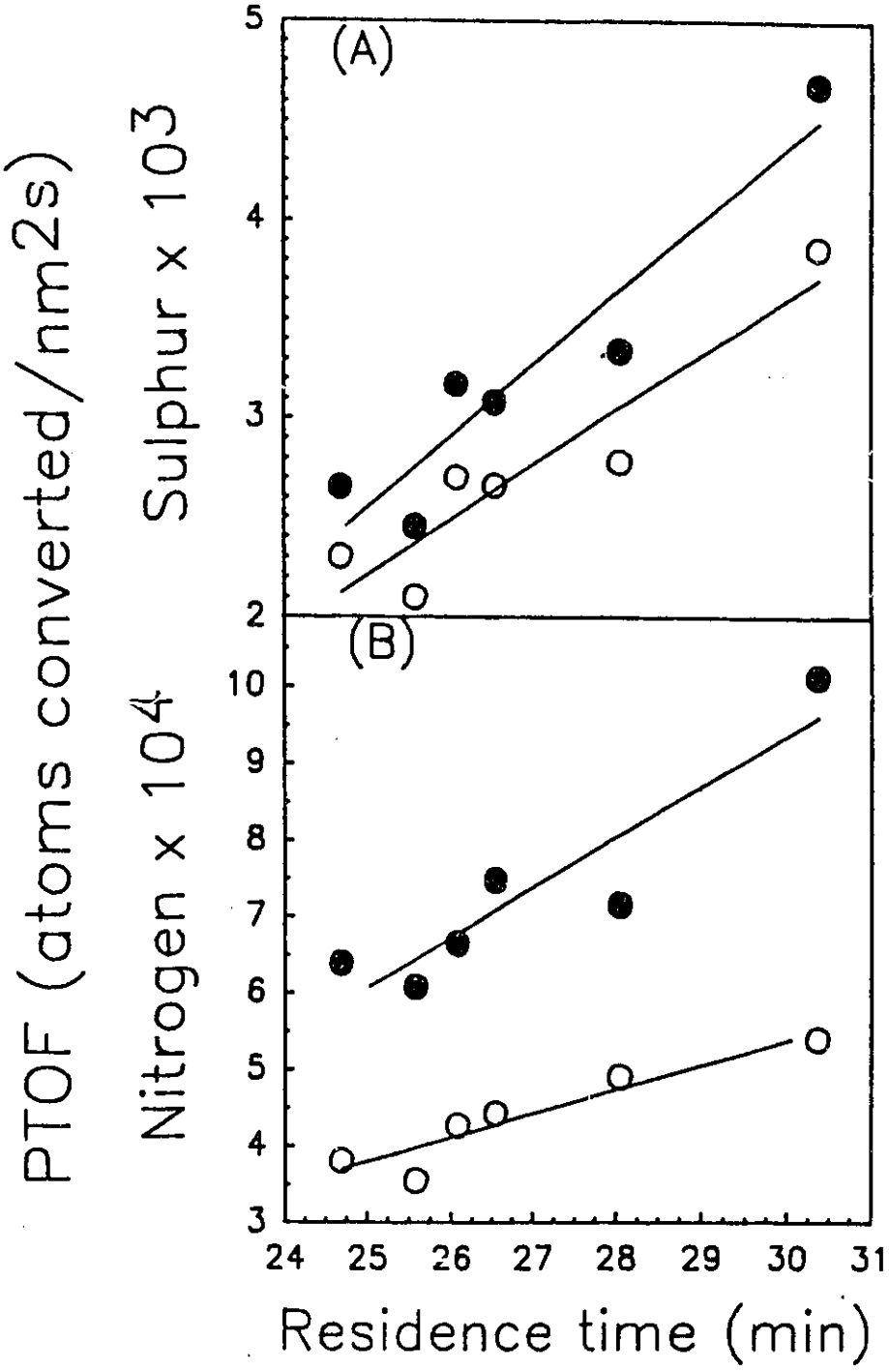

Figure 21: Pseudo turnover frequency (atoms S or N removed $(nm)^{-2}s^{-1}$) versus apparent residence time in the reactor (min). Figure 21A sulphur and Figure 21B nitrogen. Open and solid circles represent experiments at 400 and 450°C respectively.

A few laboratory studies have been reported in the literature in which zeolites were used in hydroprocessing (Kircho **et al**, 1982; Maxwell, 1987; Sambi and Mann, 1989; Vázquez **et al**, 1988a; and Vázquez **et al**, 1988b). In these studies the Brønsted acidity of zeolites increased cracking and hydroconversion. A Ni/W/zeolite Y catalyst has been reported (Maxwell, 1987) to have a higher conversion to products boiling below 300°C than amorphous aluminosilicate-based catalyst ($Ni/W/SiO_2.Al_2O_3$). Sambi and Mann (1989) reported that 25 wt % REY zeolite was optimum for $NiO-MoO_3$ catalysts. Hence, decrease in conversion in our case was probably caused by the substantial decrease in catalyst surface area.

The molecules used in this study are too large to enter the pores of H-mordenite. Therefore it is likely that the reaction sites on the external surfaces of the H-mordenite crystals are responsible for the beneficial effect shown in Figure 20. Gas oil molecules are also too large to enter the pores of the zeolites used in FCC catalysts. In this case the enhanced reaction rate is also attributed to reaction sites on the external surface of the zeolite crystals (Wojciechowski and Corma, 1986). The increase in acidic sites on zeolite catalysts used for hydrotreating coal distillates has been investigated (Kirchko **et al**, 1982). In that study, HDS rates were greater with catalysts having a HY zeolite component than with non-zeolite catalysts. Other workers (Radchenko **et al**, 1983) have

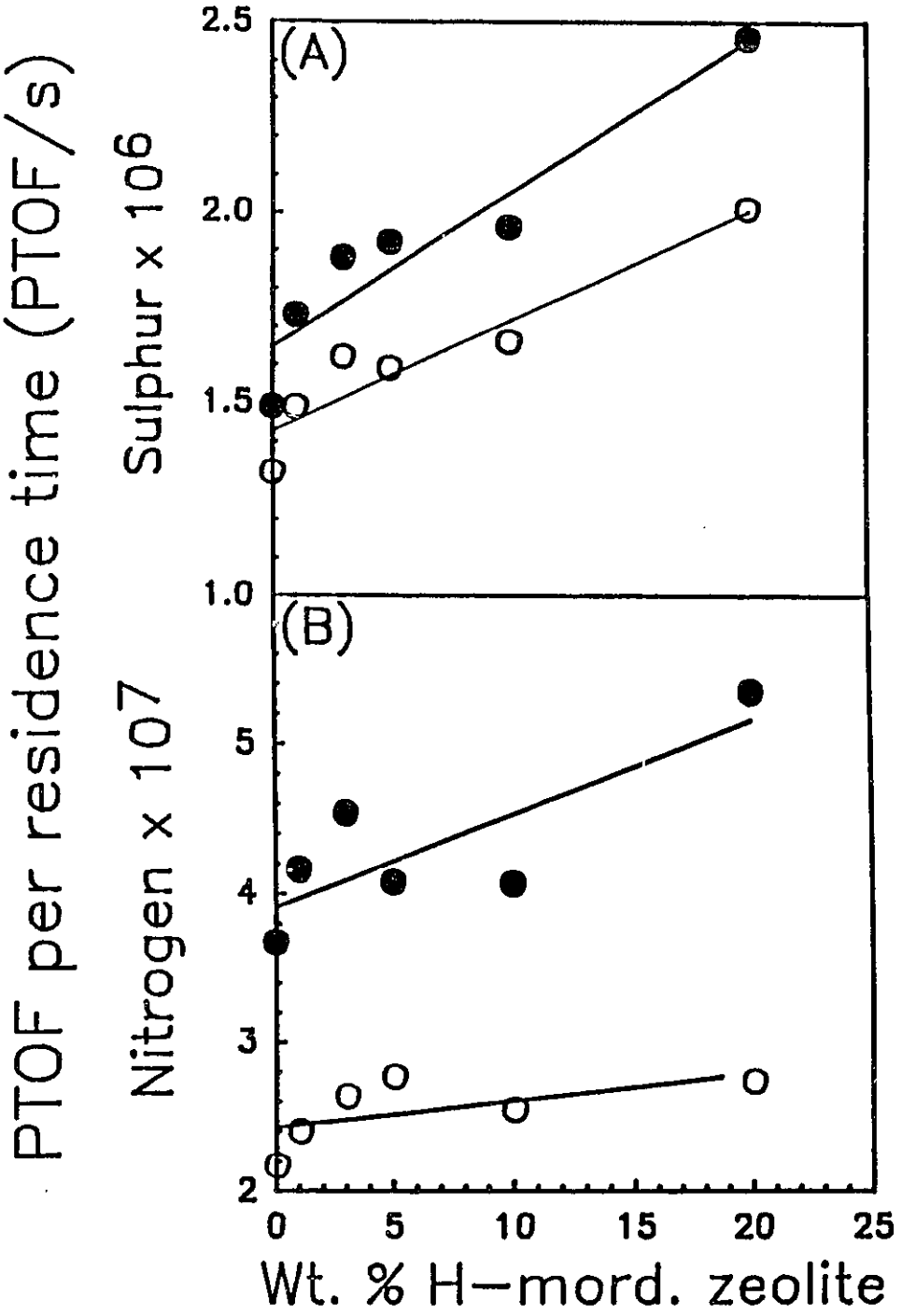

Figure 22: Pseudo turnover frequency per residence time (atoms S or N removed $(nm)^{-2}s^{-2}$) versus H-mordenite content (wt %) of the catalyst. Figure 22A sulphur and Figure 22B nitrogen. Open and solid circles represent experiments at 400 and 450°C respectively.

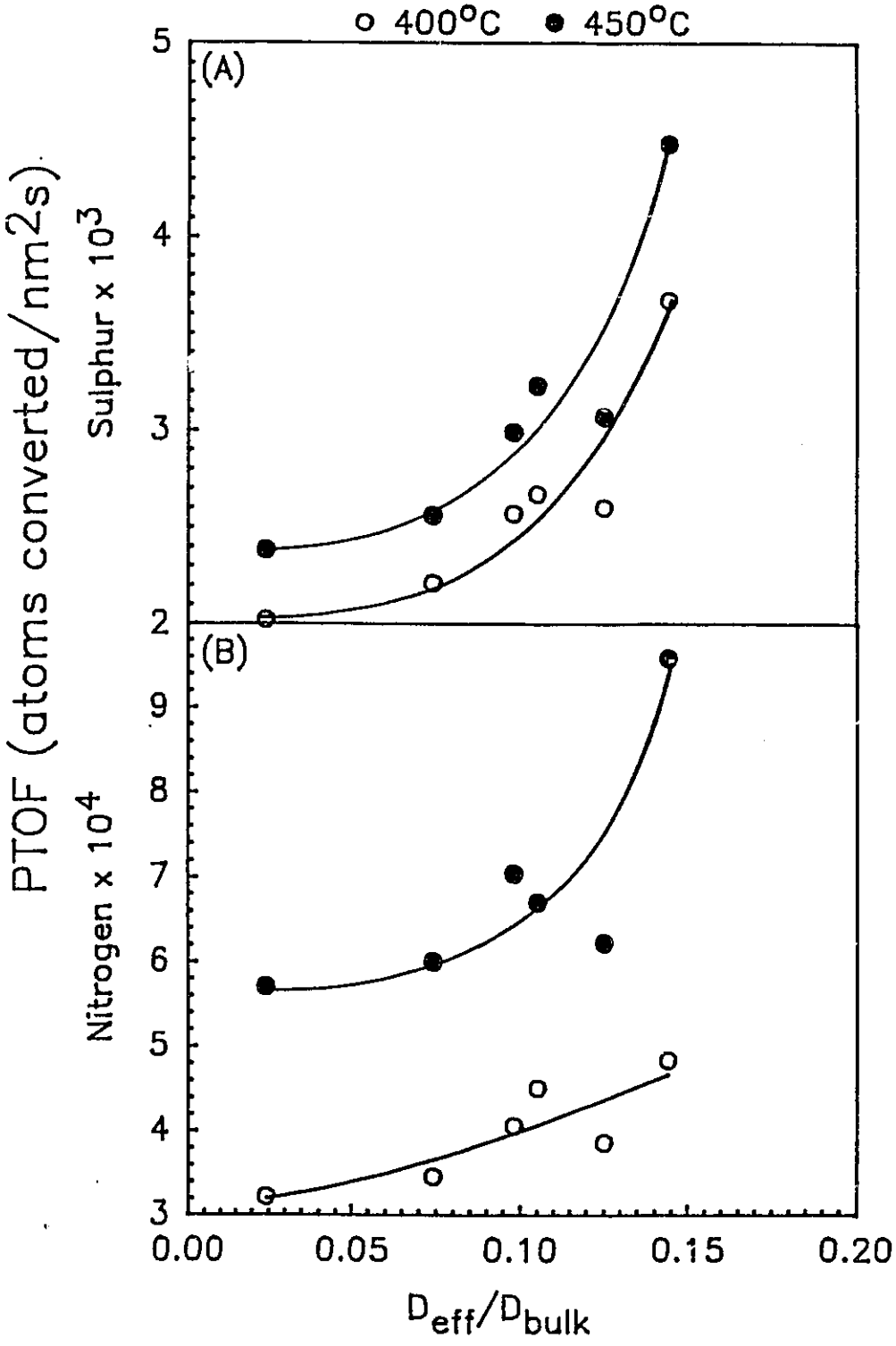

Figure 23: Pseudo turnover frequency (atoms S or N removed $(nm)^{-2}s^{-1}$) versus the ratio of the effective diffusivity to the bulk diffusivity (D_{eff}/D_B). Figure 23A sulphur and Figure 23B nitrogen. Open and solid circles represent experiments at 400 and 450°C respectively.

found an increase in catalyst acid centres as a function of zeolite content. This is consistent with the increased acidity of the catalysts used in this study as the H-mordenite increased. The catalyst acidity was determined experimentally by benzofuran TPD (section 2.1.5).

There is a modest increase in median pore diameter with catalyst H-mordenite content as shown in Table 4. The possible influence of diffusion was considered by calculating D_{eff}/D_B using the equation developed by Ternan (1987) (Equation 3, Section 1.5.9). Measurements of heavy oil molecular diameters have been made by viscosity (Kyriacou **et al**, 1988b), neutron diffraction (Ravey **et al**, 1988), membrane diffusivity (Kyriacou **et al**, 1988a), and X-ray diffraction (Speight, 1980) studies. Based on the above findings, it was decided to use a molecular diameter of 4 nm which is typical of values obtained by viscosity measurements. Using the pore diameters in Table 4, and the r_m of 2 nm , the values of λ were calculated. Using these values of λ and p equal to 2 (Ternan, 1987), the ratios D_{eff}/D_B were obtained from Equation 3.

If pore diffusion was controlling the reaction, PTOF would increase with increasing d_p, since D_{eff} would also increase with d_p. PTOF would increase with D_{eff}/D_B and eventually level out at d_p values large enough to eliminate restrictions in diffusion caused by pore size. The shape of such a curve is totally different from the shape of the curves obtained from the experimental results (Figure 23). PTOF remains almost unaffected when D_{eff}/D_B changes by a factor of 5, from 0.02 to 0.1 (small

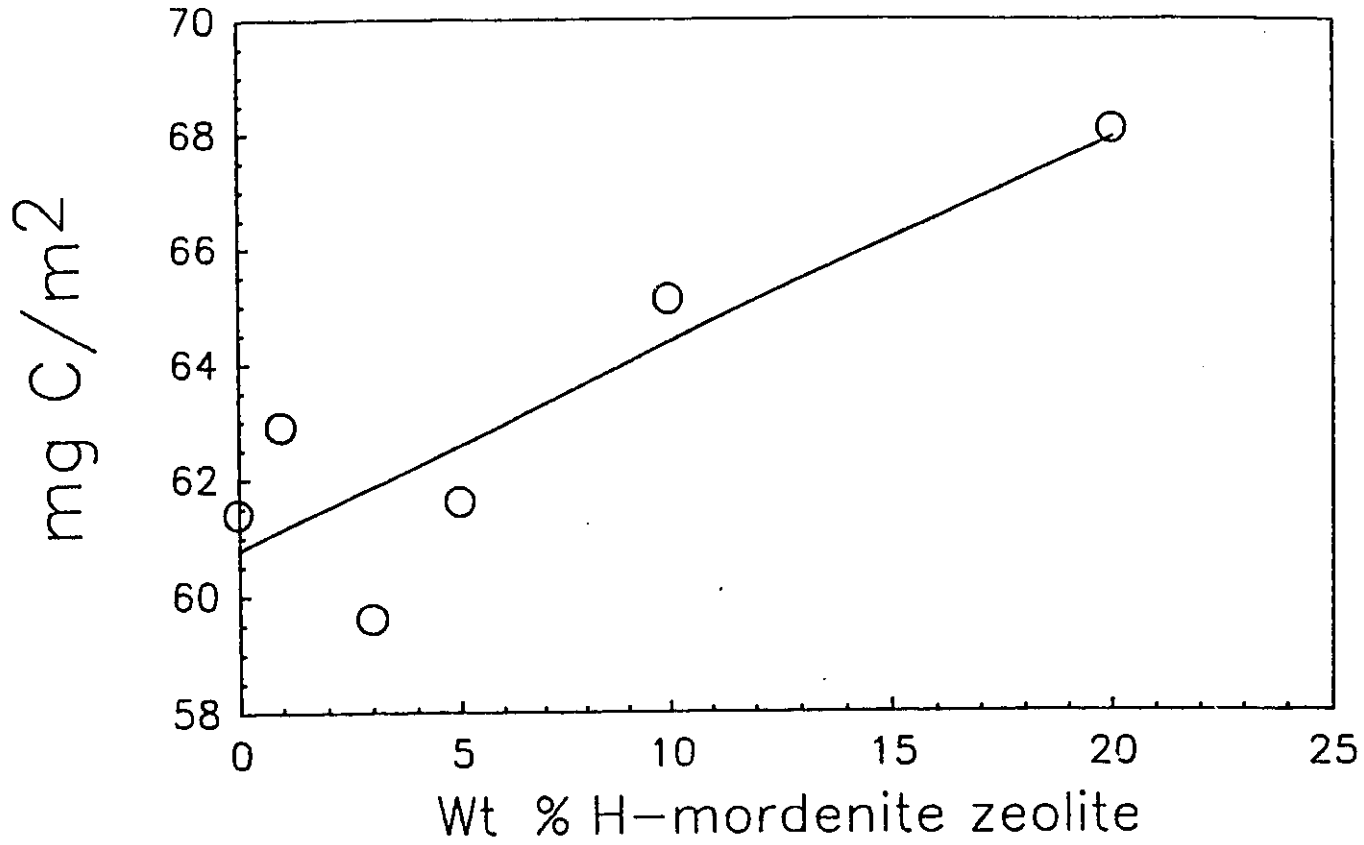

Figure 24: Amount of carbon deposited per unit surface area of the catalysts (mg C/m^2) versus catalyst H-mordenite zeolite content (wt %).

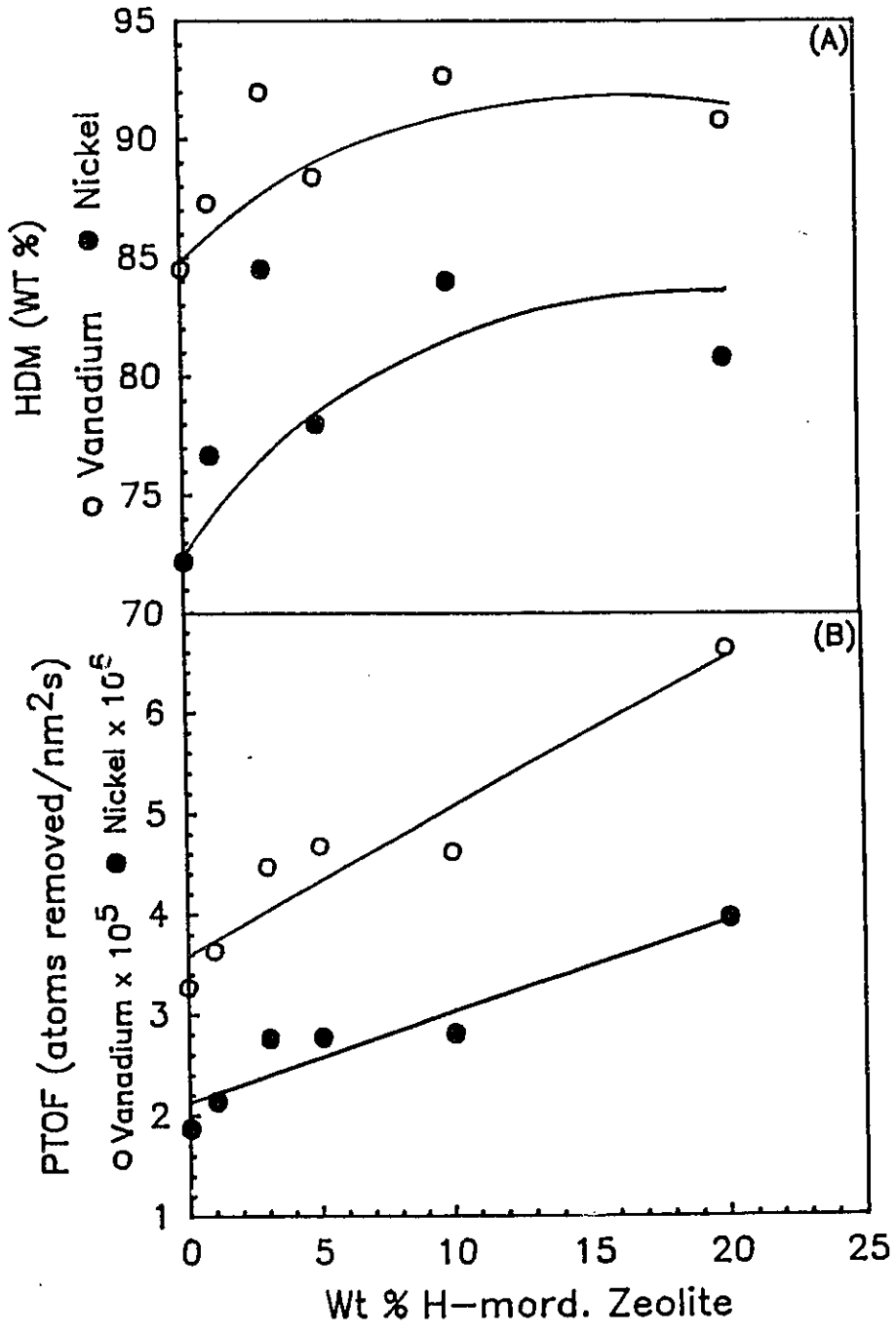

Figure 25: A - metal conversion (wt %) versus H-mordenite zeolite content (wt %) of the catalyst. B - Pseudc turnover frequency (atoms V or Ni removed $(nm)^{-2}s^{-1}$) versus H-mordenite zeolite content (wt %) of the catalyst. Open and solid circles represent vanadium and nickel respectively. All experiments at 400°C.

change of H-mordenite content, 0-5 wt %). It showed a remarkable increase when D_{eff}/D_g changed only from 0.1-0.14 (large change in H-mordenite content, 5-20 wt %). These results suggest that the chemical contribution (increased acid sites) of the mordenite caused the effect and that diffusion was not the major controlling factor of the reactions.

Figure 24 shows that the amount of carbon deposited on the catalyst increases with the H-mordenite content of the catalyst. It is possible that both the increase in the carbon deposition shown in Figure 24, and the increase in reaction shown in Figure 22 may be caused by the increased number of acidic sites in the catalyst that are located on the exterior surface of the H-mordenite crystals.

Figure 25A shows the wt % of nickel and vanadium removed at 400°C as the amount of H-mordenite was increased in the catalyst. These results clearly show an improved catalyst HDM as the amount of zeolite is increased in the catalyst. Figure 25B shows the corresponding PTOF for the metals removal given in Figure 25A as a function of the catalyst H-mordenite content. In this case a considerable increase in PTOF was obtained as the catalyst H-mordenite content was increased. Addition of H-mordenite had increased the amount of metal removed by about 10 wt %, and almost doubled the PTOF (Figure 25B). Calculation of the PTOF/θ showed a similar trend to that of Figure 22, i.e, an increase in PTOF/θ despite the increased residence time. Note that Section 2.6 explained that an increase in residence time could cause a

decrease in PTOF. It is obvious that, the addition of the H-mordenite component to the catalyst increases the conversion of the organo-metallic nickel and vanadium complexes that are in the heavy oil. Since the organo-metallic molecules are too large to enter the micropores of the mordenite structure, it is suggested that the acid sites on the external surfaces of the zeolite crystals were responsible for the increased conversion.

The activity of the catalysts for HDS, HDN, and MCR removal (Figure 15) can be compared with HDM activity (Figure 25A). Clearly the additional acid sites had a greater effect on HDM than on HDS, HDN and MCR removal. The increase in the overall metal conversion, while sulphur, nitrogen, and MCR overall conversions decreased, suggests that the mechanism by which the organo-metallic molecules interact with the catalysts in HDM reactions was probably much different from the HDS and HDN reactions. The increased zeolite in the catalyst favoured the conversion of the organo-metallic molecules despite the decrease in the total catalyst surface area in the reactor.

5.3 Catalytic Hydrocracking with Catalyst Containing an HY Zeolite Component

The results obtained from the hydrocracking reaction experiments with the catalysts containing an HY zeolite component are discussed in this section. The properties of the catalysts containing the HY zeolite component are given in Table 5. Hydrocracking reaction experiments with these catalysts were carried out at temperatures of 400 and 370°C.

Figure 26 shows a slight increase in HDN, HDS and MCR removal as the HY content is increased in the catalysts. This is probably caused by the addition of surface acid centres to the catalyst by HY zeolite. Many studies (Benesi, 1967; Haynes,Jr., 1978; Barthomeuf, 1983; Radchenko **et al**, 1983; Maxwell, 1987; and Abbot and Wojciechowski, 1989) have indicated the presence of Brønsted acid centres in HY zeolite.

Figure 27 shows that the total surface area and the bulk density of the catalysts in the reactor decreased as the HY zeolite content increased. Although the total catalyst surface area decreased (Figure 27A) a slight increase in the catalytic activity (Figure 26) was observed suggesting an improvement in the catalysts by the addition of HY zeolite. Radchenko **et al** (1983) investigated the presence of Brønsted acid centres in hydrocracking catalysts containing up to 20 wt % HY zeolite. They found that even after 320 h in use, the Brønsted acid centres were still present in the catalyst.

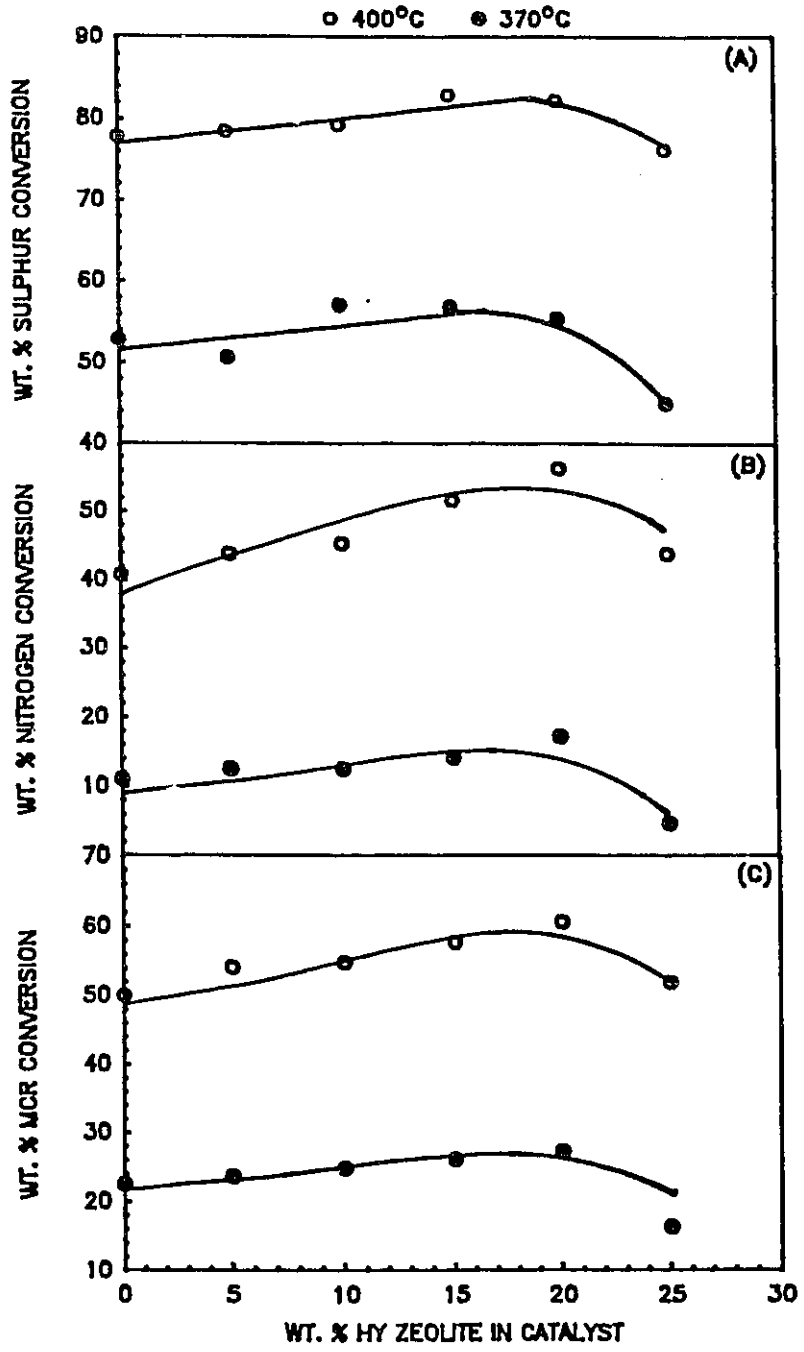

Figure 26: Conversion (wt %) versus HY zeolite content (wt %) of the catalyst. Figure 26A sulphur, Figure 26B nitrogen and Figure 26C micro carbon residue. Open and solid circles represent experiments at 400 and 370°C respectively.

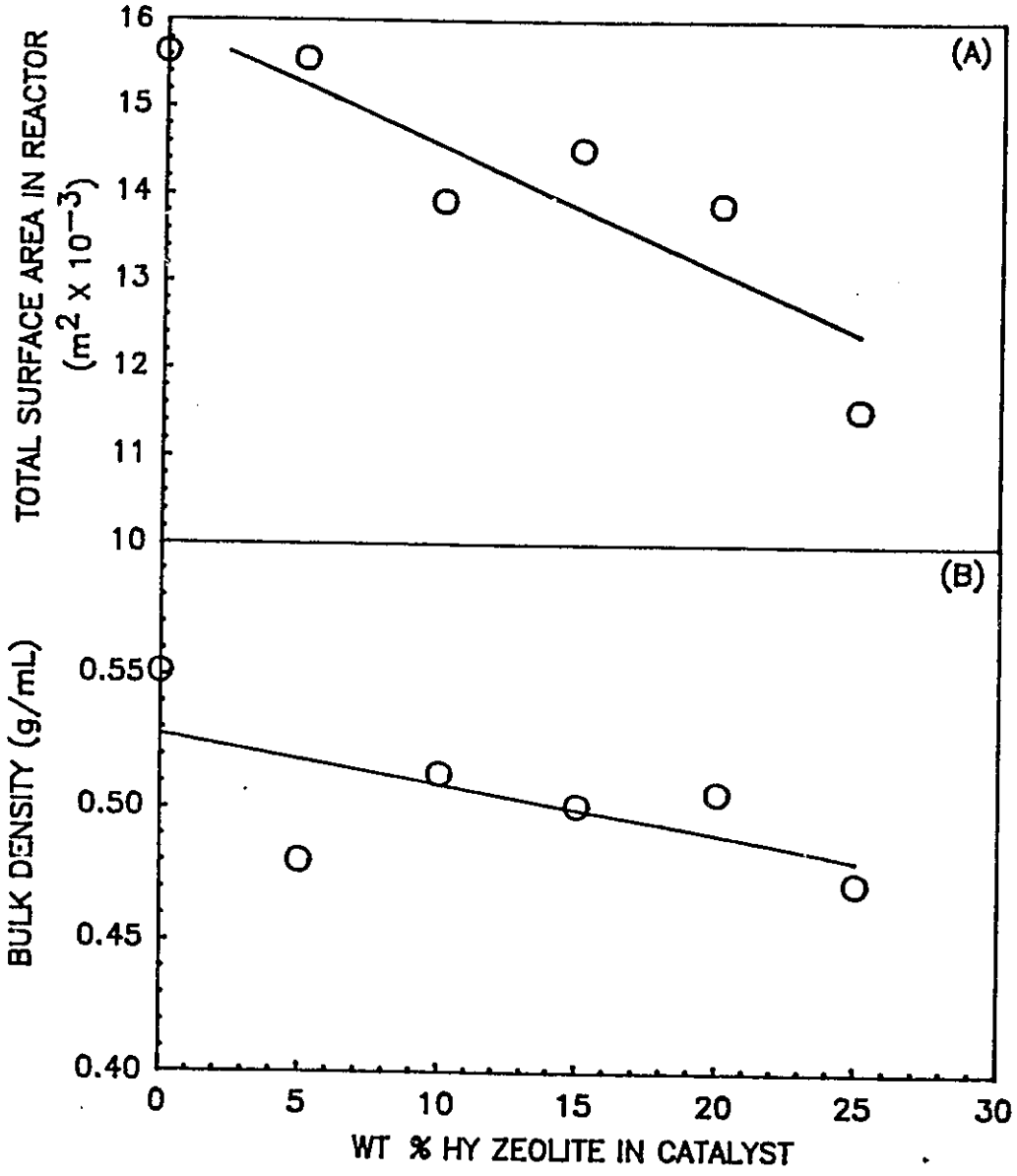

Figure 27: A -total surface area in the reactor (m^2) versus HY zeolite content (wt %) of the catalyst. B -catalyst bulk density (g/mL) versus HY zeolite content (wt %) of the catalyst.

Figure 28 shows the calculated PTOF as a function of increasing HY zeolite content in the catalysts. Like H-mordenite, HY zeolite also shows an improvement in the performance of the catalysts. Both Figures 26 and 28 suggest that 20 wt % HY in the catalyst is probably an optimum. Above 20 wt % HY both nitrogen conversion and nitrogen PTOF start to decrease. Sulphur conversion declines above 20 wt % HY but the sulphur PTOF, especially at 400°C, increased continuously, even up to 25 wt % HY zeolite content in the catalyst. At 370°C, the sulphur PTOF levels out between 15 and 25 wt % HY zeolite. These results are similar to those obtained by Sambi and Mann (1989) discussed in section 5.2.

The effect of the relative residence time on the PTOF is shown in Figure 29. The residence time in this case did not vary greatly. It ranged from 26.2 to 28.6 min with the highest and the lowest residence time occurring with the 5 and 20 wt % HY containing catalysts respectively. The results of Figure 29 have the same trend as those in Figures 26 and 28. This suggests that the small difference in residence time had no major effect on the activity of the catalysts discussed in Figures 26 and 28.

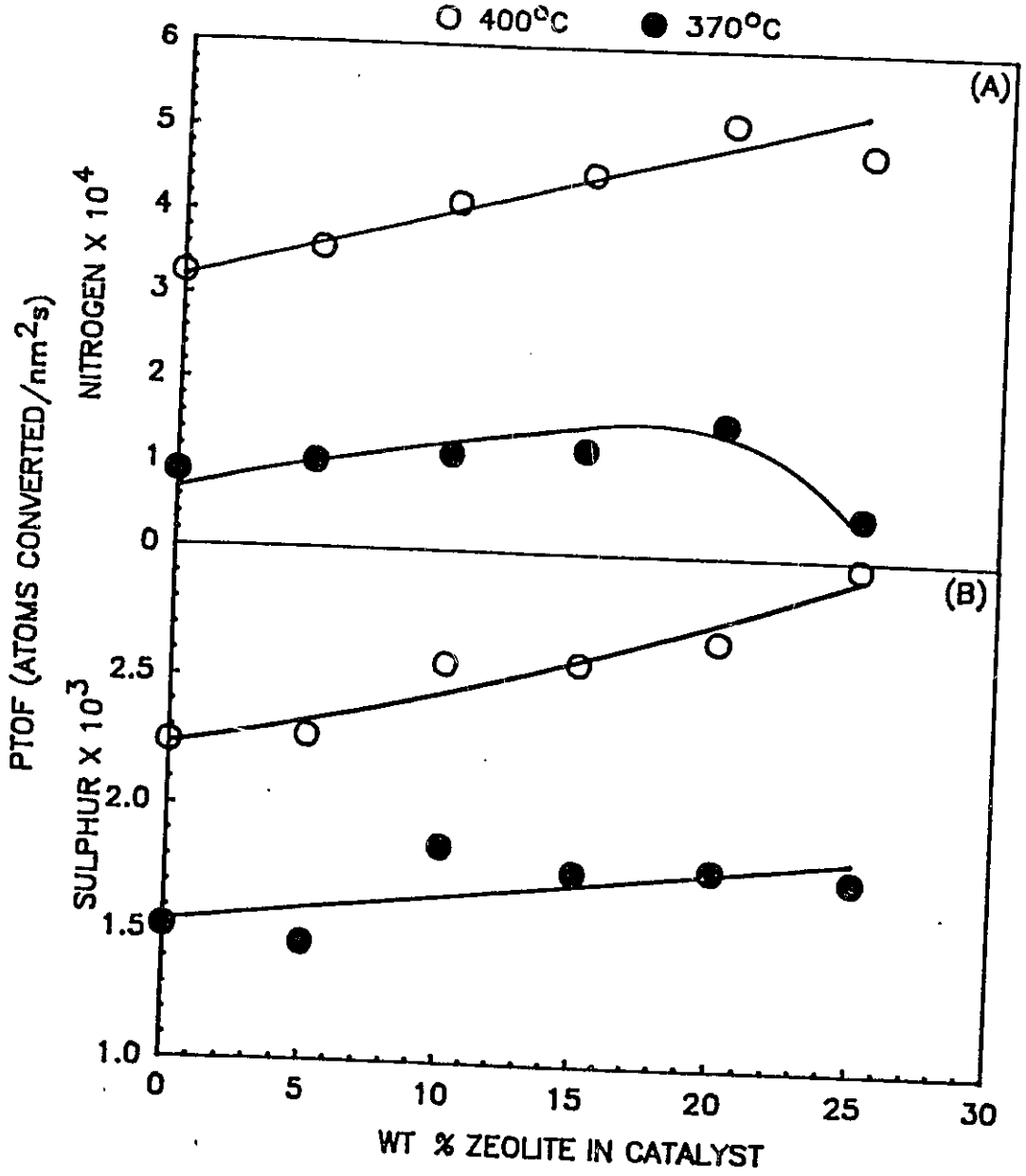

Figure 28: Pseudo turnover frequency (atoms S or N removed $(nm)^{-2}s^{-1}$) versus HY zeolite content (wt %) of the catalyst. Figure 28A nitrogen and Figure 28B sulphur. Open and solid circles are for the experiments at 400 and 370°C respectively.

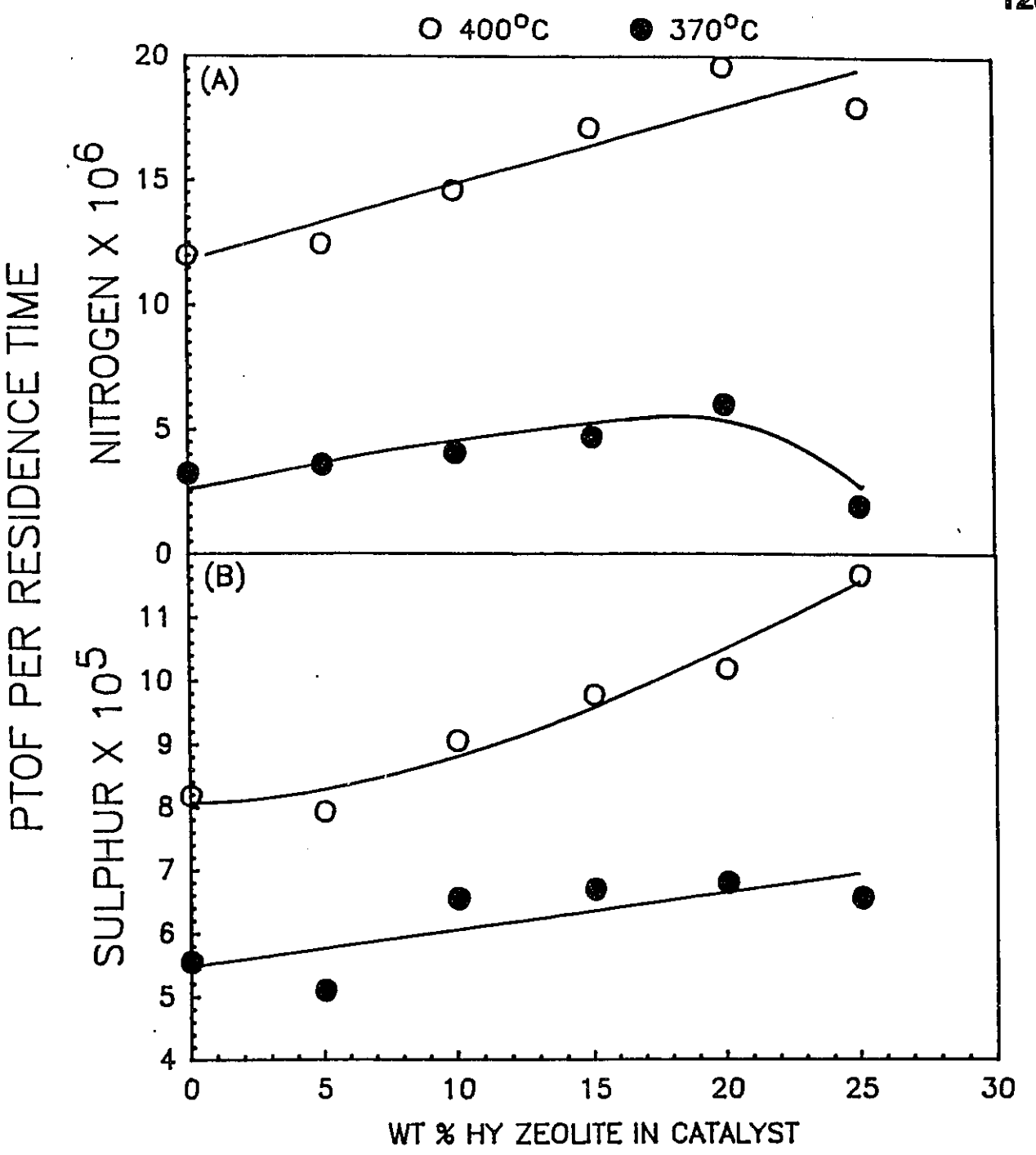

Figure 29: Pseudo turnover frequency per residence time (atoms S or N removed $(nm)^{-2}s^{-2}$) versus HY content (wt %) of the catalyst. Figure 29A sulphur and Figure 29B nitrogen. Open and solid circles represent experiments at 400 and 370°C respectively.

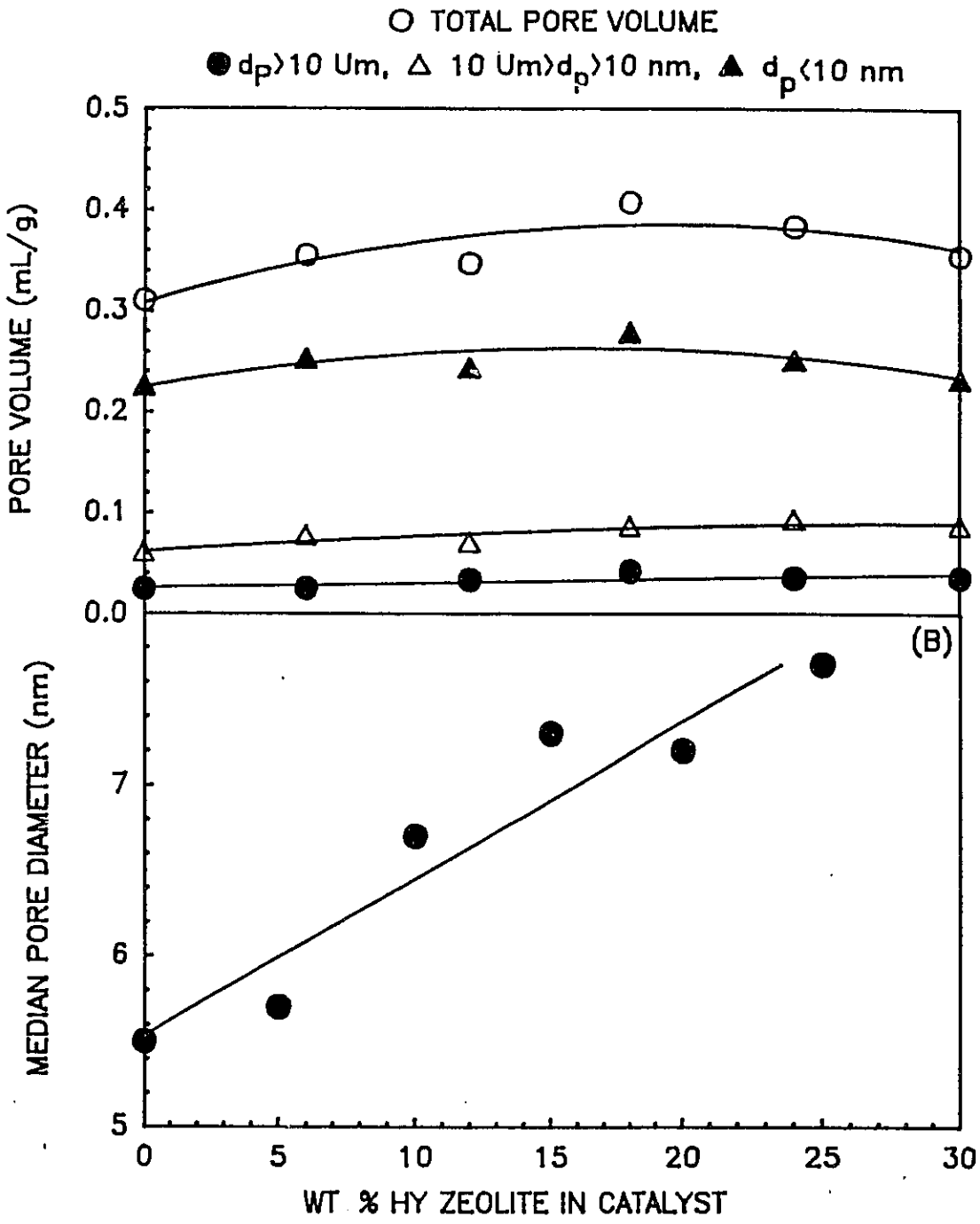

Figure 30: A - catalyst pore volume (mL/g) versus HY zeolite content (wt %) of the catalyst. Open circles are for total pore volume, solid circles for d_p > 10 μm, open triangles for 10 μm > d_p > 10 nm, and solid triangles for 3 nm < d_p< 10 nm. B - median pore diameter (nm) versus HY zeolite content (wt %) of the catalyst.

Figure 30 shows the effect of HY zeolite on the pore volume distribution and the median pore diameter. There is a very slight increase in pore volume, especially from 0 to 15 % HY zeolite. The median pore diameter increases from 5.5 nm for the catalyst with no HY to 7.7 nm for the catalyst with 25 wt % HY zeolite. Calculation of D_{eff}/D_B based on Equation 3 showed no trend which would suggest that changes in diffusion with increased HY zeolite content had a major influence on the catalytic activity.

The amount of coke left on the spent catalyst reflects the number of acid sites on the catalysts. Figure 31 shows the amount of carbon per unit area of the catalyst as a function of increasing HY zeolite in the catalyst. The increase in coke on the catalysts as HY zeolite content increased suggests that the addition of HY zeolite to the catalysts increased the number of acid sites in the catalysts. Probably the increased Brønsted acid centres increased the cracking reactions of the catalysts, causing more coke to be formed. Rustamov **et al** (1988) suggested that strong Brønsted acid sites were responsible for coke formation in a zeolite-containing aluminosilicate cracking catalyst. The increased acid centres in HY, catalysts as measured by the benzofuran TPD, is probably the cause of the increased coke in the catalyst (Figure 31) and the increased conversions shown in Figure 26 and Figure 32.

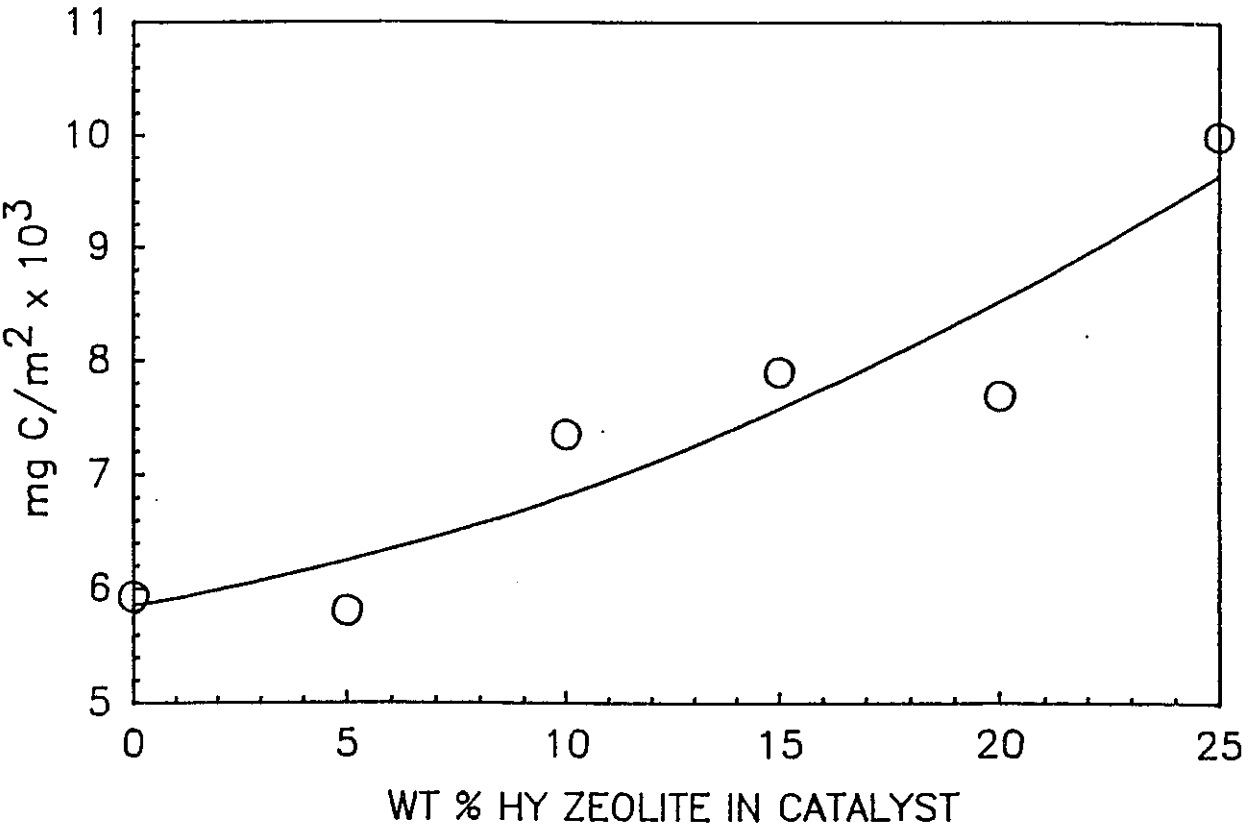

Figure 31: Amount of carbon deposited per unit surface area of the catalysts (mg C/m^2) versus catalyst HY zeolite content (wt %).

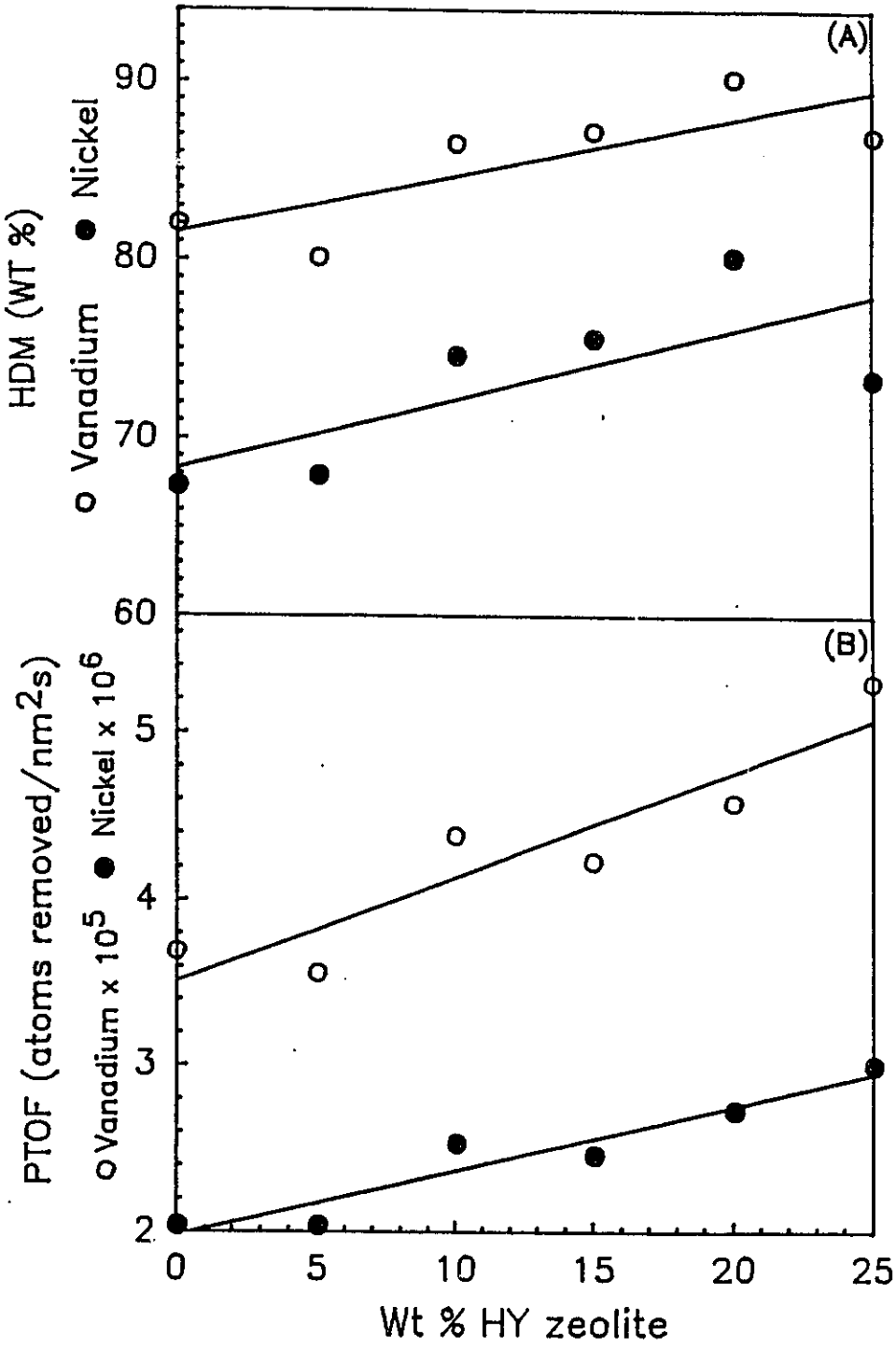

Figure 32: A - metal conversion (wt %) versus HY zeolite content (wt %) of the catalyst. B - Pseudo turnover frequency (atoms V or Ni removed ($nm^{-2}s^{-1}$) versus HY zeolite content (wt %) of the catalyst. Open and solid circles represent vanadium and nickel respectively. All experiments at 400°C.

Figure 32A shows the increase in wt % of nickel and vanadium metals removed as a function of the catalyst HY zeolite content at 400°C. Again in this case, there was a decrease in HDM with the catalyst containing 25 wt % as compared to that with 20 wt %. On the other hand, the PTOF for metals removal, Figure 32B, shows a continuous increase up to 25 wt % HY zeolite in the catalyst. The decrease in conversion with catalyst containing 25 wt % HY zeolite was probably caused by the loss in the total surface area in the reactor. The increased HDM with catalysts containing an HY zeolite component suggests also that there was an increased catalyst acidity caused by the addition of HY zeolite.

These results have shown that, the addition of HY zeolite to the $CoO-MoO_3-Al_2O_3$ hydrocracking catalyst increased the activity of the catalyst. Figure 26 shows the increased HDS and HDN while Figure 28 shows the increased PTOF both with increasing HY zeolite in the catalyst. Figure 32 shows that both the HDM conversion and the metal PTOF increased with increased HY zeolite in the catalysts. The increased catalyst activity with increasing catalyst HY zeolite content was largely caused by the increased number of acid sites in the catalysts.

5.4 Comparison Between Non-Catalytic Hydrocracking and Catalytic Hydrocracking

The results showing the sulphur, nitrogen and MCR removal for non-catalytic hydrocracking, catalytic hydrocracking with catalysts containing an H-mordenite component and the others containing an HY component are shown in Figure 10, 15 and 26 of sections 5.1, 5.2 and 5.3 respectively. These results show that at 400°C, sulphur conversion is about 5 times higher in catalytic hydrocracking than in non-catalytic hydrocracking. There was no nitrogen conversion at 400°C in non-catalytic hydrocracking, while there was about 40 wt % nitrogen conversion in catalytic hydrocracking. The MCR removal at 400°C in catalytic hydrocracking was about 7 times higher than in non-catalytic hydrocracking. At 450°C the catalytic sulphur conversion was 1.6 times higher than in non-catalytic conversion, while nitrogen and MCR conversions were about 1.3 times higher in catalytic cracking than in non-catalytic cracking. It is obvious from these results that catalysts produce higher hydrocracking conversion at much lower temperatures. Not to be forgotten are the higher liquid product yields which are obtained at higher conversion in catalytic hydrocracking. For example, while sulphur conversion of 61 wt % at 450°C in non-catalytic hydrocracking had liquid product yield of 58 wt %, a liquid product yield of 84 wt % and sulphur conversion of 98 wt % was obtained in catalytic hydrocracking at the same temperature.

Figure 33 shows the effect of temperature on sulphur, nitrogen, MCR, nickel and vanadium conversions in catalytic hydrocracking with a catalyst without a zeolite component. The results show two types of slopes: sulphur and vanadium conversion correlations have similar slopes of about 0.6, while nitrogen, MCR and nickel conversion correlations have similar slopes of about 1.0. These kinds of correlations are very useful because they can provide estimates of the temperature at which a desired conversion can be obtained. Comparing the effect of temperature on sulphur, nitrogen and MCR conversions in catalytic hydrocracking (Figure 33) and the non-catalytic conversions (Figure 10), non-catalytic conversion correlations have slopes of about 1.2 which turns out to be higher than those in catalytic hydrocracking. The non-catalytic metal conversions (Figure 14) also show a much greater increase in metal removal with increasing temperature than in catalytic hydrocracking (Figure 33). Despite the greater increase in conversion with temperature for non-catalytic hydrocracking, at any particular temperature catalytic hydrocracking produces higher conversions than non-catalytic hydrocracking. The higher conversions in catalytic hydrocracking are caused by the much higher hydrogenation rates in catalytic hydrocracking than in non-catalytic hydrocracking. These results are consistent with the results by Miki **et al** (1983), who found that the consumption of hydrogen gas in the presence of a catalyst was four times larger than in the absence of a catalyst. Therefore, the use of a catalyst helps the saturation of unsaturated compounds and makes the bonds easier to cleave.

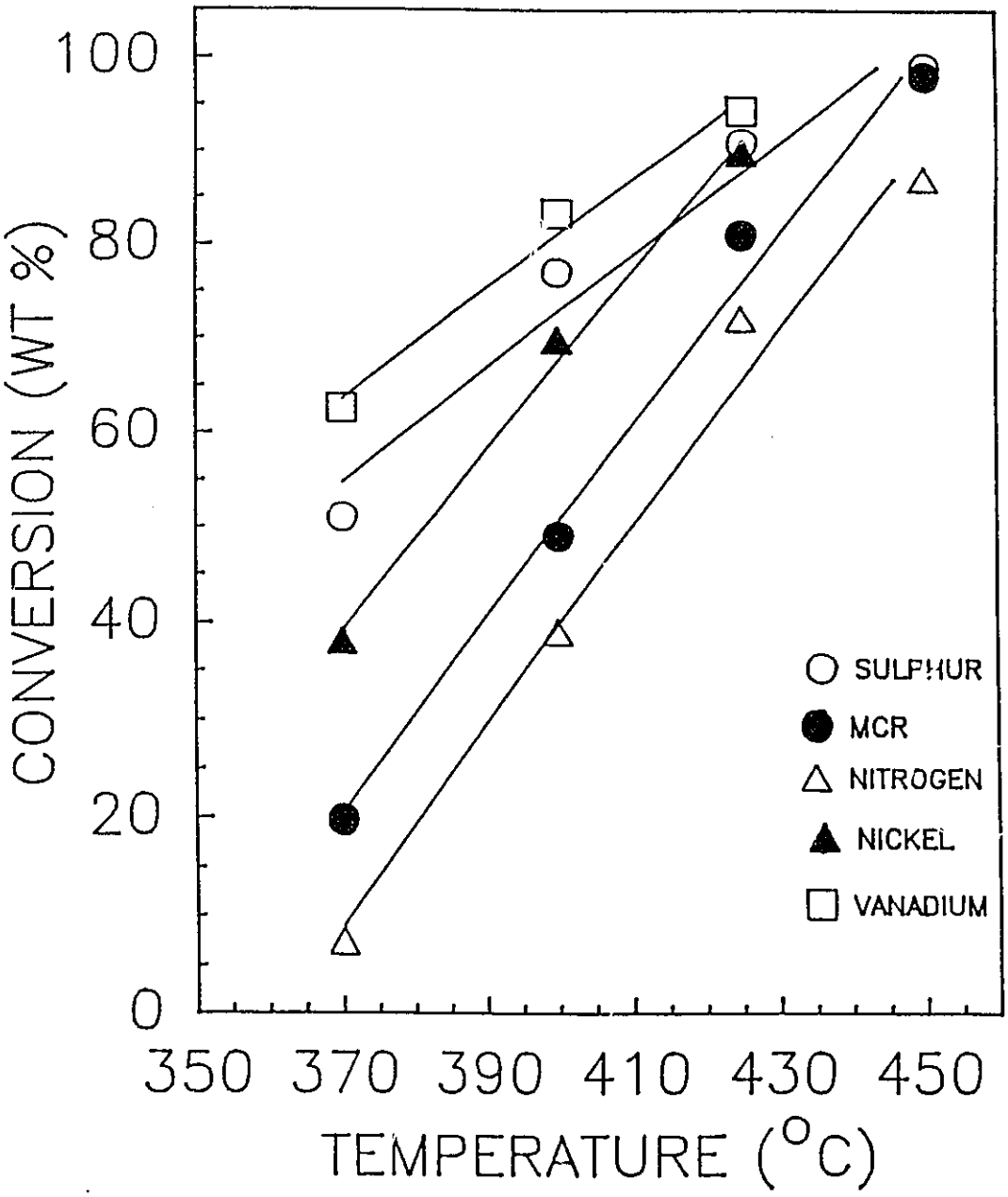

Figure 33: Conversion (wt %) versus temperature (°C) for catalytic reactions with catalyst without a zeolite component. Open circles, solid circles and open triangles are for sulphur, micro carbon residue and nitrogen respectively.

Figure 34 shows the effect of temperature on atomic hydrogen to carbon ratio (H/C) for the liquid products. Both non-catalytic and catalytic hydrocracking H/C ratios are given. At all temperatures non-catalytic hydrocracking had the smallest H/C ratio. Catalysts containing H-mordenite zeolites had the highest H/C ratio at any particular temperature. The results also show that temperature has the same effect in all cases. This is shown by the dashed lines of similar slopes in Figure 34. These correlations suggest that the hydrogenation reaction varies with the catalyst used, but that temperature has the same effect on all catalysts and also on the non-catalytic reaction. The higher H/C atomic ratios can be related indirectly to more cracking caused by the catalysts' acidity. Since H-mordenite is more acidic than HY (Benesi, 1967), greater H/C atomic ratios are obtained with H-mordenite zeolite catalysts compared to those obtained with HY zeolite catalysts.

Figure 35 shows the effect of temperature on the liquid product yield (Figure 35A) and liquid product density (Figure 35B) in catalytic hydrocracking with a catalyst without a zeolite component. Comparing Figure 35A to Figure 12, there is more liquid product yield in catalytic hydrocracking than in non-catalytic hydrocracking. In addition, the liquid product densities in non-catalytic hydrocracking (Figure 11) are much higher and therefore less desirable than those in catalytic hydrocracking (Figure 35B). Thus, compared to non-catalytic

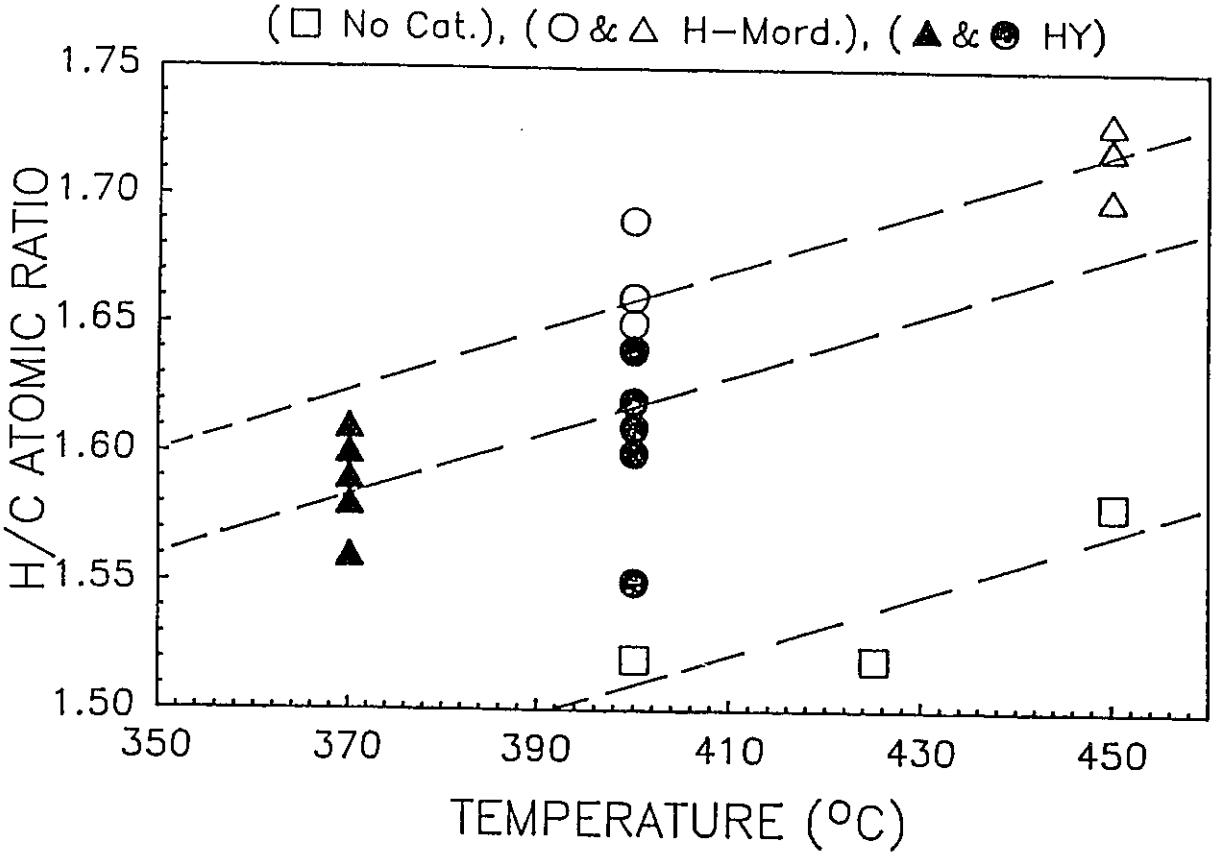

Figure 34: Liquid product hydrogen to carbon atomic ratio (H/C) versus reaction temperature (°C). Open squares for non-catalytic hydrocracking. Open circles and triangles for reactions with catalysts containing H-mordenite zeolite. Solid circles and triangles for reactions with catalysts containing HY zeolite.

hydrocracking, catalytic hydrocracking produces more liquid product with a larger portion of light fuel oil. Therefore, catalytic hydrocracking puts more hydrogen (from the gas phase) into the liquid product. As a result a greater yield of liquid product (i.e., less gas formed) having a higher H/C atomic ratio (i.e., lower density) is obtained.

We have observed that sulphur, nitrogen, and MCR conversions appeared to increase linearly with reaction temperature in both catalytic and non-catalytic reactions. The liquid product densities also appeared to decrease linearly with reaction temperature in both cases. The importance of using catalysts were: higher conversions, more liquid product yield, and lower liquid product densities, i.e., higher distillate oil yield. The correlation between H/C atomic ratio with reaction temperature grouped the liquid products obtained from the same types of catalysts or without catalyst together. Although the overall conversion using catalysts containing H-mordenite zeolite component decreased (except for HDM reactions), the liquid product obtained from these catalysts had the highest H/C atomic ratio. The addition of H-mordenite in the catalysts appeared to enhance HDM and by calculation of PTOF it was shown to have enhanced the other reactions too. The addition of HY to the catalysts appeared to improve all the reactions.

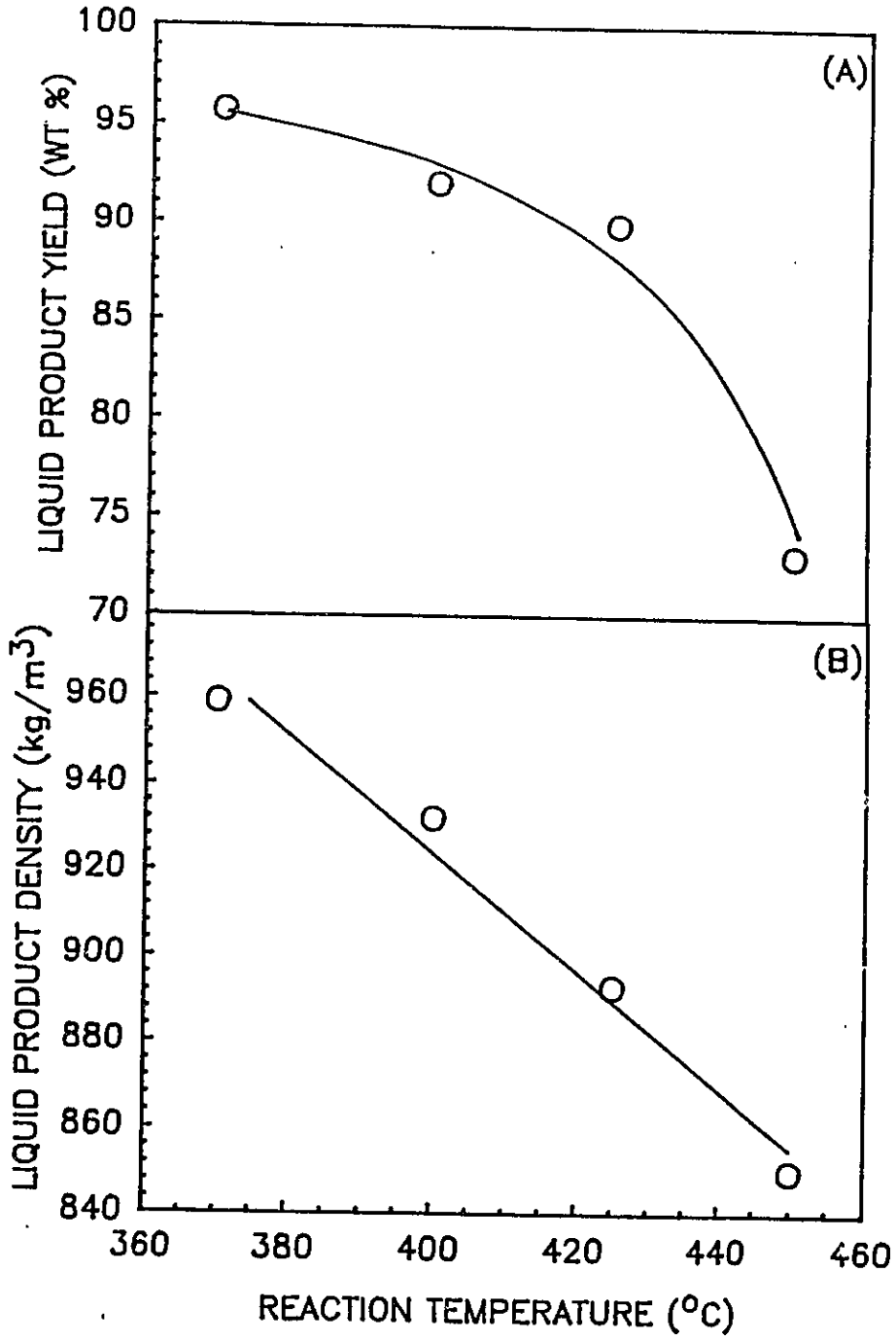

Figure 35: Effect of temperature in liquid product yield and density in catalytic hydrocracking with a catalyst without a zeolite component. Figure 35A, liquid product yield (wt %) versus temperature (°C). Figure 35B, liquid product density (kg/m^3) versus temperature (°C).

6.0 CONCLUSIONS AND RECOMMENDATIONS

6.1 Conclusions

(a) The addition of zeolite (H-mordenite or HY) to a $CoO-MoO_3-Al_2O_3$ catalyst affected several geometric properties of the catalysts:

1. The catalyst specific surface area and particle density, both measured by mercury porosimetry, decreased with increasing catalyst zeolite content.
2. The catalyst pore volume, also measured by mercury porosimetry, increased with increasing catalyst zeolite content, resulting in an increase in the catalyst median pore diameter.
3. The catalyst bulk density decreased because of the decreasing particle density and an increasing curvature of the catalyst extrudates.
4. The specific catalyst surface area measured by the BET method increased with increasing catalyst zeolite content.

(b) The H-mordenite zeolite affected the hydrocracking reactions in the following ways:

1. H-mordenite increased the overall HDM of the catalyst.
2. The overall HDS, HDN, and MCR removal were poor.
3. Further analysis based on constant residence time and constant surface area also showed increased HDS and HDN activity

4. Deposition of carbon on the catalyst increased with increasing H-mordenite content in the catalyst.
5. The increased activity of the catalysts was attributed to the increase in the number of acid sites, caused by the acidity of additional H-mordenite crystals' external surface.
6. Liquid products obtained from hydrocracking with catalysts containing H-mordenite zeolite had the highest H/C atomic ratio.

(c) The HY zeolite affected the hydrocracking reactions in the following ways:

1. HY also increased the overall HDM of the catalyst.
2. The overall HDS, HDN and MCR removal were improved.
3. Calculation of PTOF also showed improved catalyst activity with increasing HY content in the catalyst.
4. Carbon deposition on the catalyst increased with HY content.
5. The enhanced activity of the catalyst was also attributed to the increased number of reaction centres, caused by the addition of HY zeolite.

Measurement of the number of acid sites using benzofuran temperature programmed desorption showed that the number of acid sites increased with increasing catalyst zeolite (HY or H-mordenite) content.

(d) Temperature had the following effects on the hydrocracking reactions:

1. In non-catalytic hydrocracking, the logarithm of sulphur conversion appeared as a linear function of temperature. Nitrogen and MCR conversions formed linear correlations.
2. Catalytic hydrocracking with a catalyst without a zeolite component showed linear correlations between sulphur, nitrogen, MCR, and metal (vanadium and nickel) removal with the reaction temperature.
3. Liquid product densities had a linear correlation with reaction temperature in both catalytic and non-catalytic reactions.
4. Liquid products from catalytic reactions had a higher H/C atomic ratios and are therefore much lighter.

6.2 Recommendations

1. Catalysts containing zeolite (H-Mordenite or HY) are impressive HDM catalysts. Long term testing of these catalysts is recommended in order to consider their use in commercial plants.
2. Further long term studies with the catalyst containing the optimum HY zeolite content (20 wt %) are recommended. These studies will permit their performance with time to be compared with commercial hydrocracking catalysts.
3. To improve the overall HDS, HDN, and MCR conversions obtained with the catalysts containing an H-mordenite zeolite component, straight extrudates should be prepared to increase the catalyst packing (i.e., increasing bulk density).

7. REFERENCES

Abbot, J. and B.W. Wojciechowski, "The Mechanism of Paraffin Reactions on HY Zeolite", J. Catal. **115**, 1-15 (1989).

Altajam, M.A. and M. Ternan, "Hydrocracking of Athabasca Bitumen Using Co-Mo Catalysts Supported on Wide Pore Carbon Extrudates, Fuel **68**, 955-960 (1989).

Annual Book of ASTM Standards, "Petroleum Products, Lubricants, and Fossil Fuels", **05.02**, ASTM, Philadelphia, (1986) p. 23.

Atanasova, P., T. Halachev, J. Uchytil and M. Kraus, "Effect of Phosphorus on the Surface Concentration of Molybdenum and Nickel in the Oxide Form of Nickel-Molybdenum/Alumina Catalysts and on their Hydrodesulphurization Activity", Appl. Catal. **38**, 235-240 (1988).

Baltus, R.E. and J.L. Anderson, "Hindered Diffusion of Asphaltenes Through Microporous Membranes", Chem. Eng. Sci. **38**, 1959-1969 (1983).

Banerjee, D.K., K.J. Laidler, B.N. Nandi and D.J. Partmore, "Kinetic Studies of Coke Formation in Hydrocarbon Fractions of Heavy Crudes", Fuel **65**, 480-484 (1986).

Bartholic, D.B. and R.P. Haseltine, "Development of Engelhard's ART Process", Proceed. Ref. Depart., Am. Petrol. Inst. **60**, 335-339, Illinois, May (1981).

Barthomeuf, D., in "Zeolites: Science and Technology", F. Riberiro, A.E. Rodriques, L.D. Rollmann, and C. Naccache, Eds., Martinus Nijhoff, Dordrecht, (1983) p. 317-346.

Benesi, H.A., "Relationship between Catalytic Activity and Nature of Acidity of the Crystalline Zeolites, Mordenite and Faujasite", J. Catal. **8**, 368-374 (1967).

Blouri, B., F. Hamdan and D. Herault, "Mild Cracking of High-Molecular-Weight Hydrocarbons", Ind. Eng. Chem. Proc. Des. Dev. **24**, 30-37 (1985).

Boduszyski, M.M., "Asphaltenes in Petroleum Asphalts--Composition and Formation", Am. Chem. SOc. Prepr. Div. Petrol. Chem. **24**(4), 935-949 (1979).

Boduszyski, M.M., "Composition of Heavy Petroleums. 1. Molecular Weight, Hydrogen Deficiency, and Heteroatom Concentration as a Function of Atmospheric Equivalent Boiling Point up to 1400°F (760°C)", Energy and Fuels **1**, 2-11 (1987).

Bolton, A.P., "Molecular Sieve Zeolites", Academic Press, New York, (1976).

Boorman, P.M., J.F. Kriz, J.R.Brown and M. Ternan, "Hydrocracking Bitumen Derived From Oil Sands with Sulphided MoO_3-CoO Catalysts Having supports of Varying Composition", Proceed. 8th Inter. Congr. Catal. **2**, 281-291 (1984).

Boudart, M., J.S. Arrieta and R. Dalla Betta, "Correlation Between Thiophene Hydrodesulphurization Activity and number of First Sulphur Neighbors as Determined by EXAFS in Sulphided $CoMo/Al_2O_3$ Samples", J. Am. Chem. Soc. **105**, 6501-6502 (1983).

Brooks, J.D. and G.H. Taylor, in "Chemistry and Physics of Carbon Vol. 4", P.L. Walker, Jr, Ed., Edward Arnold, New York, (1968) P.243-286.

Brunet, S., S. Karmal, D. Duprez and G. Perot, "Characterization of Hydrodenitrogenation Catalysts by O_2 Chemisorption", Catal. Let. **1**, 255-260 (1988).

Burch, R. and A. Collins, "Chemisorption/Catalytic Activity Correlations for Sulphided $Ni/Mo/Al_2O_3$ Hydrodesulphurization Catalysts", Appl. Catal. **17**, 273-308 (1985).

Champagne, J.P., E.Manolakis and M. Ternan, "Molecular Weight Distribution of Athabasca Bitumen", Fuel **64**, 423-425 (1985).

Chianelli, R.R., "Fundamental Studies of Transition Metal Sulphide Hydrodesulphurization Catalysts", Catal. Rev. Sci. Eng. **26**(3 & 4), 361-393 (1984).

Decroocq, D., "Catalytic Cracking of Heavy Petroleum Fractions", Gulf (Houston) and Technip (Paris), (1984) p. 16-23

Döhler, W., D.-I.K. Kretschmar, L. Merz and K. Niemann, "VEBA-Combi-Cracking - a Technology for Upgrading of Heavy Oils and Bitumen", Prepr. Div. Petrol. Chem. **32**(2), 484-489 (1987).

Donath, E.E. in "Catalysis Science and Technology", J.R. Andersen and M. Boudat, Eds., Spurger -Verlag, Berlin (1983), p. 1-38.

Driesen, R.P.V. and N.C Stewart, "How Cities Service's H-Oil Unit is Performing", Oil & Gas J., 100-105 (1964).

Eccles, R.M., A.M. Gray and W.B. Livingston, "New Resid Conversion Scheme Set for Louisiana Refinery", Oil & Gas J. **80**(15), 121-129 (1982).

Energy, Mines and Resources Canada, "Petroleum Processing in Canada", Petroleum Sector, (1981).

Fitz, Jr. C.W. and H.F. Rase, "Effect of Phosphorus on Nickel-Molybdenum Hydrodesulphurization/Hydrodenitrogenation Catalysts of Varying Metals Content", Ind. Eng. Chem. Prod. Res. Dev. **22**, 40-44 (1983).

Fixari, B., and P.Le. Perchec, "Hydrogenation of Polyaromatics in the Presence of Hydrogen-Hydrogen Sulphide System", Fuel **68**, 218-221 (1989).

Gary, J.H. and G.E. Handwerk, "Petroleum Refining Technology and Economics", Marcel Dekker, New York, (1975).

Gavin, D.G., in "Catalysis Volume 5", G.C. Bond and G. Webb, Senior Reporters, The Royal Society of Chemistry, Burlington House, (1982) p. 220-246.

Green, D.C. and D.H. Broderick, "Processing Heavy Crudes:Residuum Hydroprocessing In the 80s", Chem. Eng. Progr.**77**, 33-39 (1981).

Gregg, S.J. and K.S.W. Sing, "Adsorption, Surface Area and Porosity", Academic Press, New York, (1982).

Hardin, A.H., R.H. Packwood and M. Ternan, "Effects of Median Diameters in Co/Mo/Al_2O_3 Catalysts on The Conversion of Athabasca Bitumen", Symp. Effect of Pore Size on Catalytic Behaviour Div. Petrol. Chem, Am. Chem. Soc., 1450-1461 Miami, Sept. (1978).

Harvey, T.G. and K.C. Pratt, "Simultaneous Hydrotreating and Hydrocracking of Heavy Feedstocks - A New Process Development", Chemica 85: Innovation Proc. Resour. Ind.; Aust. Chem. Eng. Conf. **13th**, 81-84 (1985).

Haynes, JR. H.W., "Chemical, Physical, and Catalytic Properties of Large Pore Acidic Zeolites", Catal. Rev. Sci. Eng. **17**(2), 273-336 (1978).

Heavy Oiler, UNITAR/UNDP INFORMATION CENTRE FOR HEAVY CRUDE AND TAR SANDS, Issue NO. **30**, July (1989).

Hirotani, Y., T. Takeuchi, Y. Miyabuchi, T. Aiba and M. Shigeta, "Successful Performance of a Refinery with Eureka Unit", Am. Chem. Soc. Prepr. Div Petrol. Chem. **26**(2), 465-475 (1981).

Jacobs, A.P., "Carboniogenic Activity of Zeolites", Elsevier Sci. Publ. Co., Amsterdam, (1977).

Kang, B., S. Wu, H. Tsai and J. Wu, "Effect of Catalyst Composition on the Hydrodesulphurization and Hydrodenitrogenation of Atmospheric Residual Oil", Appl. Catal. **45**, 221-238 (1988).

Kelly, J.F. and M. Ternan, "Hydrocracking Athabasca Bitumen with Alkali Metal Promoted CoO-MoO_3-Al_2O_3 Catalysts", Can. J. Chem. Eng. **57**, 726-733 (1979).

Kett, K.T., C.G. Lahn and L.W. Schuette, "Resid Conversion Route", Chem. Eng., 40-41, Dec. (1974).

Kirchko, A.A., N.F. Meged', N.N. Khor'kova, M.K. Yulin, A.A. Galkina and A.I. Mezhlumova, "Upgrading Products from Coal, Liquefaction by Hydrotreating over Zeolite Catalysts", Chem. Technol. Fuels Oils (English translation) **18**(6), 273-276 (1982).

Knözinger, H. in "Proceedings 9TH International Congress on Catalysis", M.J. Phillips and M. Ternan, Eds., **5**, Calgary (1988), p. 20-53.

Köseoglu, R.Ö. and C.R. Philips, "Hydrocracking of Athabasca Bitumen Kinetics of Formation of Gases", Fuel **67**, 552-556 (1988).

Kriz, J.F. and M. Ternan, in "Catalysis on the Energy Scene", S. Kaliaguine and A. Mahay, Eds., Elsevier Sci. Publ., Amsterdam, Netherlands, (1984) p.545-550.

Kyriacou, K.C., V.V. Sivaramakrishna, R.E. Baltus and P. Rahimi, "Measurement of Diffusion Coefficients of Oil Residual Fractions Using Porous Membranes", Fuel **67**, 15-18,(1988a).

Kyriacou, K.C., R.E. Baltus, and P. Rahimi, "Characterization of Oil Residual Fraction Using Intrinsic Viscosity Measurements", Fuel **67**, 109-113 (1988b).

Laine, J., J. Brito, S. Yunes and P. Andréu, "Acid Strength Distributions in the Mo-Al-Si and the Ni-Mo-Al oxide systems Determined by Ammonia Adsorption", React. Kinet. Catal. Lett. **25**(1&2), 5-10 (1984).

Little, D.M., "Catalytic Reforming", PennWell, Oklahama, (1985)

Matralis, H.K., A. Lycourghiotis, P. Grange and B.Delmon, "Flourinated Hydrotreatment Catalysts: Characterization and Hydrodesulphurization Activity of Flourine-Cobalt-Molybdenum/γ-Alumina Catalysts", Appl. Catal. **38**, 273-287 (1988).

Maxwell, I.E., "Zeolite Catalysis in Hydroprocessing Technology", Catal. Today **1**, 385-413 (1987).

Meier, W.M. and D.H. Olson, "Atlas of Zeolite Structure Types", Butterworths, London, 2 ed. (1987).

Meyers, R.A., "Handbook of Petroleum Refining Process", McGraw-Hill, New York, (1986).

Miciukiewicz, J., Q. Qader and F.E. Massoth, "Studies of Molybdenum-Alumina Catalysts XV. Effects of Flourine-Modified Alumina on Catalyst Properties", Appl. Catal. **49**, 247-257 (1989).

Miki, Y., S. Yamadaya, M. Oba and Y. Sugimoto, "Role of Catalyst in Hydrocracking of Heavy Oil", J. Catal. **83**, 371-383 (1983).

Mishin, I.V., H. Bremer and K.-P. Wendlandt, in "Catalysis on Zeolites", D. Kallό, and Kh.M. Minachev, Eds., AKADÉMIA KIADÓ BUDAPEST, (1988), p. 231-275

Moon, S. and S. Ihm, "Nitric oxide Chemisorption and Temperature-Programmed Desorption Study of Cobalt and Molybdenum Catalysts Supported on Activated Carbon and Alumina", Appl. Catal. **42**, 307-324 (1988).

Nag, N.K., K.S.P. Rao, K.V.R. Chary, B.R. Rao and V.S. Subrahmanyam, "Characterization of γ-Alumina-Supported Tungsten Sulfide Hydroprocessing Catalysts", Appl. Catal. **41**, 165-176 (1988).

Nandi, B.N., M. Ternan, B.I. Parsons and D.S. Montgomery, "Coke Formation During Simultaneous Hydrocracking of bitumen and Hydrogenation of Coal", Fuel **54**, 197-200 (1975)

Nandi, B.N., K. Belinko, L.A. Ciavaglia and B.B. Pruden, "Formation of Coke During Thermal Hydrocracking of Athabasca Bitumen", Fuel **57**, 265-268 (1978).

Nita K., S. Nakai, S. Hidaka, T. Mibuchi, H. Shimakawa, Ken-Ichi II and K. Inamura, in "Catalyst Deactivation", B. Delmon and G.F. Froment, Eds., Elsevier Sci. Publ. Amsterdam, Netherlands, (1987) p. 501-511.

Otterstedt, J.E., S.B. Gevert, S.G. Järås and P.G. Menon, "Fluid Catalytic cracking of Heavy (Residual) Oil Fractions: A Review", Appl. Catal. **22**, 159-179 (1986).

Papaioannou, A. and H.W. Haynes, Jr., "Alkali and Alkaline Earth Catalysts for Coal Liquefaction Applications". Am. Chem. Soc. Prepr. Fuel Chem. **34**(2), 589-596 (1989).

Parham, T.G. and R.P. Merrill, "An EXAFS Study of the Structure of Supported Cobalt Molybdate Catalysts as a Function of Sulphiding Temperature", J. Catal. **85**, 295-310 (1984).

Patmore, D.J., and C.P. Khulbe, "Residuum and Heavy Oil Upgrading with CANMET Hydrocracking Process", Prepr. Div. Petrol. Chem. **26** (2), 431-439 (1981).

Prins, R., V.H.J. De Beer and G.A. Somorjai, "Structure and Function of the Catalyst and the Promoter in Co-Mo Hydrodesulphurization Catalysts", Catal. Rev. Sci. Eng. **31**(1 & 2), 1-40 (1989).

Pruden, B.B., J.M. Denis and G. Muir, "Upgrading of Cold Lake Heavy Oil in the CANMET Hydrocracking Demonstration Plant.", Prepr. 4TH UNITAR/UNDP Conference on Heavy Crude and Tar Sands **2**(80), (1988).

Quann, R.J., R.W. Ware, C. Hung and J. Wei, in "Advances in Chemical Engineering **14**", J. Wei, J.L. Anderson, K.B. Bischoff and J.H. Seinfeld, Eds., Academic Press, New York, (1988) p. 95-259.

Rabo, J.A., "Zeolite Chemistry and Catalysis", American Chemical Society, Washington, (1976).

Radchenko, E.D., S.A. Sergienko, G.D. Chukin, A.A. Voitekhov and I.Ya. Perezhigina, "Behaviour of Zeolite-Containing Catalyst in Hydrocracking Process", Chem. Technol. Fuels Oils (English translation) **19**(6), 262-266 (1983).

Ravey, J.C., G. Ducouret and D. Espinat, "Asphaltene Macrostructure by Small Angle Neutron Scattering", Fuel **67**, 1560-1567 (1988).

Real, R.A.D., "Hydrotreating of Athabasca Bitumen Derived Heavy Gas Oil over Ni-W and Co-Mo Catalysts", Master thesis, University of Ottawa, Ottawa, (1987).

Relly, I.G., D.S. Scott, T. De Brujin, A. Jain and J. Piskorz, " A Correlation for Gas Holdup in Turbulent Coalescing Bubble Columns", Can. J. Chem. Eng. **64**, 705-717 (1986).

Ripperger, W. and W. Saum, "Cobalt-and Nickel-Molybdenum Catalysts: Their Properties and Applications for Hydrodesulphurization", J. Less-Common Metals **54**, 353-362 (1977).

Rustamov, M.I., A.A. Saidova, G.T. Farkhadova, É.I. Amerbekov, A.A. Medzhidov, and N.M. Mardanova, "Effect of Coke Deposition on the Catalytic Activity and Acid Properties of a Zeolite-Containing Aluminosilicate Cracking Catalyst", Kinet. Catal. (English translation) **28**(6 part 2), 1253-1257 (1988).

Ruthven, D.M., "Principles of Adsorption and Adsorption Processes", John Wiley & Sons, New York, (1984).

Sambi I.S., and R.S. Mann, "REY-Zeolite and Silica-Alumina Mixed Support for Hydrotreating Heavy Gas Oil", Can. J. Chem. Eng. **67**, 337-342 (1989).

Scott, J., Ed., "Zeolite Technology and Apllications: Recent Advances", Noyes Data Corporation (NDC), New Jersey, (1980) p. 106-122.

Shaheen, E.I., "Catalytic Processing in Petroleum Refining", PennWell, Oklahoma, (1980).

Sidel'kovskaya, V.G., S.A. Surin, G.D. Chukin, I.I. Skarzov, R.R. Aliev, B.K. Nefedov and L.V. Turivskaya, "Effect of Zeolite Additives on the Formation of the Active Phases of Aluminum-Nickel-Molybdenum Catalysts", Kinet. Catal. (English translation) **29**(2), 448-453 (1988).

Soodhoo, K., and C.R. Philips, "Non-Catalytic Hydrocracking of Asphaltenes", Fuel **67**, 361-374 (1988).

Speight, J.G., "The Chemistry and Technology of Petroleum", Marcel Dekker, New York, (1980).

Speight, J.G., "The Desulphurization of Heavy Oils and Residua", Marcel Dekker, New York, (1981).

Suzuki, M. and K. Onuma, "Hydrotreating Catalysts for Heavy Oils (Part2) Reaction Performance and Aging Behaviour of Bimodal Alumina Based Catalysts for Desulphurization and Demetallation", J. Japan Petrol. Inst. **27**(5), 420-428 (1984).

Suzuki, T., H. Yamada, L.P. Sears and Y. Watanabe, "Hydrogenation and Hydrogenolysis of Coal Model Compounds by Using Finely Dispersed Catalysts", Energy and Fuels **3**, 707-713 (1989).

Takeuchi, C., Y. Fukul, M. Nakamura and Y. Shiroto, "Asphaltene Cracking in Catalytic Hydrotreating of Heavy Oils. 3.[1] Characterization of products from Catalytic Hydroprocessing of Khafji Vacuum Residue", Ind. Eng. Chem. Proc. Des. Dev. **22**(2), 249-257 (1983).

Ternan, M., and M.J. Whalley, "Presulphiding of Catalysts for Hydrodesulphurization and Hydrodenitrogenation in a Bottom Feed Liquid Phase Reactor", Can. J. Chem. Eng. **54**, 642-644 (1976).

Ternan, M., E. Furimsky and B.I. Parsons, "Coke Formation on Hydrodesulphurization Catalysts", Fuel Processing Technol. **2**, 45-55 (1979)

Ternan, M. and J.F. Kriz, in "Catalyst Deactivation", B. Delmon and G.F. Froment, Eds., Elsevier Scientific Publishing Company, Amsterdam, (1980) P. 283-293.

Ternan, M., "Catalysis, Molecular Weight Change and Fossil Fuels[1]", Can. J. Chem. Eng. **61**, 133-147 (1983a).

Ternan, M., "Catalytic Hydrogenation and Asphaltene Conversion of Athabasca Bitumen", Can. J. Chem. Eng. **61**, 689-696 (1983b).

Ternan, M., "The Diffusion of Liquids in Pores", Can. J. Chem. Eng. **65**, 244-249 (1987).

Thrash, R.J. and R.H. Pildes, "The Diffusion of Petroleum Asphaltenes Through well Characterized Porous Membranes", Prepr. Am. Chem. Soc. Petrol. Div. **26**(2), 515-525 (1981).

Topsøe, H. and B.S. Clausen , in "Catalysis and Surface Science: Chemical Industries/21", H.Heinemann and G.A. Somorjai, Eds., (1984) P. 95-120.

Van Driesen, R.P., and L.L. Fornoff, "Upgrade resid with LC-Fining", Hydrocarbon Processing **64**(9), 91-95 (1985).

Vázquez, M.I., A. Escardino and A. Aucejo, "Hydrocracking of n-Heptane with a $NiO-MoO_3/HYUS$ Zeolite as Catalyst. Kinetic Study", Can. J. Chem. Eng. **66**, 313-318 (1988a).

Vázquez, M.I., A. Escardino and A. Aucejo, "Hydrocracking of n-Heptane with a $NiO-MoO_3/HY$ Ultrastable Zeolite as Catalyst. The Network of Reaction", Ind. Eng. Chem. Res. **27**(11), 2039-2043 (1988b).

Venuto, P.B., and E. Thomas Habib JR., "Fluid Catalytic Cracking with Zeolite Catalysts", Marcel Dekker, New York, (1979).

Wilson, M.F., I.P. Fisher and J.F. Kriz, "Hydrogenation of Aromatic Compounds in Synthetic Crude Distillates Catalyzed by Sulphided $Ni-W/\theta-Al_2O_3$" J. Catal. **95**, 155-166 (1985).

Wivel, C., R. Candia, B.S. Clausen, S. Mørup and H Topsøe, "On the Catalytic Significance of a Co-Mo-S Phase in $Co-Mo/Al_2O_3$ Hydrodesulphurization Catalysts: Combined in Situ Mössbauer Emission Spectroscopy and Activity Studies", J. Catal. **68**, 453-463 (1981).

Wojciechowski, B.W. and A. Corma, "Catalytic Cracking" Marcel Dekker, New York, (1986).

APPENDECIS

APPENDIX--A

Table 6: Experimental Data

Zeolite type & amount (wt%)	Temperature (°C)	Sulphur conversion (wt %)	Nitrogen conversion (wt %)	MCR conversion (wt %)	Nickel conversion (wt %)	Vanadium conversion (wt %)	Liquid product yield (wt %)	Liquid Product Density (kg/m^3)	H/C Atomic ratio
H-Mord-0	400	84.6	49.5	54.2	72.2	84.5	92.9	927	1.66
H-Mord-1	400	85.9	49.3	56.4	76.7	87.3	95.8	922	1.69
H-Mord-3	400	85.2	49.5	58.1	84.5	92.0	92.3	923	1.66
H-Mord-5	400	81.5	50.5	53.6	78.0	88.4	90.6	926	1.66
H-Mord-10	400	84.4	46.0	55.1	84.0	92.7	95.4	925	1.66
H-Mord-20	400	81.1	39.2	52.1	80.8	90.8	93.3	928	1.65
H-Mord-0	450	99.3	87.2	97.8	-	-	73.1	850	1.72
H-Mord-1	450	99.4	85.0	98.1	-	-	84.2	859	1.72
H-Mord-3	450	99.2	85.3	98.3	-	-	74.2	852	1.73
H-Mord-5	450	98.5	74.4	94.0	-	-	79.9	864	1.70
H-Mord-10	450	99.4	73.5	96.8	-	-	82.2	865	1.72
H-Mord-20	450	98.9	76.7	94.5	-	-	82.9	863	1.72
HY-0	400	77.1	37.5	48.4	67.3	82.0	92.0	932	1.64
HY-5	400	77.6	42.2	52.6	67.9	80.1	83.9	932	1.62
HY-10	400	78.6	43.8	53.4	74.6	86.5	90.6	927	1.60
HY-15	400	82.4	50.0	56.4	75.6	87.2	90.1	924	1.64
HY-20	400	81.5	54.7	59.3	80.2	90.2	81.6	922	1.55
HY-25	400	75.4	42.2	50.3	73.4	87.0	89.0	931	1.61
HY-0	370	51.1	.3	19.7	38.0	62.5	95.7	959	1.58
HY-5	370	49.0	10.3	21.2	36.8	58.4	92.6	963	1.59
HY-10	370	55.6	9.0	22.6	44.7	68.5	95.5	957	1.61
HY-15	370	55.5	11.3	23.7	44.3	69.5	94.6	962	1.60
HY-20	370	54.0	14.2	24.9	46.1	69.4	93.1	957	1.60
HY-25	370	43.3	1.5	13.6	35.1	62.0	98.5	971	1.56
Non-Catalytic	400	15.3	0	6.6	0	29.6	94.0	989	1.52
Non-Catalytic	425	31.6	19.1	44.8	31.7	57.3	92.5	957	1.52
Non-Catalytic	450	61.4	57.6	73.5	82.7	91.0	57.7	935	1.58
No Zeolite	425	91.0	72.0	81.0	89.9	94.4	89.9	893	1.67

APPENDIX--A Continues

Table 7: Experimental Data

Zeolite type & amount (wt%)	Temperature (°C)	Gas volume collected in 2 h (ft^3)	Sulphur PTOF (atoms removed $nm^{-2}s^{-1}$) x 10^3	Nitrogen PTOF (atoms removed $nm^{-2}s^{-1}$) x 10^4	Nickel PTOF (atoms removed $nm^{-2}s^{-1}$) x 10^6	Vanadium PTOF (atoms removed $nm^{-2}s^{-1}$) x 10^5
H-Mord-0	400	7.65	2.02	3.22	1.87	3.27
H-Mord-1	400	8.95	2.21	3.46	2.14	3.64
H-Mord-3	400	7.15	2.57	4.06	2.76	4.47
H-Mord-5	400	9.60	2.67	4.51	2.77	4.68
H-Mord-10	400	13.8	2.60	3.86	2.81	4.62
H-Mord-20	400	8.50	3.67	4.83	3.96	6.64
H-Mord-0	450	10.90	2.38	5.67	-	-
H-Mord-1	450	10.50	2.56	5.96	-	-
H-Mord-3	450	8.38	2.99	6.99	-	-
H-Mord-5	450	10.00	3.23	6.64	-	-
H-Mord-10	450	10.85	3.07	6.17	-	-
H-Mord-20	450	11.50	4.48	9.45	-	-
HY-0	400	8.75	2.15	2.85	2.04	3.69
HY-5	400	9.10	2.18	3.21	2.04	3.56
HY-10	400	9.75	2.46	3.74	2.53	4.38
HY-15	400	9.40	2.48	4.09	2.46	4.23
HY-20	400	9.35	2.56	4.68	2.73	4.58
HY-25	400	8.09	2.85	4.34	3.00	5.30
HY-0	370	9.20	1.43	0.55	1.15	2.82
HY-5	370	8.70	1.37	0.78	1.10	2.61
HY-10	370	9.20	1.72	0.76	1.52	3.47
HY-15	370	9.36	1.67	0.92	1.44	3.37
HY-20	370	9.20	1.70	1.21	1.57	3.52
HY-25	370	8.02	1.63	0.15	1.47	3.78
Non-Catalytic	400	9.05	-	-	-	-
Non-Catalytic	425	9.00	-	-	-	-
Non-Catalytic	450	9.02	-	-	-	-

APPENDIX--A: Continues

Table 8: experimental Data

Zeolite type & amount (wt%)	Hydrogen content in spent catalyst (wt %)	Nitrogen content in spent catalyst (wt %)	Carbon content in spent catalyst (wt %)	Amount of carbon deposited in spent catalyst ($mg\ C\ m^{-2}$) x 10
H-Mord-0	0.99	0.49	10.50	6.14
H-Mord-1	1.02	0.50	10.78	6.29
H-Mord-3	0.96	0.60	10.66	5.96
H-Mord-5	1.14	0.64	15.44	6.16
H-Mord-10	1.08	0.59	14.83	6.51
H-Mord-20	1.02	0.60	11.36	6.81
HY-0	1.84	0.47	8.28	5.93
HY-5	1.48	0.47	8.22	5.81
HY-10	1.95	0.55	9.04	7.35
HY-15	2.14	0.62	10.00	7.90
HY-20	2.60	0.43	9.35	7.69
HY-25	2.63	0.46	10.40	10.0

APPENDIX--B: CALCULATIONS

A. Percentage liquid product yield :

$$Yield\ (wt\ \%) = \frac{(wt\ of\ product)}{(wt fed)} * 100$$

B. Conversion of species X :

$$Conversion\ (wt\ \%) = \frac{(wt\ of\ X\ fed - wt\ of\ X\ out)}{(wt\ of\ X\ fed)} * 100$$

$$= \frac{(wt\ \%\ X\ in\ feed - \frac{Yield(wt\ \%)}{100}\ (wt\ \%\ X in\ product)}{(wt\ \%\ X\ in\ feed)}$$

Example:

The Boscan heavy oil used had 5.38 wt % sulphur and the liquid product yeild for the first experiment was 92.9 wt %. The product had 0.89 wt % sulphur.

$$\therefore Conversion\ (wt\ \%) = \frac{(5.38 - (\frac{92.9}{100})(0.89))}{5.38} * 100$$
$$= 84.6$$

C. Pseudo Turnover Frequency (PTOF)

By using Equation 5 of section 2.5 the PTOF were evaluated.

Example:

Using the SA value of the catalyst without H-mordenite in Table 4 (i.e., 93.9 * 194 = 18216 m^2), the sulphur conversion calculated above, molecular weight of sulphur 32, and a sulphur feed

rate of 8.339 g/h the sulphur PTOF is as follows:

$$PTOF\left(\frac{S atoms removed}{nm^2 s}\right) = \frac{84.6}{100} * 8.339 * \frac{167.288}{32} * \frac{1}{18216}$$
$$= 2.02 * 10^{-3}$$

Nitrogen and metals PTOF were calculated in a similar manner.

D. Apparent Residence Time (θ)

The apparent residence time in the reactor was calculated based on the void space between the catalyst particles and the gas hold-up in the reactor.

The reactor gas hold-up (ϵ_G) was calculated using the correlation by Relly et al (1986) which is as follows:

$$\epsilon_G = (296 * \bar{U}_G^{0.44} * \rho_L^{-0.98} * \sigma_L^{-0.16} * \rho_G^{0.19}) + 0.009$$

where ρ_L = heavy oil density around 400°C (approx. 782 kg/m^3),

ρ_G = hydrogen density (at 13.9 MPa, and 425°C = 4.79 kg/m^3),

σ_L = heavy oil surface tension (approx. 0.04 N/m),

$\bar{U}_G$ = gas velocity in the bed = V^*/A_B,

A_B = cross-sectional area of empty reactor = 5.067 cm^2 and

V^* = volumetric gas flowrate (at 13.9 MPa and reactor temperature).

The gas flowrate was calculated from the total gas which left the reactor during the duration of the steady state experiment. For each catalyst, the total gas volume for the 4 h catalyst test was divided by the time to obtain an average gas flow rate.

The void space between the catalyst particles (extra particle space) in the reactor was obtained by subtracting the volume of the catalyst from the total volume of the reactor. The volume of the catalyst in the reactor was obtained by dividing the weight of the catalyst loaded in the reactor by the catalyst particle density. The fraction (E) of the extra particle space to the total volume was obtained by dividing the volume of extra particle space by the total reactor volume.

The apparent residence time was then calculated as follows:

$$\theta = \frac{V}{V^{**}} * E * (1 - \epsilon_G)$$

Where V = volume of empty reactor (155 mL)

V^{**} = heavy oil feedrate around 400°C. This was obtained by dividing the weight of the heavy oil fed per hour by the the density of the oil {(155 g/h)/(0.782 g/mL) = 198.2 mL/h}.

Example

For the first catalyst a total of 18.55 ft^3 of gases at ambient conditions, left the reactor in 4 h. 93.9 g of the catalyst were loaded in the reactor, and the catalyst particle density was 1.441 g/mL. The experiments were run at an average temperature of 425°C.

Solution:

catalyst volume = mass/density

= (93.9 g)/(1.441 g/mL = 65.16 mL

Therefore, extra particle space fraction (E) is:

$$E = (155-65.16)/155$$

$$= 0.58$$

Volumetric gas rate:

First, we convert exit gas volume at ambient conditions, (V_1), to reactor conditions, (V_2), using ideal gas equation:

$$\frac{P_1 V_1}{T_1} = \frac{P_2 V_2}{T_2}$$

$$\rightarrow V_2 = \frac{(0.1013\ MPa)(18.55\ ft^3)(698\ K)}{(298\ K)(13.9\ MPa)} = 0.317\ ft^3$$

$$= (0.317\ ft^3)\left(\frac{28320\ mL}{1\ ft^3}\right) = 8967.5\ mL$$

Hence,

$$V^* = \frac{8967.5\ mL * \frac{1\ m^3}{10^6\ mL}}{4\ h * \frac{3600\ s}{1\ h}} = 6.227 * 10^{-7}\ m^3 s^{-1}$$

Gas Velocity in the bed:

$U_G = V^*/A_B$

$= (6.227 * 10^{-7}\ m^3 s^{-1})/(5.067 * 10^{-4}\ m_2)$

$= 1.23 \times 10^{-3}$ m/s

Using the Relly **et al** correlation:

$\epsilon_G = (296 \times 0.00123^{0.44} \times 782^{-0.98} \times 0.04^{-0.16} \times 4.79^{0.19}) + 0.009$

$=0.060$

Hence, apparent residence time:

$$\theta = \left(\frac{155\,mL}{198.2\,mL\,h^{-1}}\right)(0.58)(1-0.060) = 0.426\,h = 25.6\,\text{min}$$

E. PTOF Per Residence Time

To obtain the values of PTOF/s the values of PTOF calculated in section C are divided by the apparent residence time calculated in section D.

F. Amount of Carbon Deposited per Unit Surface Area

The data for spent catalysts composition in Table 8 (Appendix--A), and the specific surface area for the corresponding catalysts in Table 4 and 5 were used.

Basis: 100 g of spent catalyst.

$$\frac{wt\ (g)\ C}{wt\ (g)\ Cat^{a}} * \frac{1}{CSSA\ (m^2g\text{-}1)} * \frac{1000\ (mg)\ C}{(g)\,C} = (\ )\left[\frac{mg\ C}{m^2}\right.$$

Where cat^a stands for spent catalyst on hydrogen, nitrogen, and carbon free basis, and CSSA is the catalyst's specific surface area.

Example:

Let's take a spent catalyst with 10.5 % carbon, 0.99 % hydrogen, 0.49 % nitrogen, and having specific surface area of 194 m^2/g. Therefore carbon deposited is:

$$\frac{10.5\ g\ C}{(100\text{-}10.5\text{-}0.49\text{-}0.99)\ g} * \frac{1000\ mg\ C}{1\ g\ C} * \frac{1}{194\ m^2g^{-1}} = 0.614\ \frac{mg\ C}{m^2}$$

APPENDIX--C

Temperature Programmed Desorption Plots

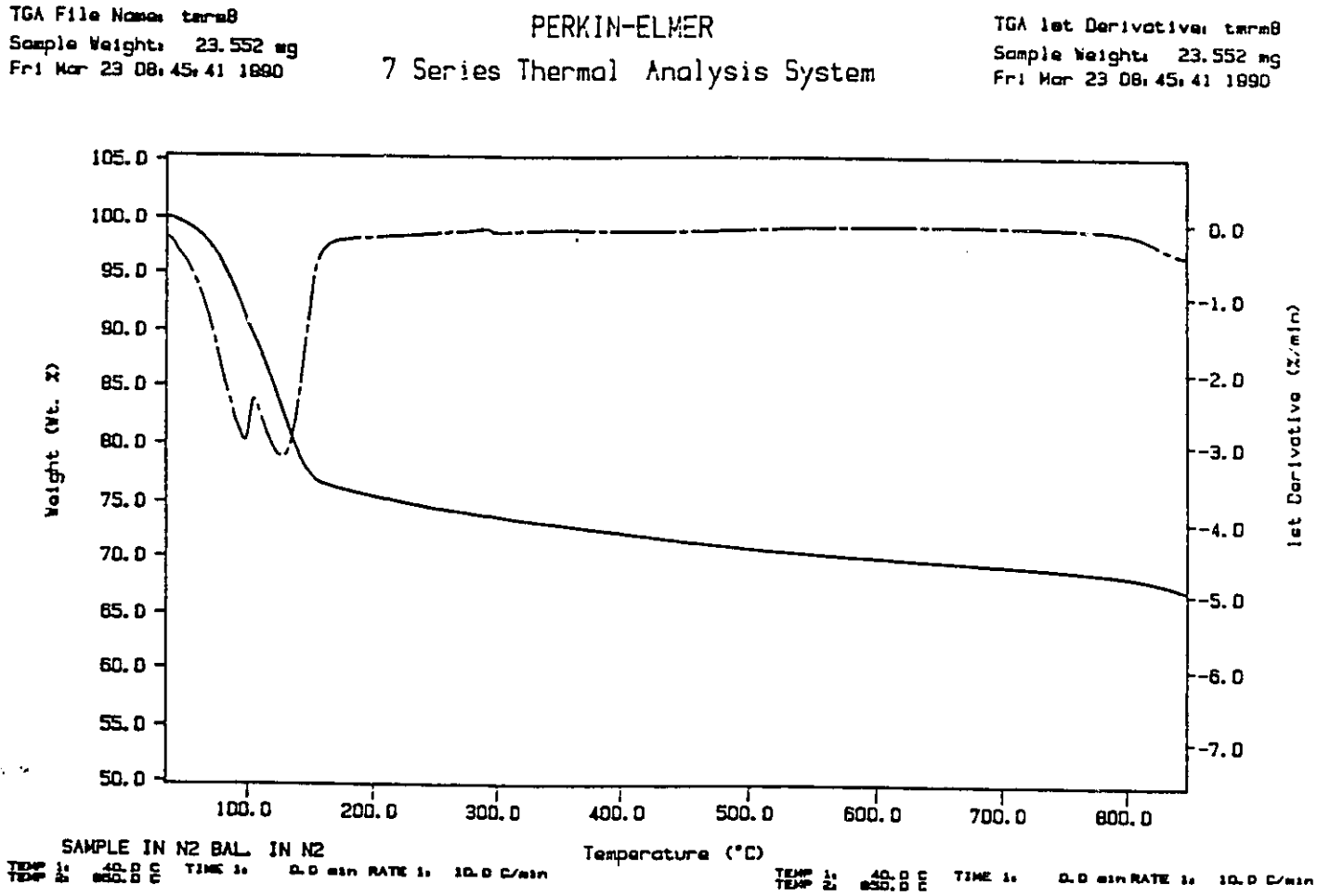

Figure 36: Temperature programmed desorption plot for the catalyst without a zeolite component

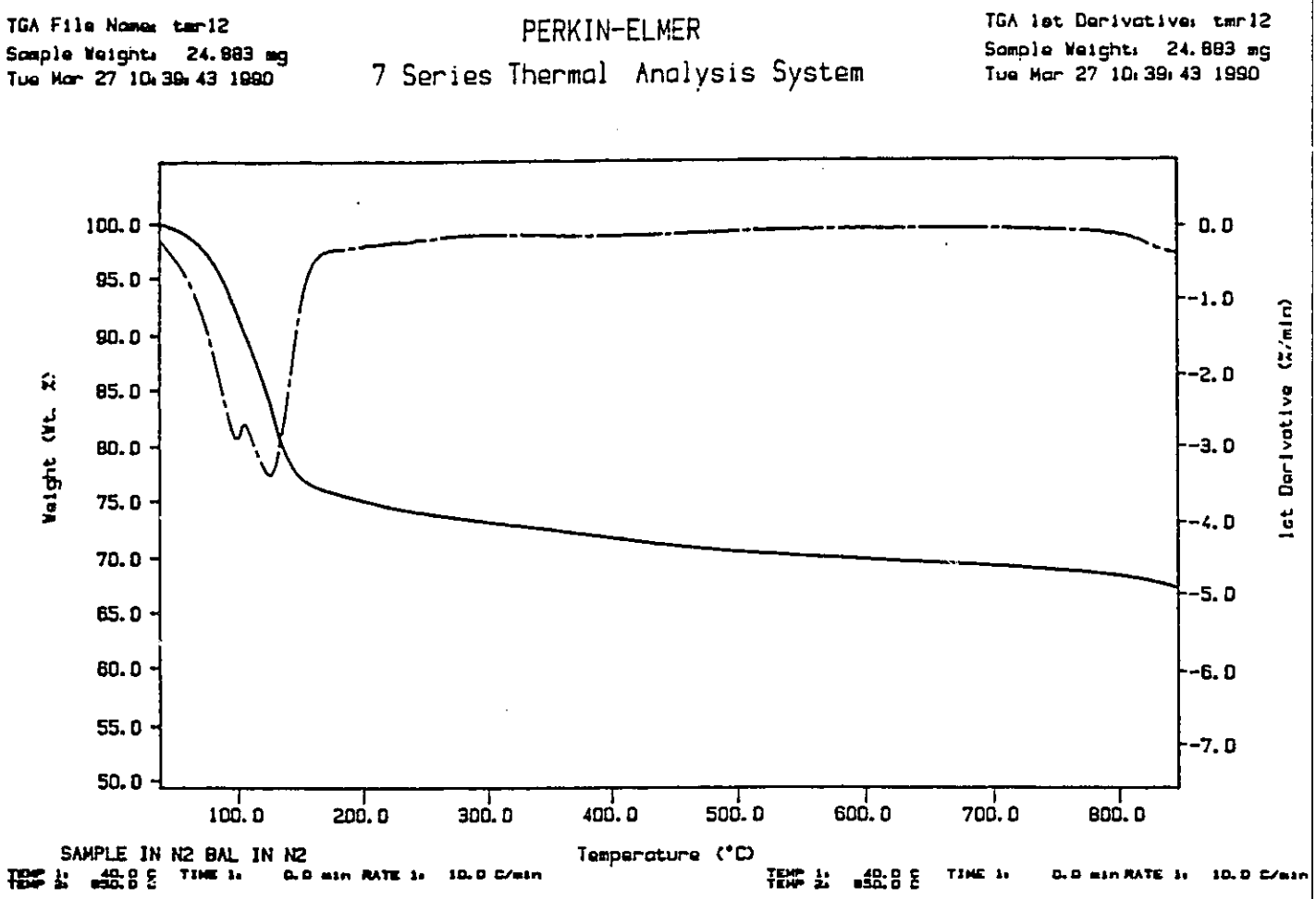

Figure 37: Temperaure programmed desorption plot for the catalyst with 10 wt % H-mordenite zeolite content

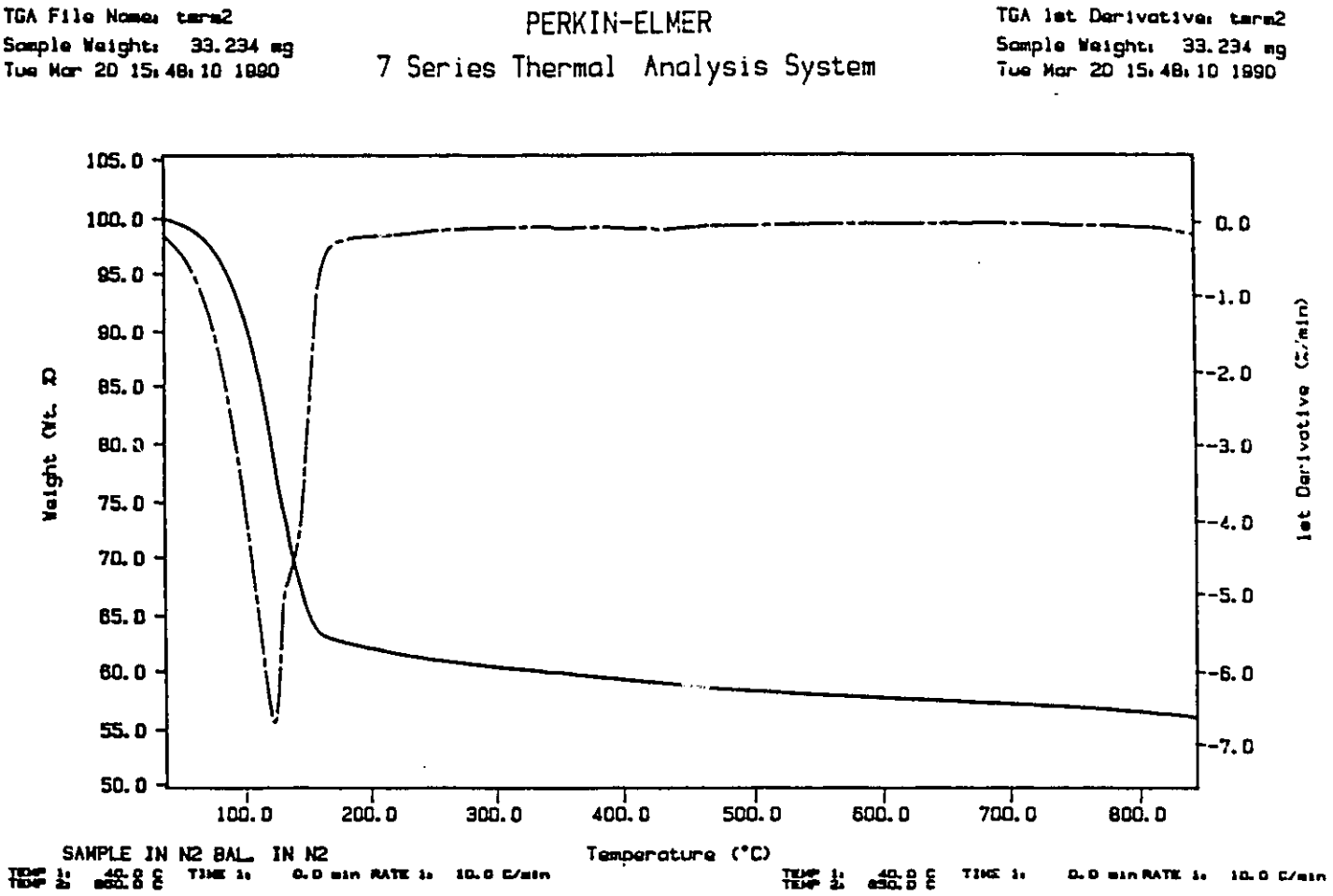

Figure 38: Temperaure programmed desorption plot for the catalyst with 20 wt % H-mordenite zeolite content

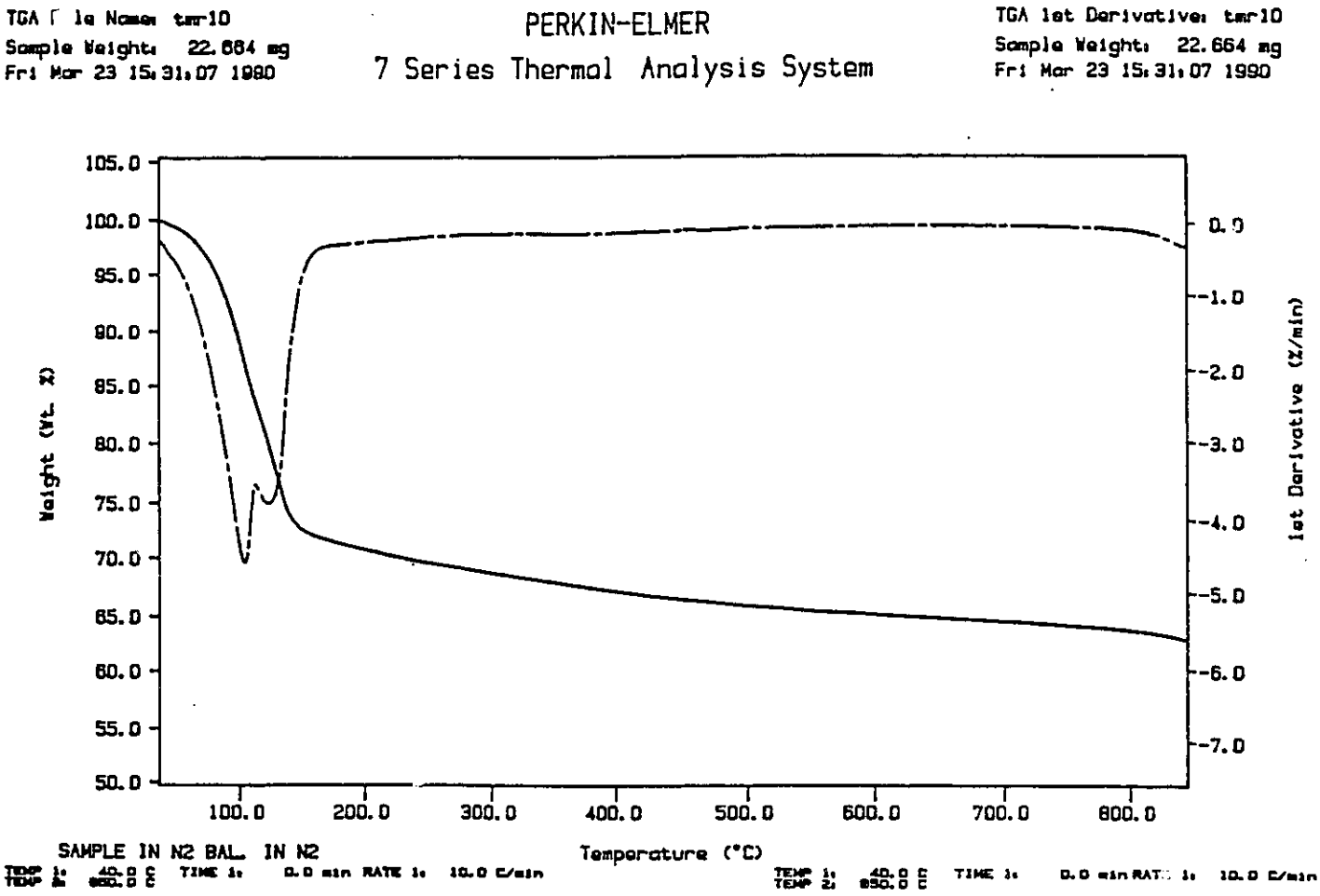

Figure 39: Temperaure programmed desorption plot for the catalyst with 20 wt % HY zeolite content